

## This is to certify that the

thesis entitled

I. CRYSTAL STRUCTURE OF A 2:1 COMPLEX OF 12-Crown-4 WITH SODIUM PERCHLORATE

and

II. PREPARATION AND CRYSTAL STRUCTURE OF (Sr/Y)Cl<sub>2</sub> O5 AND (Sr/Yb)Cl<sub>2+x</sub> presented by

Eileen Mason

has been accepted towards fulfillment of the requirements for

Ph.D. degree in Chemistry

Major professor

**O**-7639



#### OVERDUE FINES: 25¢ per day per item

RETURNING LIBRARY MATERIALS:
Place in book return to remove charge from circulation records

## I. CRYSTAL STRUCTURE OF A 2:1 COMPLEX OF 12-Crown-4 WITH SODIUM PERCHLORATE

and

II. PREPARATION AND CRYSTAL STRUCTURE OF (Sr/Y)Cl<sub>2.05</sub> AND (Sr/Yb)Cl<sub>2+x</sub>

Ву

Eileen Mason

## A DISSERTATION

Submitted to

Michigan State University
in partial fulfillment of the requirements

for the degree of

DOCTOR OF PHILOSOPHY

Department of Chemistry

### ABSTRACT

I. CRYSTAL STRUCTURE OF A 2:1 COMPLEX OF 12-Crown-4
WITH SODIUM PERCHLORATE

Ву

## Eileen Mason

The crystal structure of Na(C804H16)2ClO4 has been determined by a single crystal X-ray diffraction study. The crystal belongs to space group P2,/a with lattice parameters  $\underline{a} = 15.420$  (8)  $\mathring{A}$ ,  $\underline{b} = 15.245$  (10)  $\mathring{A}$ ,  $\underline{c} = 9.650$ (5) A,  $\beta = 92.13$  (4)°. The intensities of 4027 reflections were measured on a Picker-FACS-I automatic diffractometer (Mo  $\mathbf{K}_{\alpha}$  radiation) and refined after initial positions had been indicated by MULTAN by alternating least squares calculations with subsequent difference maps. Full matrix least squares refinement of non-hydrogen atom positions and anisotropic thermal parameters, and isotropic hydrogen thermal parameters converged at  $R_{\gamma}$  = .071 for 1401 reflections with  $|F^2|$  greater than  $3\sigma$  ( $F^2$ ). The sodium ion forms a sandwich structure with two 1204 rings. The eight-fold coordination at the metal is approximately square antiprismatic. The perchlorate is severely disordered. Cationanion interaction appears to be minimal.

# II. PREPARATION AND CRYSTAL STRUCTURE OF $(Sr/Y)Cl_{2.05}$ and $(Sr/Yb)Cl_{2+x}$

Recent developments in solid state chemistry have focused on the detection of long range order in compounds of complex stoichiometry. A series of anion excess species of composition  $M_n X_{2n+1}$  which exhibit the Vernier structure has been identified for certain rare earth ions and combinations of rare earth ions with strontium or yttrium. Attempts to prepare a similar Vernier-type species containing only strontium and yttrium have resulted in a different type of anion-excess structure. An apparently isomorphous strontium-ytterbium analog has also been prepared.

The compounds form colorless crystals which maintain the  $SrCl_2$  unit cell with Z = 4. The crystal structure was refined only for the yttrium compound which has cell parameters  $\underline{a} = \underline{b} = \underline{c} = 6.967$  (1)Å. The intensities of 2645 reflections were measured on a Picker FACS-1 automatic diffractometer (Mo K $_{\alpha}$  radiation) and initial positions indicated by a Patterson synthesis were refined by least squares calculations with subsequent difference maps. Two structural solutions are suggested.

In the proposed vacancy model, the extra  $Y^{3+}$  charge is balanced by the simultaneous removal of a  $Sr^{2+}-Cl^-$  ion pair from the  $SrCl_2$  structure. The individual ion sites are only partially occupied and are not equivalent. The

inequivalence of the sites strongly suggests that some ordering of the vacancies occurs, but the exact nature of the ordering cannot be determined. Refinement in space group P23, which specifies that the anion sites will form two distinguishable interpenetrating tetrahedra, yields a residual value of R = .1013 for 218 reflections with  $|F|^2$  greater than  $\sigma$  (F<sup>2</sup>). Refinement in space group P1, which allows all sites to refine independently, leads to a residual value R = .0873 for the same data set.

The second model describes the structure in terms of a Willis cluster of defects and includes both anion vacancies and interstitial anions. Full-matrix least squares refinement in space group Fm3m, with positions analogous to those in  $\rm UO_{2.13}$  and  $\rm (Ca/Y)F_{2.10}$ , converged at R = .0633 for 114 reflections with  $|F|^2$  greater than  $\sigma$  (F²). Refinement of all data, including reflections inconsistent with face centered symmetry converged at R = .1126 for 114 reflections with  $|F|^2$  greater than  $\sigma$  (F²). It is believed that these additional mixed index reflections indicate ordering of the defect clusters.

But love
and science - they are both gambles;
and if you try to win
the sun's light,
you must be prepared also
to lose every
day.

Diane Wakoski,
"In This Galaxy"



#### ACKNOWLEDGMENTS

Above all, I wish to thank Dr. Harry Eick for his unflagging confidence and optimism. It is largely due to his influence that I returned to graduate school at all, and, without his encouragement my hopes would surely have succumbed to the pitter patter of a myriad little defeats.

I want to extend my appreciation to Dr. A. I. Popov for providing the crystal of  $Na(12-crown-4)_2ClO_4$  and for helpful discussions.

I am grateful to Dr. W. E. Braselton and Steven Ton-sager for chemical analyses by induction coupled plasma spectrometry. The results of the analyses aided me immeasurably in this study.

I would like to thank Dr. Donald Ward for the data collections and his assistance with the crystallographic calculations.

I acknowledge the Department of Chemistry of Michigan State University and the National Science Foundation for financial support throughout my graduate career.

Lastly, I want to thank the large number of Friends and Relations who have extracted me, like Pooh, from many a Place of Great Tightness.

## TABLE OF CONTENTS

Chapter	Page
LIST OF TABLES	v
LIST OF FIGURES	vii
CHAPTER I - BACKGROUND MATERIAL IN SYMMETRY AND CRYSTALLOGRAPHY	1
Reciprocal Space	1
Methods of Data Collection	7
The Precession Method	7
Data Collection with an Automated Diffractometer	11
Transformation of Unit Cells	16
Data Reduction	23
Obtaining a Trial Structure from a Patterson Map	30
Obtaining a Trial Structure by Direct Methods	32
Refinement of the Trial Structure	38
CHAPTER II - CRYSTAL STRUCTURE OF Na(C <sub>8</sub> O <sub>4</sub> H <sub>16</sub> ) <sub>2</sub> ClO <sub>4</sub>	40
Introduction	40
Experimental	42
Structure Solution and Refinement	42
Results and Discussion	49

Chapter	Page
CHAPTER III - PREPARATION AND CRYSTAL STRUCTURE OF (Sr/Y)Cl <sub>2.05</sub> and (Sr/Yb)Cl <sub>2+x</sub>	59
Introduction	59
Experimental	69
Preparation of (Sr/Y)Cl <sub>2+x</sub> and (Sr/Yb)Cl <sub>2+x</sub>	69
Data Collection and Refinement of (Sr/Y)Cl <sub>2+x</sub>	73
Preliminary Investigation of (Sr/Yb)Cl <sub>2+x</sub>	99
Results and Discussion	105
REFERENCES	116
ANNOTATED BIBLIOGRAPHY	123
ADDUCT	3.00

## LIST OF TABLES

Table	Page
1	Crystal Data
2	Final-cycle Refinement Indicators 47
3	Positional and Thermal Parameters
	with Associated ESD's 48
4	Bond Distances and Angles 52
5	Crystal Data for (Sr/Y)Cl <sub>2.05</sub> ,
	First Data Collection
6	Results of Rhombohedral Refinement
	Positional and Thermal Parameters
	with Associated ESD's
7	Crystal Data - Second Data Col-
	lection
8	Comparison of Refinement in Space
	Group Pm3m Using Both Data Col-
	lections
9	Discrepancy Indices for Refine-
	ments with Different Cation: Anion
	Occupancy Ratios 91
10	Results of Chemical Analysis by
	Induction Coupled Plasma
	Spectrometry

Table		Page
11	The Vacancy Model Results of	
	Refinement	95
12	Structural Parameters of Average	
	Cells	98
13	The Willis Cluster Model Results	
	of Refinement	100
14	Percent Occupancy of Zr Sites	
	in Zr <sub>0.77</sub> S	109

## LIST OF FIGURES

Figure			Page
1	Relationship between the direct		
	and reciprocal lattice axes	•	4
2	Above: The reciprocal lattice		
	and the sphere of reflection.		
	Below: The direct plane. Figure		
	redrawn from Stout and Jensen, see		
	Bibliography	•	6
3	(a) A zero-level plane of the		
	reciprocal lattice whose normal,		
	t, is precessing about the direct		
	X-ray beam with precession angle $\mu$ .		
	Redrawn from The Precession Method,		
	Buerger. See Bibliography.		
	(b) Reciprocal lattice plane,		
	tangent to sphere of reflection,		
	and intersecting the sphere of		
	reflection. Redrawn from Stout and		
	Jensen. (c) Film parallel to		
	reciprocal lattice plane showing		
	circular trace of circular intersec-		
	tion with sphere of reflection. Re-		
	drawn from Stout and Jensen	_	10

Figure		Page
4	A four-circle diffractometer	12
5	Scan mode geometry. Redrawn from	
	Stout and Jensen	12
6	The sodium-dicrown unit illustrating	
	50% probability ellipsoids and the	
	atom labeling scheme. H-atoms are	
	designated by the number of the carbon	
	atom to which they are attached	50
7	The packing in Na(12C4) $_2$ C1O $_{l\!f}$ Sodium	
	ions are located at $(0.5 \pm 0.0076)$ ;	
	chlorine atoms at $(\pm 0.0033)$	55
8	The severe distortion of the per-	
	chlorate moiety is illustrated by the	
	presence of seven partially-occupied	
	oxygen atom positions surrounding the	
	chlorine atom	56
9	Clusters in $(Ca/Y)F_{2+x}$ . Above:	
	2:2:2 cluster, two F' ions, two F"	
	ions and two normal ion vacancies.	
	Below: an extended 3:4:2 cluster with	
	two F" ions and 4 F' ions. Y <sup>3+</sup>	
	positions assumed in calculating diffuse	
	scattering. Redrawn from Reference 48	62
10	The 5/11, 6/13 and 11/24 Vernier	
	structures	65

Figure		Page
11	(a) The cubic fluorite unit cell.	
	(b) Tetragonal basis cell derived from	
	the fluorite cell. (c) Rhombohedral basis	
	cell derived from fluorite unit cell. (d)	
	The rhombohedral basis cell and suggested	
	superstructures. (Figure redrawn from	
	Reference 57.)	66
12	Crystal mounting apparatus	72
13	Zero layer precession photographs	
	of (Sr/Y)Cl <sub>2+x</sub> . Above: An apparent	
	six-fold axis. Below: A pattern of	
	triplets	74
14	Relationship between the axes of the	
	rhombohedral — and cubic —	
	unit cells	80
15	$I_{max}/I$ vs $\phi$ for two representative	
	azimuthal scans. No absorption cor-	
	rection has been applied	83
16	A zero layer precession photograph	
	showing two of the cubic axes	104
17	Above: 2:2:2 Willis cluster con-	
	taining two normal anion vacancies	
	( $\square$ ) two X' interstitials ( $\bigcirc$ ),	
	two X" interstitials ( $lacktriangle$ ), and	
	cubic $(*,*,*)$ sites $(+)$ .	

Figure		Page
17	Below: A 3:4:2 Willis cluster.	
	Figure redrawn from Reference 47	107
18	Illustration of the atomic positions	
	in the monoclinic superstructure,	
	space group C2/m. The monoclinic	
	unit cell is shown by the heavy	
	lines. The NaCl-type ZrS cells	
	are shown as thin-lined cubes. Re-	
	drawn from Reference 57	109

#### CHAPTER I

## BACKGROUND MATERIAL IN SYMMETRY AND CRYSTALLOGRAPHY

The first portion of this dissertation is designed to stand apart from the remainder of the work. It is intended to provide a brief and qualitative overview of crystallography and symmetry. For the sake of brevity, the list of topics is eclectic; for the sake of simplicity, mathematical derivations have been excluded whenever possible.

Because of the generalized approach, references have been deliberately omitted.

The reader is directed to the appended bibliography for sources of more detailed analysis. Although it is not complete, the bibliography is annotated to provide a quick guide to the type and complexity of information contained in each work.

### RECIPROCAL SPACE

The experimental data required for X-ray analysis of a crystal structure consist of measurements of the direction of scattering of the X-ray beam by the crystal and the

intensities of these diffracted beams. The first value reveals the size and shape of the unit cell. The second value may be analysed to give the positions of atoms within the unit cell.

X-ray diffraction from the planes of a crystal occurs when  $n\lambda = 2d\sin\theta$ , where  $\lambda$  is the wavelength of the incident X-ray beam, d is the interplanar spacing, and  $2\theta$  is the angle between the incident beam and the diffracted beam. Bragg's Law which describes the conditions for diffraction is more easily visualized in reciprocal space than in direct space.

For each cell in direct space, a corresponding cell in reciprocal space can be constructed. The relationship between the direct and reciprocal lattices requires that for a, b, c, vectors in real space, and a\*, b\*, c\*, vectors in reciprocal space, a\* is perpendicular to b and c, etc., while a is perpendicular to b\* and c\*, etc. The reciprocal lattice can be generated by designating one direct lattice point as an origin and defining the normals from this point to all possible  $(hk\ell)$  direct lattice planes. The reciprocal lattice points will be positioned along these vectors at a distance  $1/d_{hk\ell}$  from the origin if  $d_{hk\ell}$  is the perpendicular distance between the direct lattice planes of the set  $(hk\ell)$ . The indices  $hk\ell$  will define positions in reciprocal space in the same way that the coordinates xyz define positions in direct space.

For orthogonal systems,  $\alpha=\beta=\gamma=\alpha^*=\beta^*=\gamma^*=90^\circ$  and the

reciprocal space axes are coincident with the axes in direct space. For radiation of wave length  $\lambda$ , the translation in direct space,  $t_{uvw}$ , is related to a translation in reciprocal space,  $d_{hbl}^*$ , by the relationship

$$t_{uvw} = \lambda \left( 1/d_{hk\ell}^* \right)$$

The axes of the unit cell in direct space are simply special cases of translation:

$$a = t_{100} = \lambda (1/d^*_{100})$$

$$b = t_{010} = \lambda (1/d^*_{010})$$

$$c = t_{001} = \lambda(1/d*_{001})$$

For non-orthogonal systems, the situation is more complicated because the reciprocal lattice axes will not be coincident with the direct cell axes. The interplanar distance measured along the normal may be different from the interplanar distance measured along the cell axis. For example, if the angle between a and c is  $\beta$ , then

$$d_{100} = a \sin \beta = a \sin \beta^* \quad (\beta^*=180^\circ-\beta)$$

and 
$$d_{100}^* = a^* = \frac{1}{a \sin \beta}$$

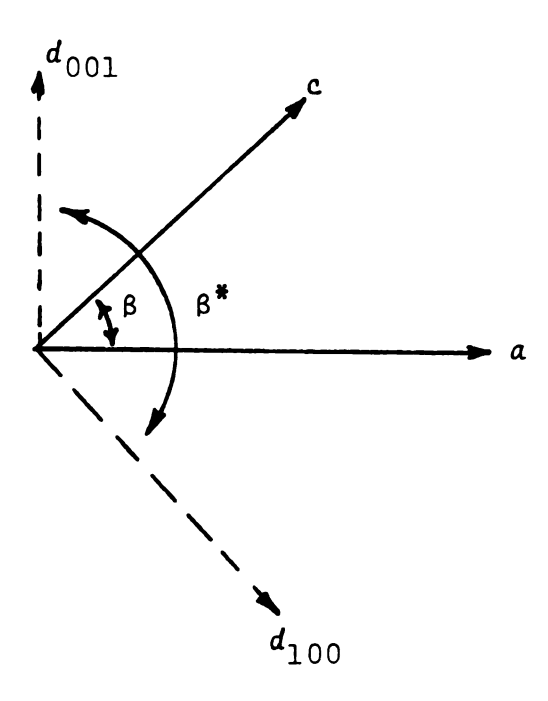


Figure 1. Relationship between the direct and reciprocal lattice axes.

Note that for 90° angles,  $\sin \beta = 1$  and  $a^* = \frac{1}{a}$ . Consider a reciprocal lattice plane in a crystal which is bathed in a beam of X-rays of wavelength  $\lambda$ . The beam is parallel to this plane, and is indicated by a line (XO) passing through the origin (0) of the reciprocal lattice.

A unit circle in direct space corresponds to a circle of radius  $1/\lambda$  in reciprocal space. Such a circle, with radius  $1/\lambda$  passes through 0. Its center (C) falls on line XO. P is any reciprocal lattice point located on the circumference of the circle. (Figure 2)

Angle OPB will be equal to 90° because it is inscribed in a semi-circle, and  $\sin$  OBP =  $\sin$   $\theta$  =  $\frac{OP}{OB}$  =  $\frac{OP}{2}$  x  $\lambda$ . Remember that P is a reciprocal lattice point. Therefore, OP equals  $1/d_{hkl}$ , and from the Bragg equation

$$\sin \theta = \frac{(1/n \cdot d_{hk\ell})\lambda}{2} = [(1/2 \ dhk\ell)]\lambda.$$

Through this derivation, we see that Bragg reflections occur whenever reciprocal lattice points fall on a circle of radius  $1/\lambda$  which is tangent to the origin of the reciprocal lattice.

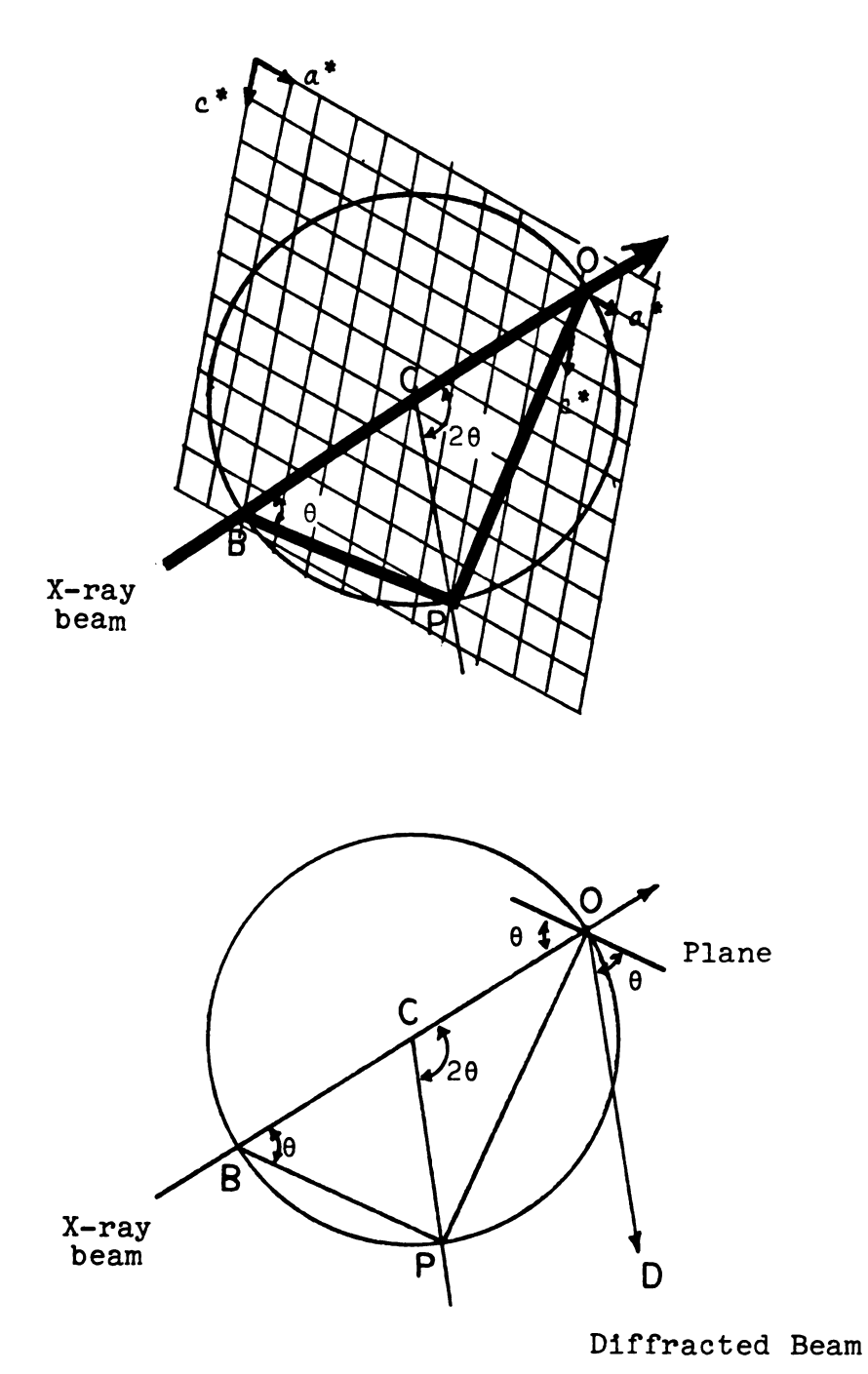


Figure 2. Above: The reciprocal lattice and the sphere of reflection. Below: The direct plane. Figure redrawn from Stout and Jensen, see Bibliography.

#### METHODS OF DATA COLLECTION

Measurements of the direction of scattering and the intensity of the scattered beam may be made photographically or electronically. The methods are complementary, for, although a diffractometer with a scintillation counter provides numerical, quantified information, film techniques are frequently more reliable guides to the symmetry of the cell, since the scintillation counter records only one reflection at a time and must be specifically positioned for each reflection. Photographic techniques record an entire plane of the reciprocal lattice on a single film and minimize the chance of overlooking reflections. Furthermore, the film is tangible and easily visualized, while the diffractometer produces pages of numbers.

In this study, photographic data collection by the precession method preceded electronic data collection with an automated diffractometer. Measurement of the films gave approximate values for the cell parameters, but the major benefit of the technique was in the identification of the correct space group. The relative intensities were considered only in relation to the symmetry properties.

## The Precession Method

In the precession method, the incident X-ray beam is parallel to a direct lattice axis and perpendicular to

a plane in the reciprocal lattice which contains 2 axes. This layer is tangent to the sphere of reflection at the origin. Arc settings on the goniometer head are used to bring the crystal into proper alignment.

The crystal is rotated at an angle,  $\mu$ , about an axis perpendicular to the beam. Movement of the crystal is such that the direct axis vector now revolves about the beam, maintaining constant angular separation of  $\mu^{\circ}$ . The reciprocal lattice zero layer now cuts the sphere and the intercepted circle precesses about the origin as the direct lattice axis precesses about the incident beam (Figure 3). Additional reflections from other layers are intercepted by a metal screen.

The film also precesses and always remains parallel to the reciprocal lattice plane. Reflections are recorded when a reciprocal lattice point falls on the intersection of the lattice layer and the sphere of reflection. Upper layers of the reciprocal lattice are recorded by moving the film closer to the crystal by a distance corresponding to the measured spacing of the rows. Each precession layer photograph gives an undistorted image of all reflections in a particular plane of reciprocal space. Measurements of the precession film, when scaled, give the cell parameters of the reciprocal lattice.

Since the symmetry of the reciprocal lattice will be the same as the symmetry of the direct lattice, examination

## Figure 3.

A zero-level plane of the reciprocal lattice whose normal, t, is precessing about the direct X-ray beam with precession angle μ. Redrawn from The <u>Precession Method</u>, Buerger. See Bibliography.

b) Reciprocal lattice plane, tangent to sphere of reflection, and intersecting the sphere of reflection. Redrawn from Stout and Jensen.

c) Film parallel to reciprocal lattice plane showing circular trace of circular intersection with sphere of reflection. Redrawn from Stout and Jensen.

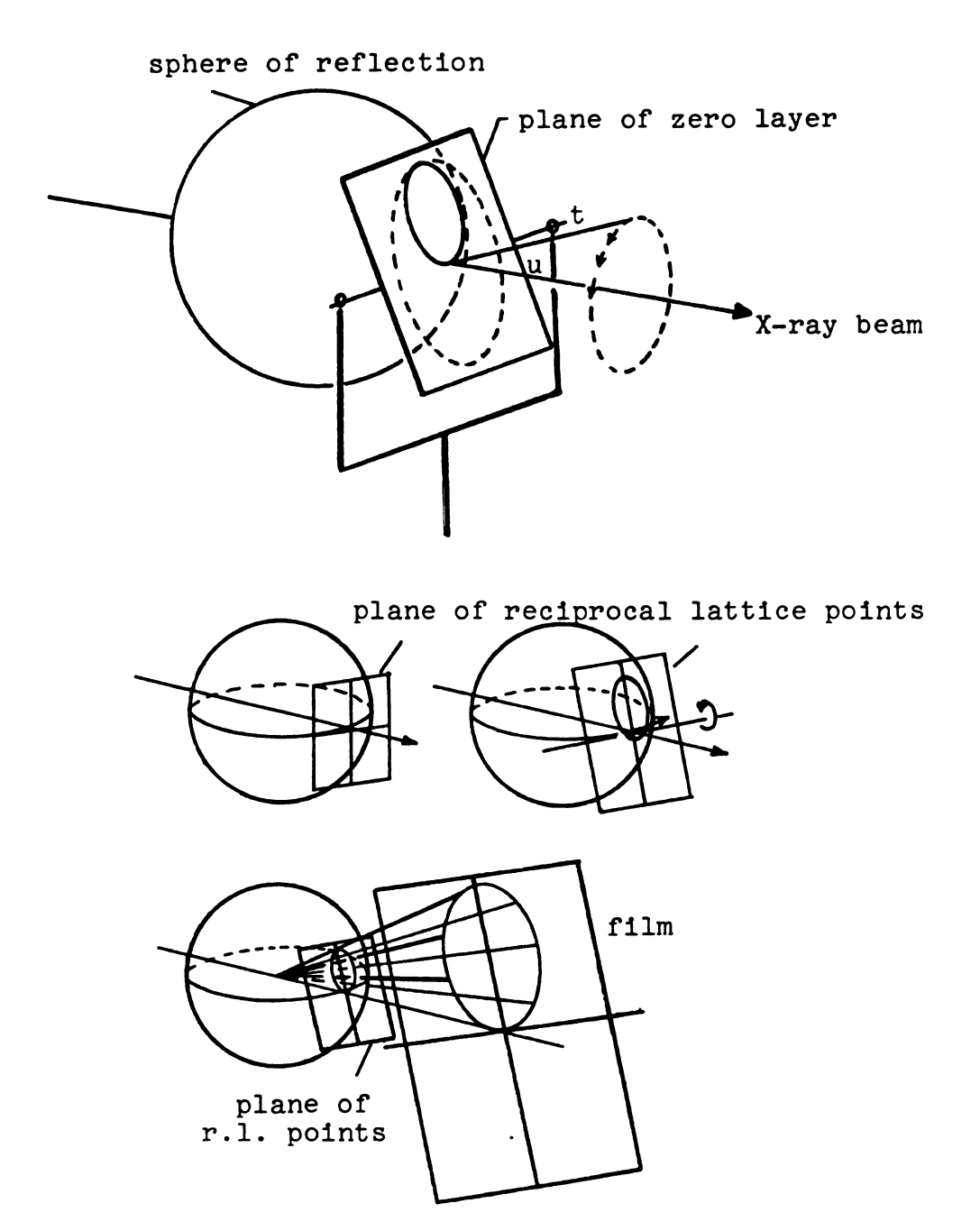


Figure 3

of a properly indexed precession film will reveal the space group of the unit cell.

It should be noted here that examination of only zero layer films may be misleading if the apparent symmetry of the zero layers is higher than that of the cell as a whole. In the zero layer, two-fold axes and mirror planes are indistinguishable. Furthermore, centering or other symmetry conditions may lead to the systematic extinction of certain classes of reflections. For example, in a face-centered cell, h,k and  $\ell$  must be all odd or all even. Hence, the HKO layer will contain only even values of h and k. This will not be obvious, however, unless the HKO plane is compared to an HKL plane where L is odd and which contains only odd valued h's and k's. Failure to recognize systematic extinctions is a major cause of improper identification of the space group. It is not possible to solve a structure accurately, if at all, if an axis of the unit cell is erroneously shortened to a fraction of its true length.

## Data Collection with an Automated Diffractometer

The four circle diffractometer has four arcs, each with 360° of freedom. The crystal orienter which contains the  $\phi$  and  $\chi$  circles is mounted within the  $\omega$  circle and rotates with it. The 20 axis is colinear with  $\omega$ . When  $\chi$  = 0°, the axis of  $\phi$  is coincident with 20 and  $\omega$ . The crystal is

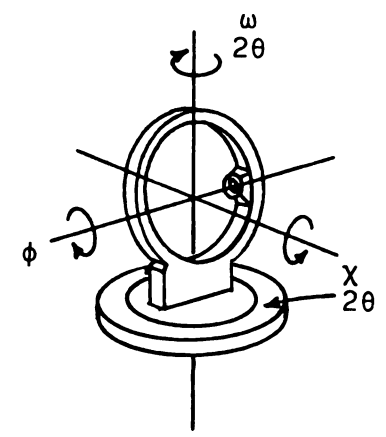


Figure 4. A four-circle diffractometer.

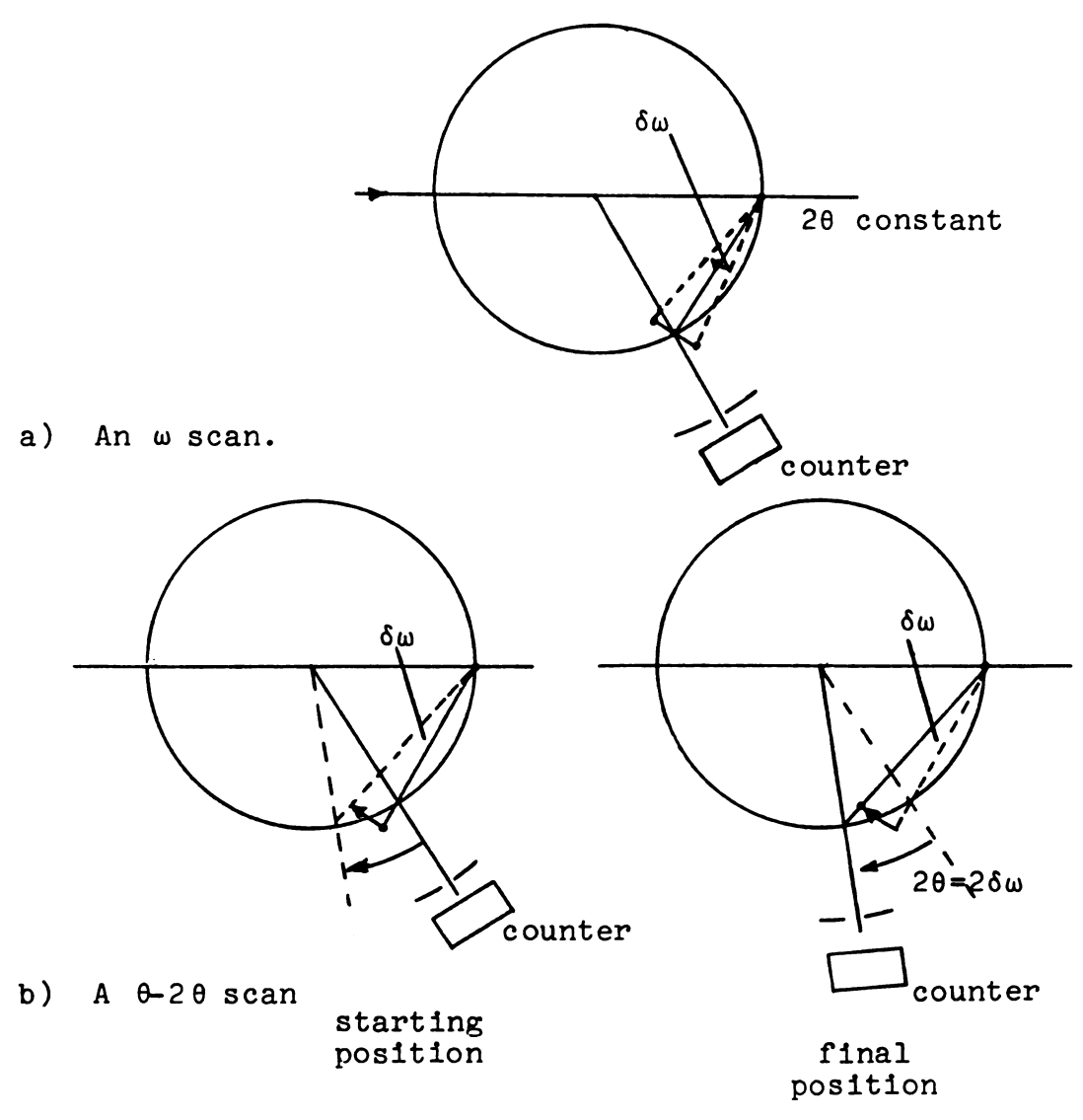


Figure 5. Scan mode geometry. Redrawn from Stout and Jensen.

mounted on a goniometer head which has a height adjustment and may have arc settings. The arc settings are not required (Figure 4).

The X-ray detector is mounted on the 20 circle. The source, which is fixed, the detector, and the center of the orientation assembly lie in a plane perpendicular to the  $\omega$  and 20 axes. Because of this restriction, it is necessary to reorient the crystal -- generally using the  $\phi$  and  $\chi$  circles -- to bring the desired reciprocal lattice point into contact with the sphere of reflection in the source/center/detector plane. After reorientation of the crystal, the detector is moved along the 20 circle until it is situated properly to record the reflection.

The values of  $\chi$ ,  $\phi$ ,  $\omega$  and 20 must be determined and individually set for each reflection to be recorded. Both the cell constants and their orientation relative to the  $\phi$  axis must be known; the angular settings are highly interdependent. A diffractometer is automated by being interfaced directly with a computer which calculates settings as needed, drives the encoder motors to the preselected angle setting, and records the angular and intensity data. On the system used in this work a PDP8/I computer was interfaced with a Picker diffractometer.

An actual reflection is not a point in reciprocal space but has finite dimensions. To measure the reflections, the detector must scan through a small region of space which encompasses the reflection. Two scanning modes are in common usage: In the  $\omega$  scan, the crystal -- and hence the reciprocal lattice -- is rotated by the  $\omega$  circle so that lattice points pass from the outside to the inside of the sphere of reflection while the detector is stationary at the precalculated 20 setting. The detector observes a region of space along an arc centered at the lattice origin and passing through the reciprocal lattice point. In the 0-20 mode, the counter moves at an angular rate twice that of the crystal, scanning along a portion of the straight line connecting the lattice point and the origin. This is approximately perpendicular to the arc traced in the  $\omega$  scan (Figure 5).

The advantage of one scan mode over the other depends on the nature of background intensity as much as the shape of the reflections. A common technique for measuring background is to obtain counts with the detector stationary at the beginning and end of the scan range, average the values obtained, and, after correcting the rate to the actual scan time, to subtract the background from the net counts of the reflection. If the background is uniform, either scan mode will be acceptable. An  $\omega$  scan however is perpendicular to the streaks caused by white radiation and will not reveal this increase in background intensity, while in the  $\theta$ -2 $\theta$  scan mode, the detector moves along the radiation streak and will give a more reliable evaluation of the intensity of the reflection.

The use of crystal monochronometers has greatly reduced the problems of white radiation, reflecting almost pure  $K_{\alpha_1}$  and  $K_{\alpha_2}$  radiation. At small diffraction angles, the  $\alpha_1\text{-}\alpha_2$  divergence is small and a restricted scan range will encompass both peaks. At higher values of sine however,  $K_{\alpha_1}$  and  $K_{\alpha_2}$  gradually diverge, and reflections tend to be broader and more diffuse. The scan range must therefore be increased. If an extended range is used for all reflections, then the intensities of the low-e reflections may be inflated by integration over too great a width. For this reason, the computer varies the scan width with 20 so that an optimum scan range will be employed for all reflections.

Variations in background intensity due to the diffraction of white radiation are systematic and predictable, but other factors may complicate the separation of background and reflection intensity. Scattering of X-rays by air, the mounting materials, protective capillaries and amorphous materials present with the crystal may lead to random and unpredictable variations in background intensity. The crystal support and amorphous material may also absorb X-rays and lead to reduced intensity of the diffracted beam. Since it is difficult to correct for these influences, they should be minimized. A beam collimator will lessen air scattering and use of the thinnest possible mounting and capillaries will reduce both scattering and absorption.

The quality of the crystal itself will also affect the

resolution of the reflections; a flat, diffuse reflection will not be easily separated from the background. Broad and split reflections and reflection peaks with shoulders are generally due to crystal flaws. A small fragment attached to the main crystal will lead to additional reflections. Depending on the intensity and location of these reflections, the main crystal may be unsuitable for analysis.

Real crystals are rarely perfect but exhibit a mosaic structure composed of small, slightly misaligned crystallites. The degree of misalignment, the mosaic spread, affects the shape of the reflections: when it is too great,
reflection peaks are excessively broad, but when misalignment of the crystallites is less than 0.5° it is actually
beneficial, helping to maintain the same magnitude of extinction for reflections of both high and low intensity. A
discussion of extinction will be included in the data reduction section.

## TRANSFORMATION OF UNIT CELLS

It is possible that the space group initially identified may be lower in symmetry than the true space group. In general, however, this will not interfere with solution of the structure, since a higher symmetry cell of the same volume can be found analytically, or the higher symmetry space group may become apparent as refinement proceeds.

When a different choice of unit cell is made, it is necessary to re-index the data in terms of the new unit cell. It is possible to use matrix multiplication to transform direct lattice vectors and the indices of planes or individual reflections from one cell to another. A related matrix will transform reciprocal lattice vectors, coordinates of positions in the unit cell, and zone axis symbols.

The first step in interconverting two unit cells is to define the unit vectors of one in terms of the other. Perhaps the easiest way to do this is to draw a picture of the two cells and verify the relationship geometrically, and to write a series of equations of the type:

$$a_2 = s_{11}a_1 + s_{12}b_1 + s_{13}c_1$$
 $b_2 = s_{21}a_1 + s_{22}b_1 + s_{23}c_1$ 
 $c_2 = s_{31}a_1 + s_{32}b_1 + s_{33}c_1$ 

that is:

$$\begin{pmatrix} a_1 \\ b_1 \end{pmatrix} \begin{pmatrix} s_{11} & s_{12} & s_{13} \\ s_{21} & s_{22} & s_{23} \\ s_{31} & s_{32} & s_{33} \end{pmatrix} = \begin{pmatrix} a_2 \\ b_2 \\ c_2 \end{pmatrix}$$

To convert the unit vectors of cell 2 to cell 1, the inverse matrix must be used, i.e.,:

$$\begin{pmatrix} a_2 \\ b_2 \\ c_2 \end{pmatrix} \begin{pmatrix} s_{11} & s_{12} & s_{13} \\ s_{21} & s_{22} & s_{23} \\ s_{31} & s_{32} & s_{33} \end{pmatrix} = \begin{pmatrix} a_2 \\ b_2 \\ c_2 \end{pmatrix} \begin{pmatrix} t_{11} & t_{12} & t_{13} \\ t_{21} & t_{22} & t_{23} \\ t_{31} & t_{32} & t_{33} \end{pmatrix} = b_1$$

Similarly, the indices  $h_i k_i l_i$  are transformed to  $h_j k_j l_j$ .

Transformation of reciprocal cell vectors requires not only exchange of the S and T matrices, but also interchange of the rows and columns within each matrix. Thus,

$$\begin{pmatrix} a_1^* \\ b_1^* \\ c_1^* \end{pmatrix} \begin{pmatrix} \dagger_{11} & \dagger_{21} & \dagger_{31} \\ \dagger_{12} & \dagger_{22} & \dagger_{32} \\ \dagger_{13} & \dagger_{23} & \dagger_{33} \end{pmatrix} = a_2^*$$

and

$$\begin{pmatrix} a_{2}^{*} \\ b_{2}^{*} \end{pmatrix} \begin{pmatrix} s_{11} & s_{21} & s_{31} \\ s_{12} & s_{22} & s_{32} \\ s_{13} & s_{32} & s_{33} \end{pmatrix} = b_{1}^{*}$$

These matrices are used to convert the positions  $x_{i}y_{i}z_{i}$  to  $x_{j}y_{j}z_{j}$ . Again, the two conversion matrices share an inverse relationship.

Interconversion is straightforward, provided that the  $s_{ij}$  and  $t_{ij}$  elements are all integral. Since S and T are inverses, this condition is satisfied only if the elements are equal to  $\pm 1$  or 0. This will be true if the new cell has the same volume as the old cell. Transformation becomes more complex, however, when fractional matrix elements are required to transform the cell originally chosen into one with a different volume.

Although the multiplication of matrices containing non-integral elements is well defined mathematically, physical interpretation is ambiguous, since h,k and  $\ell$  are required to be integral.

As an example, consider the interconversion of two of the possible hexagonal and cubic cells considered for  $(Sr/Y)Cl_{2+x}$ .

$$a_h = -1/2 \ a_{cu} + 1/2 \ c_{cu}$$

$$b_h = 1/2 \ a_{cu} - 1/2 \ b_{cu}$$

$$c_h = a_{cu} + b_{cu} + c_{cu}$$

This leads to the matrix relationship:

$$\begin{pmatrix} a_h \\ b_h \end{pmatrix} \begin{pmatrix} -2/3 & 2/3 & 1/3 \\ -2/3 & -4/3 & 1/3 \end{pmatrix} = b_{cu}$$

$$\begin{pmatrix} a_h \\ c_h \end{pmatrix} \begin{pmatrix} 4/3 & 2/3 & 1/3 \end{pmatrix} = c_{cu}$$

Consider now the transformation of the hexagonally-indexed reflections (001), (002), and (003) to their cubicly-indexed counterparts:

$$\begin{pmatrix} 0 \\ 0 \\ -2/3 \\ -4/3 \end{pmatrix} = 1/3$$

$$\begin{pmatrix} -2/3 \\ -4/3 \\ 2/3 \\ 1/3 \end{pmatrix} = 1/3$$

$$1/3$$

$$\begin{pmatrix} 0 \\ 0 \\ -2/3 \\ -2/3 \\ -4/3 \\ 2/3 \\ 1/3 \end{pmatrix} = 2/3$$

$$\begin{pmatrix} 0 \\ -2/3 \\ -4/3 \\ 2/3 \\ 1/3 \end{pmatrix} = 2/3$$

$$\begin{pmatrix} 0 \\ 0 \\ 0 \\ -2/3 \\ -4/3 \\ 2/3 \\ 1/3 \end{pmatrix} = 1$$

$$\begin{pmatrix} 0 \\ -2/3 \\ -4/3 \\ 2/3 \\ 1/3 \end{pmatrix} = 1$$

If we clear the fractions by multiplying each set of indices by the lowest common denominator, we find that  $(001)_h$  and  $(003)_h$ , two parallel planes, are now both represented by the same cubic indices,  $(111)_c$ . The multiplication has forced the planes to become equivalent.

If, in order to avoid this pitfall, all the indices are multiplied by the same factor, we find that

$$\begin{pmatrix} 1_{h} \\ 1_{h} \end{pmatrix} \begin{pmatrix} -2/3 & 2/3 & 1/3 \\ -2/3 & -4/3 & 1/3 \end{pmatrix} = -5/3 \stackrel{\times 3}{\rightarrow} \overline{5}_{cu}$$

$$\begin{pmatrix} 1_{h} \\ 1_{h} \end{pmatrix} \begin{pmatrix} 4/3 & 2/3 & 1/3 \end{pmatrix} = 7/3 \stackrel{\times 3}{\rightarrow} \overline{5}_{cu}$$

Since the original transform matrix was obtained geometrically, multiplication by the inverse of this matrix should restore the indices  $(lll)_h$ . However, this is not the case:

$$\begin{pmatrix} 1_{cu} \\ \overline{5}_{cu} \\ 7_{cu} \end{pmatrix} \begin{pmatrix} -2/3 & 2/3 & 1/3 \\ -2/3 & -4/3 & 1/3 \\ 4/3 & 2/3 & 1/3 \end{pmatrix} = \begin{pmatrix} 1_{cu} \\ \overline{5}_{cu} \\ 7_{cu} \end{pmatrix} \begin{pmatrix} -1/2 & 0 & 1/2 \\ 1/2 & -1/2 & 0 \\ 1 & 1 & 1 \end{pmatrix} = 3_{h}$$

Although multiplication of the entire set of indices maintains the separate identities of parallel planes, it redefines the unit cell.

If the unit cell parameters have been determined correctly, it is a straightforward procedure to transform

this unit cell to an equivalent cell of higher symmetry, provided such a cell exists. However, if certain classes of reflections have been overlooked, leading to an incorrect unit cell determination, it may not be possible to reindex the reflections in terms of the correct cell.

The outlook for successful transformation is especially bleak if the original cell is too small and both the length and direction of the axes are to be changed.

Upper layer precession photographs are crucial to proper space group identification and may be required for the correct determination of the unit cell axis lengths. If upper layer photographs are to be obtained, the crystal must be oriented with a principal axis parallel to the X-ray beam. Unfortunately, the arcs of the goniometer head are limited to adjustments of  $\pm 25^{\circ}$ , and it may be necessary to remount the crystal to achieve a suitable orientation. Remounting a crystal is frequently such a tedious task that it is impossible in actual practice.

This problem does not arise with a four circle diffractometer which has full freedom in all planes. With this
instrument, difficulties in identifying the proper unit
cell arise because reflections can be overlooked easily and
this can lead to incomplete data collection. The correct
directions of the axes may be identified, but the assumed
lengths may be a fraction of their true values. Such a data
set can be reindexed successfully, but it will contain "holes"

and a satisfactory structural solution may not be obtainable until the missing data have been collected.

## DATA REDUCTION

Since X-rays and crystals are both periodic, the pattern of diffraction will also be periodic and hence can be described by a Fourier series in three dimensions.  $F_{hkl}$  the structure factor for the unit cell for the reflection (hkl) is given by

$$F_{hk\ell} = \{ \sum_{j} f_{j} \cos 2\pi (hx_{j} + ky_{j} + lz_{j}) + i \sum_{j} f_{j} \sin 2\pi (hx_{j} + ky_{j} + lx_{j})$$

$$= \sum_{j} f_{j} e^{i2\pi (hx_{j} + ky_{j} + lz_{j})}$$

where  $f_j$  is the scattering factor of the i<sup>th</sup> atom and  $x_j$ ,  $y_j$  and  $z_j$  are its fractional coordinates.

The structure factor can also be written:

$$F_{hk\ell} = \sum_{j} f_{j} \cos \phi_{j} + i f_{j} \sin \phi_{j},$$

where  $\phi_j$  is the value of the phase scattered by the j<sup>th</sup> atom.

Unfortunately, the fractional coordinates cannot be calculated directly since the phase angles are not measurable quantities and must be surmised from the intensity data.

As in all wave phenomena, the intensity of the wave is proportional to the square of its amplitude and the intensity of each reflection is a measurable quantity.

The result of a collection of X-ray diffraction data is a list of intensities and scattering angles identified by indices h, k and  $\ell$ . While the angular parameters are determined by the dimensions of the lattice, the intensities are governed by the nature and arrangement of the unit cell contents.

After all background has been removed, the intensity of each reflection will be given by:

$$I = K|F_0|^2(Tv)(Lp)(Ab)$$

where K is a scale factor, Tv is related to the thermal motion of the atoms, Lp is a geometric effect and Ab includes absorption and extinction corrections.

Lp, being proportional to  $1/\cos\theta$ , is totally independent of the cell contents.

Calculation of the absorption correction may be aided if the number and types of atoms in the unit cell is known, but no knowledge of atomic positions is required.

Absorption reduces the intensity of reflections. In any absorption phenomenon, the intensity, I, of a beam passing through an absorber of thickness  $\tau$  is given by

I =  $I_0e^{-\mu\tau}$ , where  $I_0$  is the intensity of the incident beam and μ is the linear absorption coefficient. The absorption coefficient increases rapidly but not linearly with increasing atomic number, and is also dependent on the wavelength of the radiation used. Mass absorption coefficients, ( $\mu/\rho$ , where  $\rho$  is density) for most elements and most common radiations are listed in the <u>International Tables for X-ray Crystallography</u>, vol. III and absorption coefficients for compounds can be calculated. For a compound of density  $\rho$ , made up of  $X_n$ % of element  $E_n$ , the linear absorption coefficient for radiation of wavelength  $\lambda$  is given by

$$\mu_{\lambda} = \rho \sum_{n} (X_{n}/100)(\mu/\rho)_{\lambda, E_{n}}$$

If uncorrected, absorption serves to reduce the thermal parameters to values less than the true values. Absorption effects are most noticeable for reflections collected at low values of  $\sin\theta$ . If the crystal is spherical, absorption varies exponentially with  $\sin^2\theta$ .

For irregularly shaped crystals, the path length of the beam through the crystal,  $\tau$ , will vary with the orientation of the crystal relative to the incident beam. In this case, it is possible to correct for absorption by calculating the path length through the crystal of the beam diffracted from every infinitesimal portion of the crystal and then integrating over the entire crystal volume. The crystal is

described in terms of the planes which comprise its faces and the distance of these planes from an arbitrary center. Calculation of a path length for each reflection is tedious and not exactly straightforward. Computer programs can apply such an analytic correction to every reflection.

Unfortunately, difficulties arise in the cases where absorption effects are the greatest: in crystals containing In these cases, where the greatest portion of heavy atoms. the diffracted beam may be reflected by the outermost planes, the calculation of the pathlength will be extremely complex. An analytic correction may be not merely nonproductive but actually counterproductive if the calculated path length does not correspond closely to the actual path length. attempted correction may increase the intensity differences of equivalent reflections rather than reduce the differ-The best alternative may be to use an empirical ences. absorption correction based on azimuthal scans of individual reflections. In such a correction, the reduced intensity of a reflection is multiplied by an appropriate factor to restore it to its original value. No knowledge of the unit cell contents is required. If the azimuthal scan is made for a reflection at  $\chi = 90^{\circ}$ , the magnitude of the correction factor will depend on the values of  $\phi$  and  $2\theta$  and will simultaneously correct for absorption by mounting materials. An empirical correction adjustable for all four setting parameters,  $\phi$ ,  $\chi$ ,  $\omega$  and 20 would be even better.

Extinction is another process which results in an attenuation of intensity of a beam passing through a crystal. It arises from the geometry of diffraction. Each ray reflected at a Bragg angle can also undergo a second reflection back into the primary beam. Since a phase shift of  $\pi/2$  occurs with each reflection, the twice-reflected beam differs in phase from the primary beam by  $\pi$ , and the triply-reflected beam traveling in the direction of the Bragg reflection differs in phase from the once-reflected beam by  $\pi$ . Because of the phase shift, addition of rays reflected  $\pi$  times and rays reflected ( $\pi$ -2) times leads to a reduction of intensity. In a perfect crystal, the intensity of the diffracted beam would be proportional to  $|F_0|^2$ .

Correction factors can be calculated for situations in which primary correction is significant, but mosaic structure prevents the extension of perfect planes over appreciable regions of space and primary extinction is usually negligible.

Secondary extinction, however, is frequently encountered and often appreciable. It arises for intense reflections when such a large percentage of the incident beam is reflected by the very first planes encountered that the deeper planes are subjected to a lower intensity and hence produce reflections of lower intensity than expected. A large crystal will suffer more from secondary extinction as will

a crystal containing heavy atoms, or one in which the mosaic blocks are very nearly parallel. Reflections at low values of  $\sin\theta/\lambda$  are also subject to greater secondary extinction effects, as they are generally stronger reflections.

Since secondary extinction frequently mimics absorption, the correction is customarily added to the linear absorption coefficient.

The thermal parameters and scale factor can be estimated from knowledge of the nature of the cell contents without knowledge of the position of those contents. A very good approximation of these values can be derived by Wilson's method, noting that for a random distribution of N atoms, the local expectation value of

$$\left|\overline{F_{hk\ell}}\right|^2 = \sum_{j=1}^{N} f_j^2(hk\ell)$$

Consider now the relationship between  $|F_{hk\ell}|^2$  and  $|F_{obs}|^2$ , which is known only on an arbitrary scale.

$$|F_{obs}|^2 = K |F_{hkl}|^2$$

and

$$|\overline{F_{obs}}|^2 = K |\overline{F_{hk\ell}}|^2 = K \sum_{j=1}^{N} f_j^2(hk\ell)$$

Let us now assume that the effects of thermal motion can be described by including an additional factor so that

$$f^2 = {}^2e^{-(2B \sin^2\theta)/\lambda^2}$$

where of is the scattering factor at 0°K as listed in the International Tables for Crystallography.

Then

$$q = \frac{|\overline{F_{obs}}|^2}{\sum_{j=0}^{\infty} f_{j}^2} = Ke^{-(2B \sin^2 \theta)/\lambda^2}$$

and

$$\ln q = \ln K - (2B \sin^2 \theta)/\lambda^2$$

The best fitting straight line drawn through the plot of  $\ln q$  vs.  $\sin^2 \theta/\lambda^2$  will have a slope of -2B and an intercept of  $\ln K$ . The values of B and K can be adjusted from these approximate values during refinement.

After appropriate manipulations,

$$I_{corr} = K |f|^2 exp (-2B sin^2 \theta/\lambda^2)$$

The structure factor of the cell is the sum of the scattering

factors of all atoms within the cell. If positions are chosen for all atoms in the asymmetric unit, amplitudes and phases of the structure factor can be calculated, and the calculated value compared to the observed value. Good agreement of these values as reflected in the discrepancy index,

$$R = (F_{obs} - F_{calc})/F_{obs}$$
,

usually indicates that the structure proposed is correct.

Until phase angles can be measured directly, crystallographic strategy will concentrate on methods of deriving suitable trial structures.

## OBTAINING A TRIAL STRUCTURE FROM A PATTERSON MAP

One method of obtaining a trial structure is by analysis of a Patterson map. The Patterson function is given by the equation

$$P(UVW) = \frac{1}{V_c} \sum_{\text{all } h, k, \ell} \sum_{\text{l}} |F|^2 \cos 2\pi (hU + kV + \ell W)$$

It requires knowledge only of the indices and  $|F|^2$  value for each diffracted beam. Because no phase information is required, only the relative positions of atoms will be

calculated.

P(UVW) is evaluated at every point in a region identical to the asymmetric unit. The value of P at each point corresponds to the sum of the appearances of the structure when the origin of the Patterson cell has been superimposed on every possible position in the structure. In other words, the structure is viewed from each atom in turn. A vector is drawn from this atom to every other atom in the structure. The height of the peak at the terminus of this vector is equal to the product of the atomic numbers of the atoms joined. The vectors are then superimposed at the origin of the Patterson map and their heights are summed.

The map is always centrosymmetric because interatomic vector B-A will always have the same magnitude and the opposite direction as vector A-B. If N atoms are contained in the unit cell, there are  $N^2$  interatomic vectors and  $(N^2-N)/2$  vectors in the Patterson map. Unless the number of atoms in the unit cell is very small, the number of Patterson vectors is so large that the complexity of the map limits its usefulness.

Nonetheless, the Patterson function is a powerful tool for analyzing structures containing heavy atoms. In these cases, the vector between the two heavy atoms produces a very intense peak which is readily recognizable. The co-ordinates of this peak can be related to the coordinates of this atom in the structure by examination of the symmetry

requirements of the space group of the unit cell.

The heavy atom will have a much larger atomic scattering factor than the lighter atoms and will probably dominate the phase angles for the entire structure. Hence, it may be possible to begin refinement of a trial structure even if no other atomic position is known.

## OBTAINING A TRIAL STRUCTURE BY DIRECT METHODS

If the species under study contains no heavy atom, interpretation of the Patterson map may be extremely difficult. In such cases, direct methods may be used to extract phase information from intensity data. Direct method calculations are simplified by using a normalized form of the structure factor,  $\mathbf{E}_{hk\ell}$ . Since atoms have finite size, the values of the scattering factors decrease with increasing  $\sin\theta$ . The E-values, on the other hand, are not dependent on  $\sin\theta$  because the atoms are treated as zero-dimensional points. For this reason, the E's are a good indication of the intensity of a reflection relative to other reflections of the same class rather than relative to all other reflections. A relatively intense high order reflection will have a large |E|, even though a rather small  $|F_0|$  may have been observed.

The value of E is given by:

$$|E_{hk\ell}|^2 = (K |F_{o,hk\ell}|^2)/\epsilon \sum_{j=1}^{N} g_j^2$$

where  $g_j$  is the spherically averaged scattering factor of the  $j^{\rm th}$  atom. If the molecule is known to contain well-characterized fragments, the molecular scattering factors of these groups can be used as g-values in the calculation of the E's.

The  $\varepsilon$  factor in the denominator depends only on symmetry, and compensates for the mutual cancellation of the expansion of  $|F_{hk\ell}|^2$  for certain classes of reflections.

The phases of a few reflections must be known if direct phasing methods are to be applied to other reflections. In a centrosymmetric space group, the phase angle must be either 0 or  $\pi$ , and the phase angle will determine only the sign of  $(F_{o,hkl})/|F_{o,hkl}|$ .

and the numerical values of all indices must be linearly independent.

Knowledge of these phases can be used to derive the phases of other reflections by the use of the relation-ship

$$[s(hkl)][s(h'k'l')][s(h-h',k-k',l-l')] \approx +1.$$

where "s" means "sign of" and " $\approx$ " means "is probably equal to", and the signs are multiplied such that (+)(+) = +, (+)(-) = (-)(+) = - and (-)(-) = +.

A more general form of this equation, the  $\Sigma_2$  relationship, is given by

$$s[E_{hk\ell}] \approx s[h, \xi, (E_{h,k,\ell})(E_{h,k,\ell})(E_{h,k,k,\ell})]$$

The summation is carried out over all vector pairs of known sign which form a closed triangle, a vector triplet, with hkl,  $e \cdot g \cdot$ ,

$$hk\ell = 8\overline{15}; h'k'\ell' = 9\overline{55}; h-h', k-k', \ell-\ell' = \overline{140}.$$

This relationship would be of little value if the probability of the correctness of the statement could not be evaluated. Fortunately, the probability of a positive phase is expressed by the formula:

$$P_{+hk\ell} = \frac{1}{2} + \frac{1}{2} \tanh[(\sigma_3/\sigma_2^{3/2})\alpha']$$

where  $\sigma_n = \sum_{j}^{Z_j} \Gamma_j (Z_j = \text{the atomic number of the } j^{\text{th}} \text{ atom})$ and  $\alpha' = |E_{hk\ell}| \sum_{h'k'\ell'}^{\Sigma} E_{hk\ell} E_{h-h',k-k',\ell-\ell'}$ .

The initial application of this method should be with reflections with large |E|, since these relationships will have the greatest probability and will participate in the greatest number of vector triplets.

Eventually, no more phases will be able to be assigned with confidence. In this case, new series can be begun by applying the  $\Sigma_2$  formula to reflections and assigning symbolic signs., <u>i.e.</u>, A, B, C, etc. At the end of the assignments, these symbolic signs must be evaluated as + or -.

Another limitation of the  $\Sigma_2$  formula arises in space groups lacking glide plane or screw axis symmetry. Unless some other means of generating negative signs exists, the  $\Sigma_2$  formula will produce only positive  $E_{hk\ell}$ 's. Current computing methods use the inventory of phases determined by high-probability  $\Sigma_2$  relationships as a basis for deriving other phases with the tangent formula:

$$\tan \phi_{a} = \frac{\sum_{b}^{E} E_{b} E_{a-b} \sin (\phi_{b} + \phi_{a-b})}{\sum_{b}^{E} E_{b} E_{a-b} \cos (\phi_{b} + \phi_{a-b})}$$

The tangent formula can also be used in phase assignment for

non-centrosymmetric systems, but its application is limited by the complexity of the calculations. An additional feature is the possibility of weighting the E's, so that those which are established with greater certainty have a greater effect in establishing  $\phi$ .

Remember, however, that the original origin-defining reflections were chosen semi-randomly, and phases were assigned arbitrarily. While it is possible to choose a "good" starting set of reflections, it is not always possible to identify the best starting set until the phase assignment is complete. Since different starting sets can be chosen, different phase sets will be derived. The best phase set can be determined by calculating figures of merit for each set.

One indicator of the plausibility of a phase set is the absolute figure of merit, given by M =  $(Z-Z_{\rm rand})/(Z_{\rm exp}-Z_{\rm rand})$ . The Z's are related to the probability weightings of the tangent formula. "Z" is derived from the weighted tangent formula and the absolute values of E's. All these are measurable quantities.  $Z_{\rm rand}$  is calculated for a random distribution of atoms, and  $Z_{\rm exp}$  is derived from the phase set assignment. For a correct phase set determination, Z will equal  $Z_{\rm exp}$  and the absolute figure of merit should equal one. In practice, correct sets usually have values in the range of 1.2 ± -0.2, but on occasion, a correct phase set has had an absolute figure of merit as low as 0.7.

The  $\psi_0$  figure of merit is completely independent of the tangent formula and is based solely on the values of E:

$$\psi_{o} = \sum_{a} \sum_{b} E_{b} E_{a-b}$$

The summation over b includes all terms available from the set of phases under consideration, while the summation over a includes reflections for which  $\mathbf{E}_a$  is approximately equal to zero. The expected value of  $\psi_O$  for a reliable phase set determination is small.

The  $\psi_{\text{O}}$  value is sensitive to molecular position.

The third figure of merit is the well known crystallographic "R index" calculated for E's rather than F's:

$$R = \sum_{a} \frac{|\langle E_a |_{obs} - |E_a |_{calc}|}{\sum_{a} |E_a |_{obs}}$$

It is frequently found that a combined figure of merit is more reliable than any one index. The combined figure of merit may be given by

$$C = \omega_1 \frac{M-M_{\min}}{M_{\max}-M_{\min}} + \omega_2 \frac{(\psi_0)_{\max}-\psi_0}{(\psi_0)_{\max}-(\psi_0)_{\min}} + \omega_3 \frac{R_{\max}-R}{R_{\max}-R_{\min}}$$

The  $\omega_j$ 's are weighting factors which are generally assumed to be unity. The maximum value of C is  $\omega_1 + \omega_2 + \omega_3$  and the phase set that has a figure of merit closest to this value deserves the greatest consideration.

Once phases have been reliably determined, the E's can be combined in a three dimensional Fourier synthesis in the same manner as the original F's, and a map of the synthesis can be used to establish initial positions for a trial structure.

# REFINEMENT OF THE TRIAL STRUCTURE

Once a trial structure has been identified, difference maps rather than electron density maps can be prepared. a difference map,  $|F_c|$  is calculated using the phase angle determined for the trial structure.  $|F_c|$  is then subtracted from  $|F_o|$ . A positive region indicates that more electron density is needed in that area, while negative areas are oversupplied with electron density by the trial structure. At early stages of the refinement, large peaks can indicate the proper positions for additional atoms, while a deep hole indicates that the atom at that position should probably be removed. A trench about an atomic position or a residual peak at an atomic position suggests that the temperature factor should be expanded or contracted. If the atomic site has a negative value but an adjacent area is positive, the input atom should probably be moved toward the peak.

Refinement of a structure may be carried out by alternating difference maps with least squares fitting sequences. The difference map indicates the region of the asymmetric unit where the trial structure is weak and suggests the type of adjustment needed. The least squares fit adjusts all variables to bring the calculated structure into the best possible agreement with the observed data. Although a low discrepancy index from the least squares calculation is one measure of the goodness of fit, a flat difference map is one of the best criteria of a good structure determination.

## CHAPTER II

# CRYSTAL STRUCTURE OF Na(C804H16)2C104

### INTRODUCTION

Since the early 1960's, there has been an upsurge of interest in the coordination complexes of macrocyclic compounds which may serve as models for certain naturally occurring bioinorganic systems. Macrocycles display an unusual affinity for the alkali and alkaline earth metal ions, and, indeed, the tendency for the oxygen atoms of crown ethers to coordinate to these species significantly exceeds their tendency to coordinate with transition metal ions. 1 Many different physicochemical techniques have been used to study the thermodynamics and kinetics of these species. 2 Nuclear magnetic resonance of alkali metal nuclei in solution has also provided some indirect knowledge of structure as well. 3-6 However, only direct crystallographic or electron microscope methods can unequivocably determine (a) the actual size of the cavity in the ligand; (b) conformational changes that occur in the complexation of anions of different sizes; (c) the geometry of coordination about the cation; and

(d) the effect of counterions on the packing of the unit

cell and the molecular geometry. Structural analysis can also complement the findings of other experimental techniques in regard to solvent-cation interaction and its effect on complexation.

It has been found that the configuration of a macrocyclic complex depends on the relative sizes of the complexed ion and the cavity. If the cavity is significantly larger than the ion, the ligand wraps around the ion, forming a three-dimensional structure. If the cavity is only slightly larger, the macrocycle will tend to pucker so that all of the hetero-atoms are coordinated. When the size of the hole is commensurate with the size of the metal ion, the coordination geometry will be planar. In cases where the cavity is smaller than the ion, the macrocycle retains its planar configuration, but the metal ion remains outside the plane of the ligand, and a sandwich structure is noted.

The formation of 2:1 "sandwich" compounds of Na<sup>+</sup> with 12-crown-4 has been confirmed by crystallographic studies describing structures containing several water molecules within the crystal lattice.<sup>7,8</sup> Although not complexed to the metal ion, the water molecules were found to form a hydrogen-bonded network that interacted with the anion. In contrast, this investigation describes an anhydrous species and reveals that the aqueous array is not necessary for the stability of the crystal, and seems to have little effect on the stability of the metal-crown complexation as

evidenced by the Na-O bond distances. Furthermore, cationanion interactions are not noted, even in the absence of water-anion interactions.

### EXPERIMENTAL

Crystals of Na(12-C-4)<sub>2</sub>ClO<sub>4</sub> were prepared by A. J. Smetana and provided by Professor A. I. Popov. The crystal selected was mounted on a glass fiber, aligned, and examined by the precession method to identify the space group and to determine preliminary lattice constants. The crystal was then moved to a Picker FACS-I automatic diffractometer for data collection. The data were reduced and standard deviations were calculated as a function of counting statistics. Details of crystal data and data collection are given in Table 1.

### STRUCTURE SOLUTION AND REFINEMENT

Initial information about the structure was obtained from MULTAN<sup>10</sup> and refinement was carried out using the entire system of Zalkin's programs<sup>11</sup> (MAGPIK, ABSORB, INCOR, ORDER2, FORDAP, LESQ, DISMAT, DISTAN, HFINDR, LSPLAN), ORTEP<sup>12</sup> and systems written and/or modified locally for use on the CDC6500 and the Cyber 750. ORFLS<sup>13</sup> was also used to refine the multiplicities of the partially occupied oxygen positions of the perchlorate, a group which is characteristically

Table 1. Crystal Data.

formula	C <sub>16</sub> H <sub>32</sub> O <sub>8</sub> Na <sup>+</sup> C1O <sub>4</sub> -		
formula weight	474.87		
space group	P2 <sub>1</sub> /a (#14) monoclinic		
systematic absences	$0\underline{k}\underline{1}, \underline{k} = 2\underline{n} + 1$		
	$\underline{h}00, \underline{h} = 2\underline{n} + 1$		
a, Å	15.420 ± .008		
b, Å	15.245 ± .010		
с, Å	9.650 ± .005		
β, deg.	92.13 ± .04		
Unit cell parameters were cal square fit of 18 strong refle 35° $\leq$ 20 $\leq$ 40°.	culated from a least- ections in the range		
v, Å <sup>3</sup>	2267.0		
D <sub>calc</sub> , g cm <sup>-1</sup>	1.391		
crystal description	.08 mm x .20 mm x .59 mm colorless parallelipiped mounted approximately along the normal to (110)		
radiation	Mo $K_{\alpha}$ , graphite mono-chromatized		
$\mu$ , cm <sup>-1</sup>	1.972		
scan type	0-20		
limit Bragg angle, deg	0 <u>&lt;</u> 2θ <u>&lt;</u> 50		
background count time, sec	20		
scan speed, deg in 2θ/min	2.0		
unique data, no.	4027		
unique data with $F > 3\sigma(F)$ , no.	1401		
F(000)	1008		
P - see Reference 9	0.02		
Q - see Reference 9	0		
scan range	.65° below $\alpha_1$ to 0.65° above $\alpha_2$		

disordered.

Initial positions for the atoms were as indicated by MULTAN. Two groups were input: the Na<sup>+</sup>-dicrown unit, and the perchlorate moiety. Thirty-two number sets were calculated, with Set 30 equivalent to Set 17. Set 18 was chosen as a basis for initial positioning of the atoms because it had the highest combined figure of merit.

	ABS FOM	PSI ZERO	RESID	COMBINED FOM
Rel. wts for combined FOM	1	1	1	•
Max. value Min. value Set 18	1.0154 .4705 1.0154	1.752 .867 .972	44.27 26.64 26.64	2.881 .8798 2.8811

The 23 atoms positioned by MULTAN at the most-likely distances and angles were input to LESQ and the positions of the remaining atoms were identified from difference maps. These were found to be close to the positions indicated by MULTAN. Refinement of the crown rings proceeded smoothly through a series of least squares calculations and difference maps. Hydrogen positions were postulated by HFINDR and were not refined, although thermal parameters were refined isotropically.

The structure was refined in sections: each ring with its hydrogens was treated separately and the perchlorate was refined either independently or with one ring at a time.

Refinement of the perchlorate moiety was complicated by the disorder of this anion. MULTAN initially indicated seven oxygen atoms surrounding the chlorine atom. "Bond lengths" from the central peak to these seven peaks varied from 1.14 Å to 1.83 Å, and "bond angles" centered on the "chlorine" position varied from  $34^{\circ}$  to  $164^{\circ}$ .

After isotropic refinement of the Cl atom, the Na atom and the carbon and oxygen atoms of both rings, the four highest peak positions were chosen as potential sites for perchlorate oxygen atoms. These were all located at a reasonable distance from the chlorine atom (Cl-O bond distance in  $\text{ClO}_4^-$  should be about 1.45 Å), but after refinement, the angles at the chlorine atom varied from 80.92° to 136.84°.

Shifting the origin and dividing the chlorine into first two and then three positions, and fixing the chlorine in a special position resulted in substantial increases in the residual.

Pairs of peaks with approximately correct bond distances and angles relative to the chlorine position were chosen from the difference map and additional positions for oxygen atoms were calculated by HFINDR. Several tetrahedra were constructed. Invariably, least squares refinements would indicate that geometric perfection was not compatible with reality.

Attempts were made to identify two tetrahedral units,

centered on either a single chlorine atom or distinct chlorine atoms. The occupation of each site was refined as a variable in ORFLS. Again, these efforts were not successful. As one peak was removed from the difference map, another would appear. When three oxygen atom positions suggested that another oxygen atom should be located at a fourth position, the ballooning thermal parameters and holes in the difference map revealed that the fourth position was not occupied as expected.

During these calculations, the atoms were refined isotropically in order to facilitate the separation of the distinct positions for each configuration. When anisotropic thermal parameters were used, the painstakingly separated locations merged. Finally, seven positions were left surrounding the chlorine atom, and these positions were close to those postulated by MULTAN.

A new series of refinements was begun by using the positions originally indicated by MULTAN. The final results of refinement, including the final shift to error ratios are listed in Table 2. Positional parameters with associated errors are listed in Table 3.

Atomic scattering factors were taken from the <u>International Tables for X-Ray Crystallography</u> as were the real and imaginary dispersion corrections. An anomalous scattering factor of zero was assumed for hydrogen.

The final difference Fourier map, while reflective of

Table 2. Final-cycle Refinement Indicators.

 $R_1 = (\Sigma | F_0 - F_c |) / \Sigma F_0) = .0712 \text{ for 1401 data with } F > 3\sigma(F)$ 

 $R_2 = \{\Sigma(\text{wtg x } |F_0 - F_c|^2)/\Sigma \text{wtg x } F_0^2\}^{1/2} = .0756 \text{ for } 4027 \text{ data}$ (including zero-weighted data)

Standard deviation of an observation of unit weight =

$$\{\Sigma(\text{wtg x } |F_o-F_c|^2)/N_{\text{ref}}-N_{\text{par}}\}^{1/2} = 2.409.$$

Shift-to-error ratios:

maximum (non-H) .28377 average (non-H) .03475

Final difference map:

max. positive density  $(e^{R-1}) = 1.484$ 

max. negative density  $(e^{\alpha-1}) = -1.672$ .

Table 3. Positional and Thermal Parameters with Associated ESD's.

			(A)	Sodium Dienown	Non-Hydror	eri Atoms			
Atom	x	у	2	B <sub>11</sub>	B <sub>22</sub>	F <sub>33</sub>	B <sub>12</sub>	P13	B <sub>23</sub>
Na Na	.0127(3)	.2478(5)	.4924(5)	4.2(6)	5.0(6)	3.2(7)	.0(5)	<i>-</i> .€(5)	3(6)
		.1040(4)	.3812(6)	4.4(3)			4(3)	-1.3(3)	-1.3(3)
011	.0369(3)	.062(3)	.326(9)	4.8(5)			4(4)	3(5)	-2.1(5)
c <sub>12</sub>	038(1) 115(1)	.081(1)	.410(2)	6.0(6)			6(5)	-1.8(5)	.5(5)
c <sub>13</sub>									
014	1294(4)	.1717(4)	.4251(6)	6.3(3)		4.5(3)	.0(3)	.0(2)	.0(3)
<sup>3</sup> 15	1755(9)	.212(1)	.310(2)	3.4(4)			1(4)	-1.2(4)	1.8(5)
$^{\mathrm{c}}$ 1 $\epsilon$	160(1)	.309(1)	.321(2)	4.6(5)	6.5(6)	6.1(6)	.7(5)	5(4)	.5(5)
017	0727(3)	.3328(4)	.3160(6)	5.2(3)	4.8(3)	4.5(3)	.3(3)	-1.1(2)	.1(3)
c18	042(1)	.335(1)	.182(1)	5.0(5)	6.3(6)	3.7(4)	.7(4)	6(4)	.3(4)
C19	.056(1)	.332(1)	.195(2)	8.1(6)	5.5(6)	3.7(4)	8(5)	.1(4)	1.2(4)
0110	.0905(3)	.2591(4)	.2724(6)	5.2(3)	6.8(4)	4.0(3)	1.3(3)	2(2)	5(3)
$c_{111}$	.093(1)	.193(1)	.193(2)	4.6(5)	11.2(9)	4.3(5)	.7(5)	.6(4)	-1.3(6)
$c_{112}$	.107(1)	.108(1)	.295(2)	4.2(5)	8.5(7)	5.4(5)	2(5)	.5(4)	-1.7(5)
021	.1637(4)	.2406(4)	.5922(6)	5.4(3)	6.0(4)	4.8(3)	1.7(3)	5(2)	3(3)
c22	.2006(7)	.3208(8)	.648(1)	5.1(5)			3(5)	-2.5(4)	9(5)
c <sub>23</sub>	.1659(7)	.3954(9)	.561(1)	4.9(5)			-3.0(5)	1.3(5)	-1.2(5)
024	.0689(4)		.5549(6)	6.0(3)		5.1(3)	1.3(3)	5(3)	-1.4(3)
C <sub>25</sub>	.0322(9)	.4349(9)	.669(1)	10.0(7)	4.8(6)	4.7(5)	1.7(5)	1.4(5)	9(4)
c <sub>26</sub>	0626(8)	.4131(9)	.674(1)	6.1(6)		8.2(7)	2.0(5)	-1.0(5)	-1.0(5)
027	0742(3)	.3190(4)	.€75€(5)	6.0(3)		3.9(3)	1.0(3)	.2(2)	.0(3)
c <sub>28</sub>	0638(8)	.287(1)	.811(1)	6.6(6)			1(5)	.2(4)	8(5)
C <sub>29</sub>	0533(8)	.189(1)	.794(1)	5.9(6)	11.2(8)	5.1(6)	-2.8(6)	2.0(5)	9(6)
0210	.0220(4)	.1680(4)	.7157(5)	5.7(3)	6.2(3)	3.9(3)	.6(3)	-1.6(2)	2(3)
C <sub>211</sub>	.1018(7)	.1719(9)	.790(1)	5.8(5)	6.5(6)	6.4(5)	1.2(5)	-2.9(4)	.4(5)
c <sub>212</sub>	.1703(7)	.170(1)	.686(1)	5.2(5)		5.8(5)	2.2(4)	.9(4)	.3(5)
A+	x	Y	Z Mul		lorate Atoms	ъ			B
Atom		•		t. B <sub>11</sub>	B <sub>22</sub>	B <sub>33</sub>	B <sub>12</sub>	B <sub>13</sub>	B <sub>23</sub>
Cl	.2477(4)	.4705(2) .00	33(8)	7.8(3)	9.8(2)	5.4(3)	- 4.2(2	)1(3	) 1.1(2)
031	.3396(8)	.474(1) .00	7(2) .716	(4) 7.6(7)	15.4(1.5)	11.3(1.2	.4(8)	2.3(8	) .9(9)
032	.24(2)	.49(2)14	(3) .486	(3) 17.3(2.2)	) 10.1(1.8)	8.0(1.5	) - 5.7(1.	.6) -6.3(1	.5) 1.2(1.3)
033	.179(5)	.484(4) .04	9(8) .404	(3) 41.0(8.9)	47.2(10.2	) 15.6(4.1	) -25.7(8	.0) 18. <b>9</b> (5	.0) .1(5.4)
034	.236(1)		9(2) .791		) 13.3(1.3)	8.4(1.0			) -2.8(9)
035	.243(2)	.557(2)04	2(3) .542	2(4) 23.9(2.6)	21.2(2.3)	22.2(3.1	) - 8.1(2	.6) -8.4(2	.5) 19.6(2.5)
036	.237(1)	.3779(7)01				9.0(8)	- 6.3(1	.0) 1.5(7	) -4.1(9)
037	.160(3)	.467(3)04	2(5) .309	13.0(2.9)	9.1(2.3)	8.8(2.3	) - 2.9(2	.0) -9.5(2	.5) 1.5(1.7
				(C) Hydro	ogen Atoms				
Atom	х	Y	Z	Biso	Atom	x	Y	Z	Biso
H <sub>12A</sub>	0268	0088	. 3254	7.8(2.3)	H <sub>22A</sub>	.2711	.3187	.6444	8.2(2.4)
H <sub>12B</sub>	.0506	.0846	.2201	9.2(7.8)	H <sub>22B</sub>	.1818	.3290	.7550	4.3(1.7)
H <sub>13A</sub>	1050	.0519	.5123	9.0(2.8)	H <sub>23A</sub>	.1892	. 3887	.4566	12.1(3.4)
		.0518	. 3584	3.5(1.6)	H <sub>23B</sub>	.1894	.4569	.6063	6.2(2.1)
H <sub>13B</sub>	1723	.0710			£ 3D	.0397			9.7(3.1)
<sup>Н</sup> 13В	1723 2446		.3153	4.5(1.7)	Hoea	.0391	.5059	.6633	3.1(3.1)
<sup>Н</sup> 13В Н <sub>15А</sub>	2446 1515	.1986 .1879	.3153 .2130	4.5(1.7) 4.1(1.6)	H <sub>25A</sub> H <sub>25B</sub>	.0655	.4106	.7632	4.8(1.8)
<sup>H</sup> 13B <sup>H</sup> 15A <sup>H</sup> 15B	2446	.1986 .1879	.2130 .4186	4.1(1.6) 14.6(4.0)	н <sub>25В</sub>				
H <sub>13B</sub> H <sub>15A</sub> H <sub>15B</sub> H <sub>16A</sub>	2446 1515	.1986 .1879 .3308	.2130	4.1(1.6) 14.6(4.0) 5.2(1.8)	H <sub>25B</sub> H <sub>26</sub> a	.0655	.4106	.7632	4.8(1.8)
H <sub>13B</sub> H <sub>15A</sub> H <sub>15B</sub> H <sub>16A</sub> H <sub>16B</sub>	2446 1515 1854	.1986 .1879 .3308 .3398	.2130 .4186	4.1(1.6) 14.6(4.0)	H <sub>25B</sub> H <sub>26</sub> a H <sub>26</sub> b H <sub>28</sub> a	.0655 0968	.4106 .4405	.7632 .5834	4.8(1.8) 17.2(5.1)
H13B H15A H15B H16A H16B H18A	2446 1515 1854 1960 0618 0653	.1986 .1879 .3308 .3398 .3954 .2788	.2130 .4186 .2349	4.1(1.6) 14.6(4.0) 5.2(1.8)	H <sub>25B</sub> H <sub>26</sub> a H <sub>26</sub> b H <sub>28</sub> a	.0655 0968 0888	.4106 .4405 .4410	.7632 .5834 .7679	4.8(1.8) 17.2(5.1) 6.1(2.1)
H13B H15A H15B H16A H16B H18A H18B	2446 1515 1854 1960 0618	.1986 .1879 .3308 .3398 .3954 .2788	.2130 .4186 .2349 .1305	4.1(1.6) 14.6(4.0) 5.2(1.8) 5.4(1.9)	H <sub>25B</sub> H <sub>26</sub> A H <sub>26</sub> B H <sub>28</sub> A H <sub>28</sub> B	.0655 0968 0888 1208	.4106 .4405 .4410 .3017	.7632 .5834 .7679 .8706	4.8(1.8) 17.2(5.1) 6.1(2.1) 7.6(2.4)
H13B H15A H15B H16A H16B H18A H18B	2446 1515 1854 1960 0618 0653	.1986 .1879 .3308 .3398 .3954 .2788	.2130 .4186 .2349 .1305 .1232	4.1(1.6) 14.6(4.0) 5.2(1.8) 5.4(1.9) 6.8(2.2)	H <sub>25B</sub> H <sub>26</sub> A H <sub>26</sub> B H <sub>28</sub> A H <sub>28</sub> B H <sub>29</sub> A	.0655 0968 0888 1208 0064	.4106 .4405 .4410 .3017 .3153	.7632 .5834 .7679 .8706 .8633	4.8(1.8) 17.2(5.1) 6.1(2.1) 7.6(2.4) 13.0(3.6)
H13B H15A H15B H16A H16B H18A H18B H19A	2446 1515 1854 1960 0618 0653	.1986 .1879 .3308 .3398 .3954 .2788 .3920	.2130 .4186 .2349 .1305 .1232 .2459	4.1(1.6) 14.6(4.0) 5.2(1.8) 5.4(1.9) 6.8(2.2) 14.5(3.7)	H <sub>25B</sub> H <sub>26A</sub> H <sub>26B</sub> H <sub>28A</sub> H <sub>28B</sub> H <sub>29A</sub> H <sub>29B</sub>	.0655 0968 0888 1208 0064 1110	.4106 .4405 .4410 .3017 .3153 .1635	.7632 .5834 .7679 .8706 .8633 .7397	4.8(1.8) 17.2(5.1) 6.1(2.1) 7.6(2.4) 13.0(3.6) 9.2(2.8)
H13B H15A H15B H16A H16B H18A H18B H19A H19F H111A	2446 1515 1854 1960 0618 0653 .0784	.1986 .1879 .3308 .3398 .3954 .2788 .3920 .3290	.2130 .4186 .2349 .1305 .1232 .2459	4.1(1.6) 14.6(4.0) 5.2(1.8) 5.4(1.9) 6.8(2.2) 14.5(3.7) 6.8(2.1)	H <sub>25B</sub> H <sub>26A</sub> H <sub>26B</sub> H <sub>28A</sub> H <sub>28B</sub> H <sub>29A</sub> H <sub>29B</sub> H <sub>211A</sub>	.0655 0968 0888 1208 0064 1110	.4106 .4405 .4410 .3017 .3153 .1635	.7632 .5834 .7679 .8706 .8633 .7397 .8963	4.8(1.8) 17.2(5.1) 6.1(2.1) 7.6(2.4) 13.0(3.6) 9.2(2.8) 6.7(2.1)
H13B H15A H15B H16A H16B H18A H18B H19A	2446 1515 1854 1960 0618 0653 .0784 .0807	.1986 .1879 .3308 .3398 .3954 .2788 .3920 .3220 .1863	.2130 .4186 .2349 .1305 .1232 .2459 .0909	4.1(1.6) 14.6(4.0) 5.2(1.8) 5.4(1.9) 6.8(2.2) 14.5(3.7) 6.8(2.1) 18.5(4.8)	H <sub>25B</sub> H <sub>26A</sub> H <sub>26B</sub> H <sub>28A</sub> H <sub>28B</sub> H <sub>29A</sub> H <sub>29B</sub>	.0655 0968 0888 1208 0064 1110 0465 .1086	.4106 .4405 .4410 .3017 .3153 .1635 .1593	.7632 .5834 .7679 .8706 .8633 .7397 .8963	4.8(1.8) 17.2(5.1) 6.1(2.1) 7.6(2.4) 13.0(3.6) 9.2(2.8) 6.7(2.1) 10.0(2.9)

the disorder in the perchlorate region, does not indicate either the absence or the gross mispositioning of atoms. The relatively high residual electron density in the area of the anion will be discussed later.

# RESULTS AND DISCUSSION

The sodium ion has a coordination number of eight and is coordinated in a sandwich configuration between the two 12C4 rings, being too large to fit into the cavity defined by the ring oxygen atoms (see Figure 6). The coordination about the cation may be described as a slightly distorted square antiprism. A few representative angles are tabulated below to indicate the extent of distortion.

ATOM 1	ATOM 2	ATOM 3	ANGLE	ANGLE OF IDEAL SQ. ANTIPRISM
014 014 017 014 014 0110	011 011 011 011 011	017 0110 0110 024 027 021	46.11° 91.77° 45.66° 71.79° 45.47° 62.00°	45.00° 90.00° 45.00° 70.46° 42.81° 63.91°
0110	011	0210	98.61°	100.49°

The square antiprismatic configuration allows the closest approach of the rings to reduce cavity size to fit the metal ion. Sodium-oxygen distances average 2.49(5) Å, in excellent agreement with the calculated distance of 2.54 Å  $(CN_{Na} = 8; CN_{O} = 3).^{16}$ 

Each set of four crown ether oxygen atoms coordinated

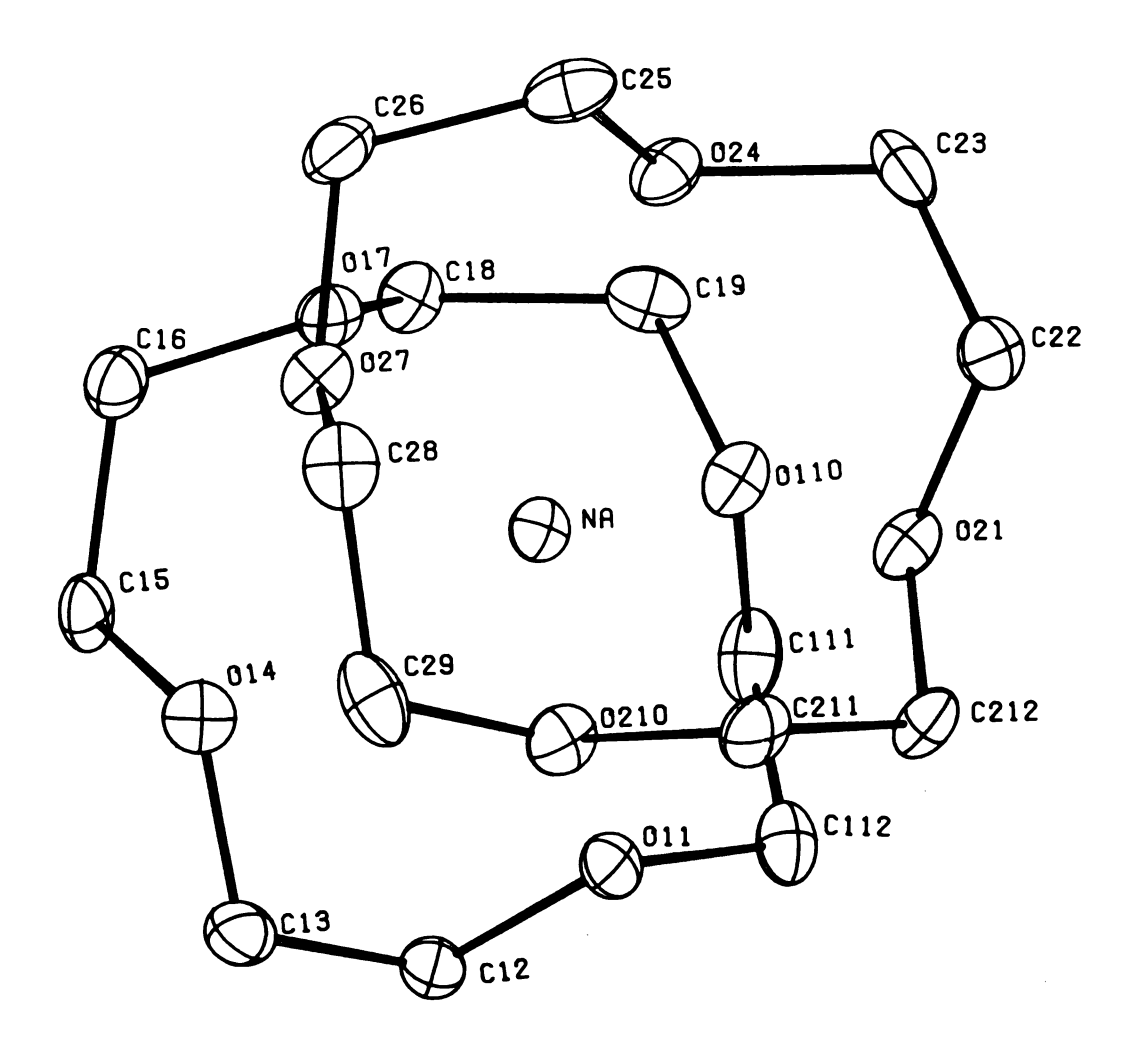


Figure 6. The sodium-dicrown unit illustrating 50% probability ellipsoids and the atom labeling scheme. H-atoms are designated by the number of the carbon atom to which they are attached.

to the cation is essentially planar. Displacements from planarity for both Ring 1 and Ring 2 are 0.01 Å. The Na<sup>+</sup> ion is centered between the planes at a distance of 1.53 Å from each. Within the ring, C-O and C-C distances average 1.40 Å and 1.50 Å, respectively, with C-O-C and O-C-C angles averaging 113.6° and 109.9°. Complete bond and angle information for the non-hydrogen atoms is listed in Table 4.

All values are in good agreement with published 12C4 structures.<sup>7,8</sup> The Na-O distances are slightly larger for 12C4-Na<sup>+</sup> complexes (2.49 Å) than for 15C5 complexes (2.39 Å)<sup>17</sup> but smaller than for 18C6 complexes (2.94 Å).<sup>18</sup> Because of the differences in coordination number and geometry, it would not be meaningful to correlate these bond distances to physical properties.

Hydrogen atoms were refined isotropically, but all other atoms were refined anisotropically. The degree of anisotropy among atoms of the same species varied but the variations do not appear to be related to proximity to the disordered anion.

The perchlorate groups form a layer with all chloride ions restricted to the region  $z=\pm.00334$ . The sodium-dicrown units form another layer, with the sodium ions falling at  $z=.5\pm.007564$ . Thus, each ion is approximately centered in a rectangular parallelepiped of counter ions. (The x- and y-dimensions of this coordination polyhedron are approximately equal. This follows directly from the fact

Table 4. Bond Distances and Angles.

C<sub>112</sub>-O<sub>11</sub>-C<sub>12</sub>

116.0 (32)

	rown Rings - D	istances (Å)	
0 <sub>11</sub> -c <sub>12</sub>	1.408 (39)	o <sub>21</sub> -c <sub>22</sub>	1.444 (6)
c <sub>12</sub> -c <sub>13</sub>	1.490 (54)	C <sub>22</sub> -C <sub>23</sub>	1.501 (13)
c <sub>13</sub> -o <sub>14</sub>	1.409 (16)	c <sub>23</sub> -0 <sub>24</sub>	1.495 (15)
0 <sub>14</sub> -C <sub>15</sub>	1.435 (18)	0 <sub>24</sub> -c <sub>25</sub>	1.386 (12)
c <sub>15</sub> -c <sub>16</sub>	1.486 (22)	C <sub>25</sub> -C <sub>26</sub>	1.502 (15)
c <sub>16</sub> -o <sub>17</sub>	1.401 (16)	c <sub>26</sub> -0 <sub>27</sub>	1.446 (19)
0 <sub>17</sub> -C <sub>18</sub>	1.394 (12)	0 <sub>27</sub> -c <sub>28</sub>	1.398 (11)
c <sub>18</sub> -c <sub>19</sub>	1.512 (22)	C <sub>28</sub> -C <sub>29</sub>	1.512 (16)
C <sub>19</sub> -O <sub>110</sub>	1.431 (17)	C <sub>29</sub> -O <sub>210</sub>	1.444 (17)
0 <sub>110</sub> -C <sub>111</sub>	1.392 (18)	0 <sub>210</sub> -C <sub>211</sub>	1.402 (13)
c <sub>111</sub> -c <sub>112</sub>	1.519 (24)	c <sub>211</sub> -c <sub>212</sub>	1.484 (12)
c <sub>112</sub> -o <sub>11</sub>	1.389 (18)	c <sub>212</sub> -0 <sub>21</sub>	1.408 (12)
C	rown Rings - A	ngles (Deg)	
° <sub>11</sub> -° <sub>12</sub> -° <sub>13</sub>	111.4 (50)	°21-°22-°23	107.8 (57)
c <sub>12</sub> -c <sub>13</sub> -o <sub>14</sub>	112.2 (21)	C <sub>22</sub> -C <sub>23</sub> -O <sub>24</sub>	111.5 (89)
C <sub>13</sub> -O <sub>14</sub> -C <sub>15</sub>	114.6 (11)	C <sub>23</sub> -O <sub>24</sub> -C <sub>25</sub>	114.2 (85)
0 <sub>14</sub> -C <sub>15</sub> -C <sub>16</sub>	107.0 (13)	0 <sub>24</sub> -c <sub>25</sub> -c <sub>26</sub>	111.0 (74)
C <sub>16</sub> -C <sub>16</sub> -O <sub>17</sub>	114.6 (12)	c <sub>25</sub> -c <sub>26</sub> -o <sub>27</sub>	109.9 (103)
c <sub>16</sub> -o <sub>17</sub> -c <sub>18</sub>	113.4 (11)	c <sub>26</sub> -0 <sub>27</sub> -c <sub>28</sub>	110.2 (87)
O <sub>17</sub> -C <sub>18</sub> -C <sub>19</sub>	107.1 (11)	o <sub>27</sub> -c <sub>28</sub> -c <sub>29</sub>	104.6 (73)
c <sub>18</sub> -c <sub>19</sub> -o <sub>110</sub>	114.7 (12)	c <sub>28</sub> -c <sub>29</sub> -o <sub>210</sub>	111.5 (107)
c <sub>19</sub> -o <sub>110</sub> -c <sub>111</sub>	112.2 (11)	c <sub>29</sub> -o <sub>210</sub> -c <sub>211</sub>	115.5 (84)
0 <sub>110</sub> -C <sub>111</sub> -C <sub>112</sub>	106.1 (14)	O <sub>210</sub> -C <sub>211</sub> -C <sub>212</sub>	106.6 (66)
C <sub>111</sub> -C <sub>112</sub> -O <sub>11</sub>	109.0 (14)	c <sub>211</sub> -c <sub>212</sub> -o <sub>21</sub>	112.6 (84)
C 0 C	116 0 (22)	C	112 0 (52)

C<sub>212</sub>-O<sub>21</sub>-C<sub>22</sub>

112.9 (52)

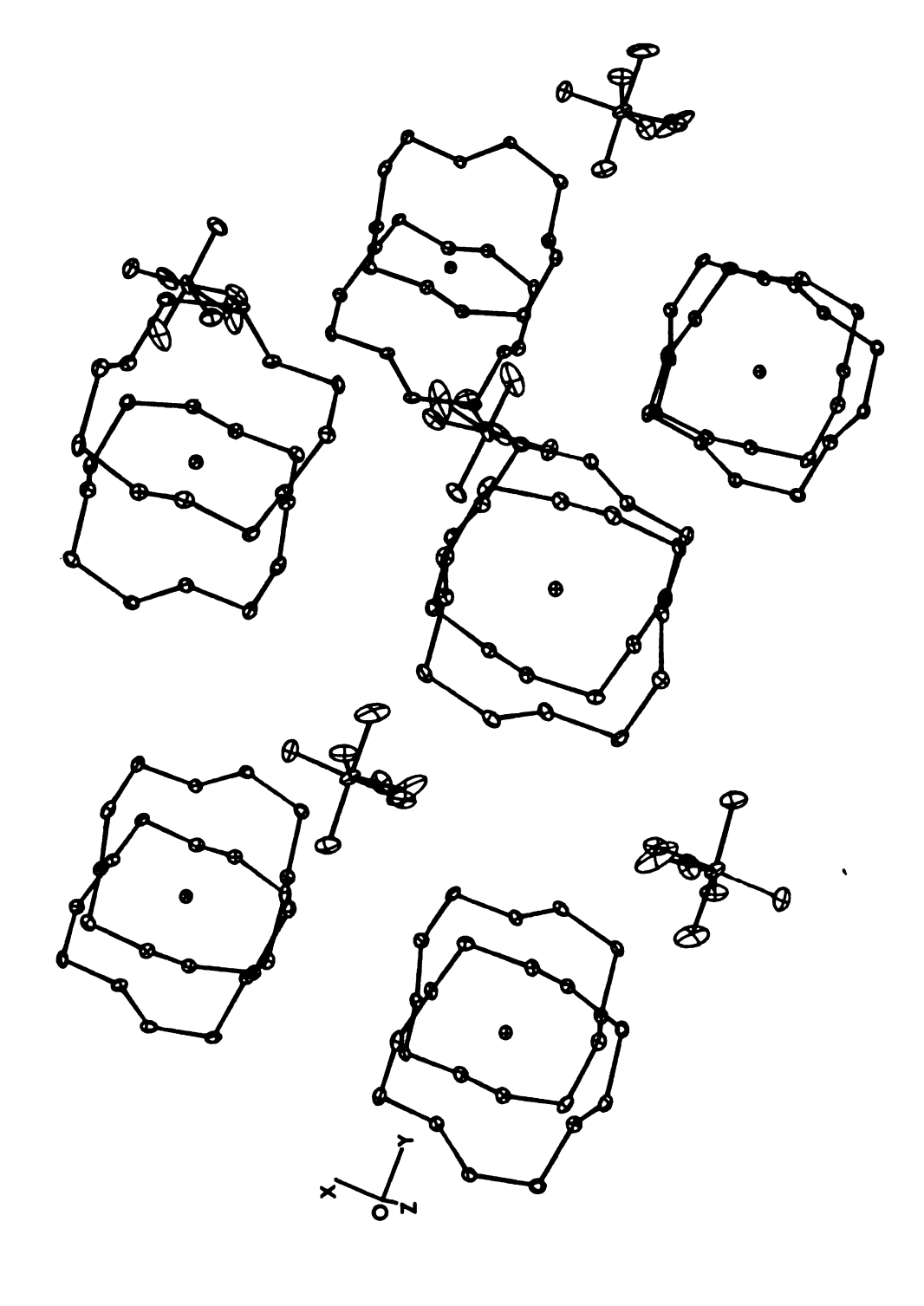
Table 4. Continued.

	Perchlorate Dis	tances (Å)	
c1-0 <sub>31</sub>	1.42 (1)	c1-0 <sub>35</sub>	1.39 (3)
C1-0 <sub>32</sub>	1.42 (29)	<sup>C1-0</sup> 36	1.43 (1)
C1-0 <sub>33</sub>	1.18 (8)	c1-0 <sub>37</sub>	1.41 (5)
c1-0 <sub>34</sub>	1.44 (2)		
	Perchlorate Ar	ngles (Deg)	
031-01-032	93.7 (125)	032-01-037	70.1 (126)
031-01-033	153.4 (37)	033-01-034	57.4 (38)
031-C1-034	97.5 (11)	0 <sub>33</sub> -c1-0 <sub>35</sub>	85.1 (33)
031-01-035	90.7 (14)	033-01-036	96.3 (31)
031-01-036	98.7 (9)	0 <sub>33</sub> -C1-0 <sub>37</sub>	42.0 (42)
0 <sub>31</sub> -c1-0 <sub>37</sub>	163.4 (22)	034-01-035	98.3 (14)
032-01-033	106.5 (13)	034-01-036	104.2 (10)
032-01-034	115.5 (124)	035-01-036	154.2 (15)
032-01-035	59.5 (124)	0 <sub>35</sub> -c1-0 <sub>37</sub>	84.2 (23)
032-01-036	95.8 (124)	036-C1-037	79.9 (20)

that the  $\underline{x}$ - and  $\underline{y}$ -dimensions of the cell are approximately equal.) (See Figure 7.) There does not appear to be any significant interaction either between the perchlorate and the sodium ions, or between the perchlorate and the dicrown unit as a whole. Further evidence for this lack of interaction may be found in the severe disorder of the perchlorate moiety. Perchlorate groups are frequently found to be disordered,  $19^{-24}$  but are often well-behaved when directly coordinated or hydrogen-bonded to another group. 25

In this case, seven partially-occupied oxygen positions surround the chlorine atom. (See Figure 8.) Major deviations from the expected tetrahedral angles and 1.45 Å bond lengths are noted. The actual values are given in Table 4. Neither the angular distribution, nor the superposition of the unit cell symmetry with the tetrahedral symmetry of the free ion, nor the pattern of occupancy supports the hypothesis that there are two separate but distinctly tetrahedral anion configurations.

Thermal parameters for the perchlorate oxygen atoms are extremely high and most are strongly anisotropic. The chlorine atom also deviated markedly from spherical electron distribution; however, attempts to resolve the positions with the largest thermal parameters into two or more positions failed. Similarly, attempts to position atoms in a less-distorted tetrahedral configuration always resulted in sharp disagreement with the observed distribution of



The packing in Na(12C4) $_2$ ClO $_4$ . Sodium ions are located at (0.5 ± 0.0076); chlorine atoms at (±0.0033). Figure 7.

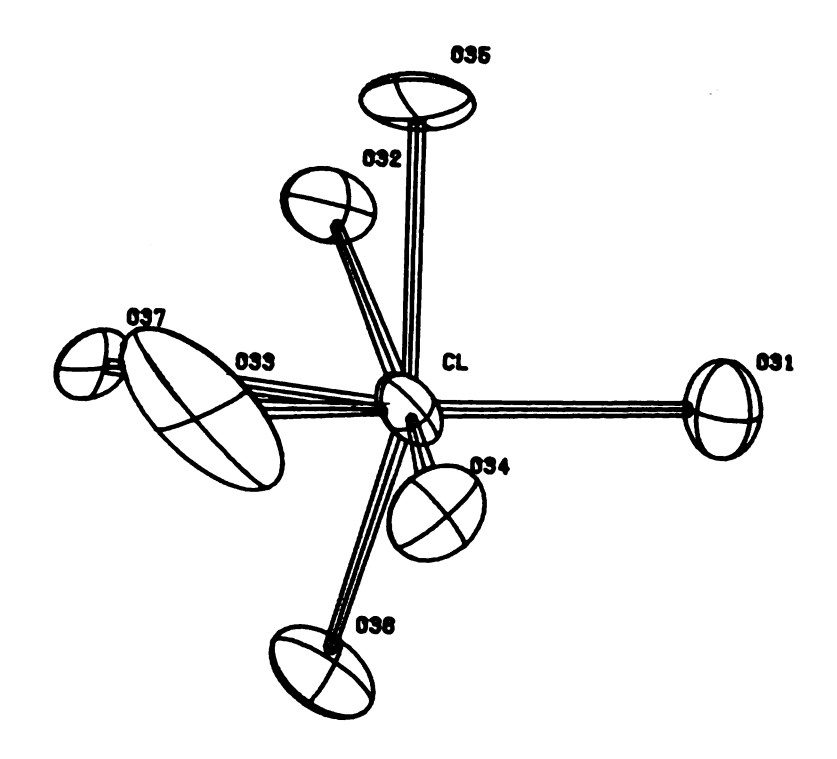


Figure 8. The severe distortion of the perchlorate moiety is illustrated by the presence of seven partially-occupied oxygen atom positions surrounding the chlorine atom.

electron density.

Another unusual feature of this analysis is the presence of the largest peak in the final difference Fourier map (1.48 eÅ<sup>-3</sup>) within an Angstrom of the chlorine position. Attempts to refine this residual peak as a partially-occupied chlorine center were unsuccessful. Since this "bonding distance" would place another atom within the radius of the Cl-O bonding sphere, it appears that this and other similar peaks are artifacts and do not represent real atomic positions. The ellipsoidal representation of electron density cannot reflect the directional bonding in the predominately covalent perchlorate. These peaks may correspond to the area enclosed in the ellipsoid, but outside the tetrahedron enclosing the bonding electrons of chlorine.

Perhaps the most meaningful conclusion is that the anion is nearly spherical and oriented semirandomly. In such a case, the excessively large thermal parameters and resultant unexpected bond lengths and angles may reflect an unsuccessful attempt to describe a curved surface of electron density as an ellipsoid. One may also speculate that the perchlorate anions exhibit long-range structural modulation, but that the intensity differences due to this ordering are too subtle to be detected by the diffractometer.

It is possible that certain anomalously large temperature factors of the ring atoms and the relatively high background noise on the difference map are artifacts of the

unresolved disorder about the perchlorate.

Sandwich structures of transition metals have been noted in which the cation with its aqueous (or anionic) coordination sphere was nestled between two large crown rings. 26,27 Alkali metal crown complexes can also show water-cation coordination if the metal is complexed to only one crown ether. 18 In dicomplexed species, aqueous layers may form infinite, two-dimensional networks between crown layers. 7,8 An unusual aspect of this structure is the absence of solvent molecules, a condition which permits the disorder of the perchlorate: the anion cannot be held in place by interaction with a solvent network, and it is prevented by the crown ligands from interacting with the cation.

#### CHAPTER III

# PREPARATION AND CRYSTAL STRUCTURE OF (Sr/Y)Cl<sub>2.05</sub> and (Sr/Yb)Cl<sub>2+x</sub>

#### INTRODUCTION

In the past 10 to 15 years, sustained interest in the atypical low valent and mixed valent metal halides has been evidenced by inorganic chemists and materials scientists alike. Since any metal with more than one oxidation state (or any mixture of metals with different oxidation states) has the potential to form a mixed valent compound, it is not surprising that a bewildering array of phases has been identified. The Ln-LnX<sub>3</sub> systems have proven especially rich in this type of chemistry. <sup>28-36</sup>

Although phase diagrams are available for a number of these halide systems, they are subject to repeated revisions as new phases are discovered. 37-41 Often, it is learned that the phases were hindered by kinetic rather than by thermodynamic barriers. Many phases exhibit extremely complex stoichiometry and their structural characterization has lagged far behind their identification.

Complex combining ratios are characteristic of the defect structures. These nonstoichiometric compounds

may maintain very similar physical properties even though their range of stable existence may span several atomic percent of one or more components. Current thinking in solid state chemistry now views these species not in terms of point defects and random, local distortions, but in terms of defect ordering, extending even to long range structural modulation. Short range ordering can also lead to a clustering of defects over a limited microdomain, while long range ordering results in a lattice superstructure which can be detected by the presence of weak X-ray reflections occurring in an orderly fashion. Neutron diffraction and electron microscopy are even more powerful methods for investigation of ordering.

The concept of long range ordering has led to the reevaluation of many structures with the specific intent of searching for defect ordering. Many systems, such as alloys, certain oxides, and many minerals, are now thought to be well-ordered compounds rather than solid solutions. Among the species subjected to reexamination are a number of fluorite-related structures, both anion-deficient and anion-excess, including oxides, oxide fluorides and other halides. Indeed, cubic solutions of the mineral yttrofluorite and related phases of the general type (Ca,Y, RE) $F_{2+x}$ , for  $0 \le x \le 0.5$ , can serve as representative examples of nonstoichiometry.

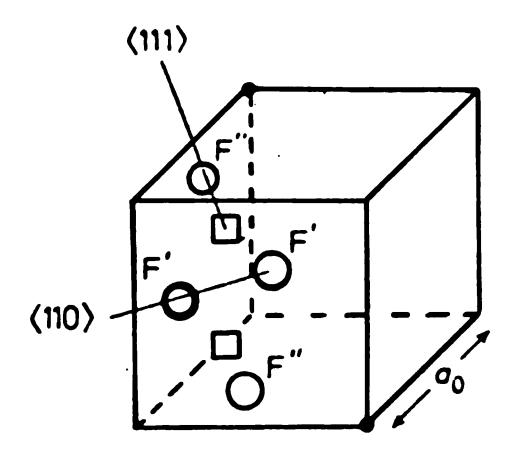
In the late 1950's, Brauer and Müller 43 determined

that at 500°C the solubility limit of LaCl<sub>3</sub> in SrCl<sub>2</sub> was about 22.5 mole percent. At this concentration, the fluorite structure of SrCl<sub>2</sub> was retained and cell parameters increased less than 0.03Å. They hypothesized that extra anions were accommodated interstitially at ½½ and the translations of this position. This model, however, does not address the problem of accommodating additional anions in a structure which is already closely packed.

In 1963, B. T. M. Willis published the results of a very precise neutron diffraction study of UO<sub>2+x</sub>, 44,45 another anion-excess derivative of the fluorite structure. For the composition UO<sub>2.13</sub>, he found that interstitial anions did not occupy the large cubic holes at ½½, ½00, 0½0 and 00½, but that the oxygen atoms located at ½½ and the symmetric equivalents of this position were shifted along <111> towards the center of the cell, and the "interstitial" oxygen atoms were shifted about 1 Å away from ½½ along <110>. A model consistent with the observed data requires that the defects be clustered if extremely short anion-anion distances are to be avoided.

Neutron diffraction studies of (Ca/Y)F<sub>2.10</sub> by Fender and coworkers 46-48 were also consistent with this model. (See Figure 9.)

The structure of YbCl<sub>2</sub> was once classified as a fluorite. Later, more precise measurements by Fishel<sup>49</sup> suggested that it would be described more exactly as an



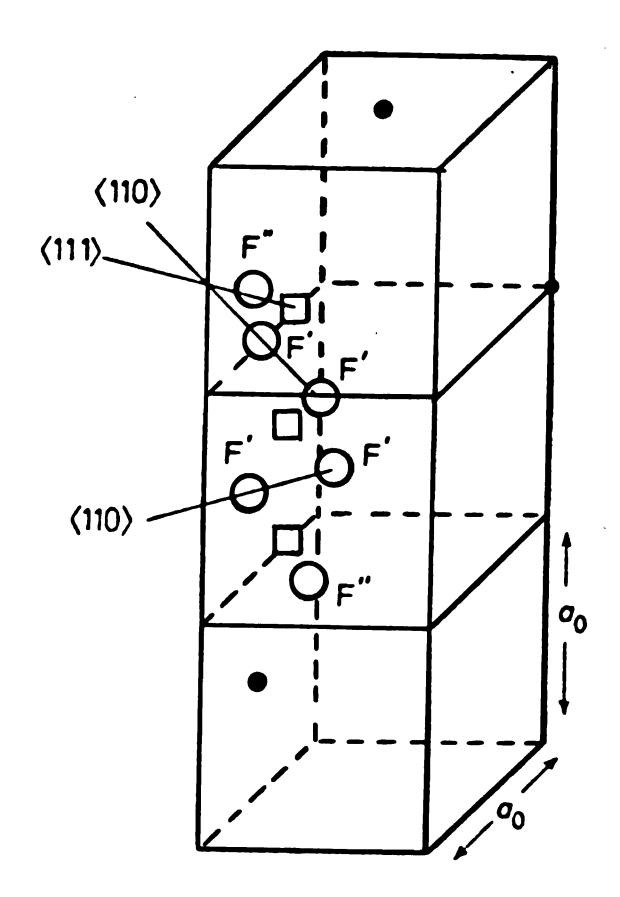


Figure 9. Clusters in (Ca/Y)F<sub>2+x</sub>. Above: 2:2:2 cluster, two F' ions, two F" ions and two normal ion vacancies. Below: an extended 3:4:2 cluster with two F" ions and 4 F' ions. •Y3+ positions assumed in calculating diffuse scattering. Redrawn from Reference 48.

orthorhombic CeSi structure: two orthorhombically distorted fluorite cells lined up in the **b** direction. Fishel also prepared a new ytterbium chloride and characterized it by X-ray powder diffraction. Chemical analysis established the formula as YbCl<sub>2.26</sub>.50

Subsequently, Lüke initiated a project to grow a single crystal of this phase and to determine its structure. When he was unable to prepare a single crystal suitable for X-ray analysis, he substituted a trivalent heteroion for Yb(III). The structure solved was for the compound  ${\rm Yb_5ErCl_{13}}^{51}$  and proved to be isostructural with Fishel's "YbCl<sub>2.26</sub>". The difference in reported composition is ascribed to inaccurate chemical analysis.

 ${
m Yb}_6{
m Cl}_{13}$  can be described as another ordered and regular variant of the fluorite structure. Six fluorite units lined up in the **b** direction are required to accommodate the additional anions in  ${
m Yb}_6{
m Cl}_{13}$ . This compound may be regarded as a Vernier structure with overlaid hexagonal and rectangular networks. It is one member of a homologous series of structures of composition  ${
m M}_n{
m X}_{2n+1}$  formed by the rare earth halides and certain mixtures of the rare earth and alkaline earth halides.

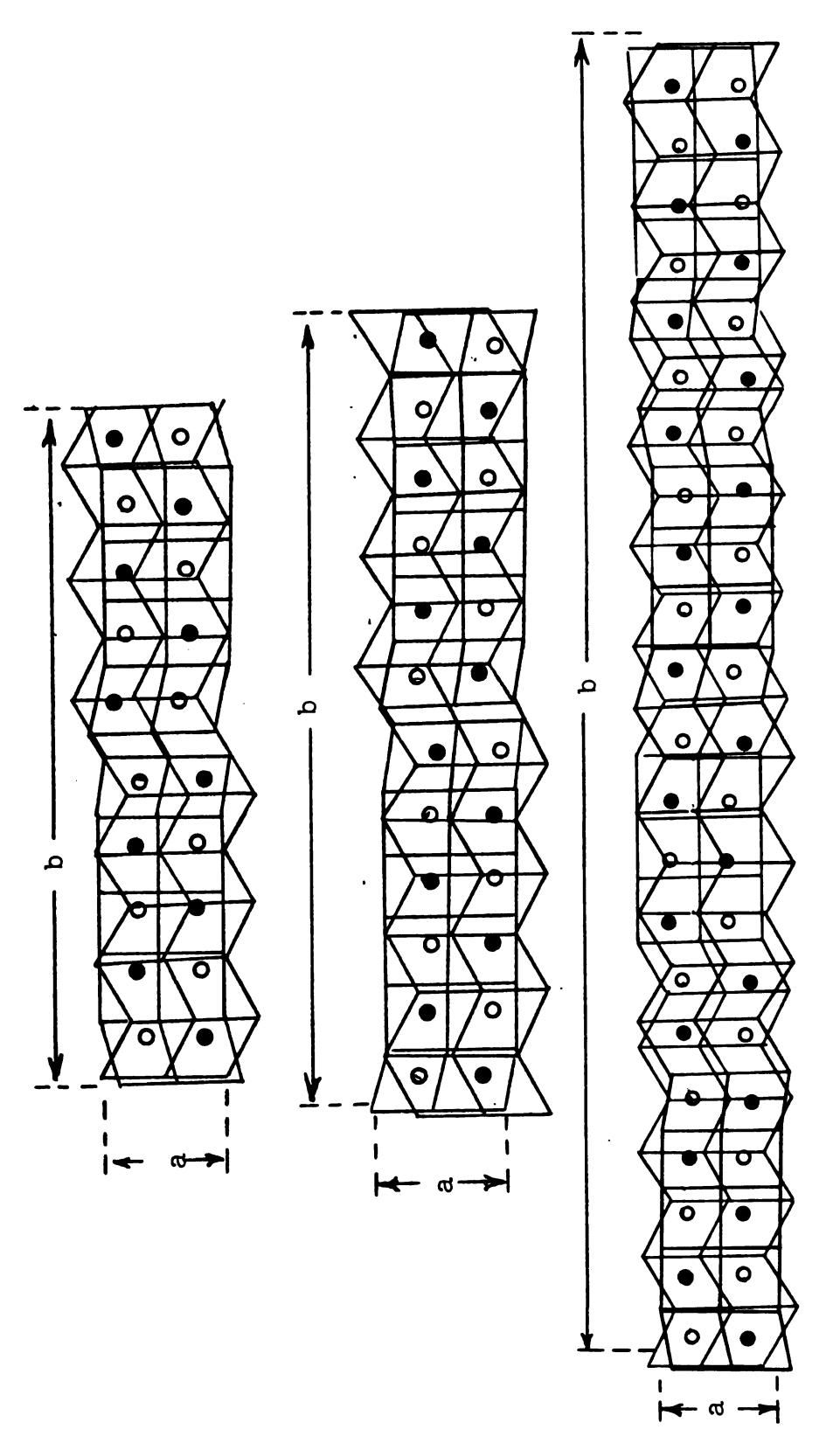
Lüke's work was beautifully complemented by that of Bärnighausen who simultaneously solved the structure of  $\mathrm{Dy}_5\mathrm{Cl}_{11}$  and the isostructural  $\mathrm{Sr}_4\mathrm{DyCl}_{11}$ . The ordering of this last compound appears to be in direct conflict

with the Brauer-Müller results.

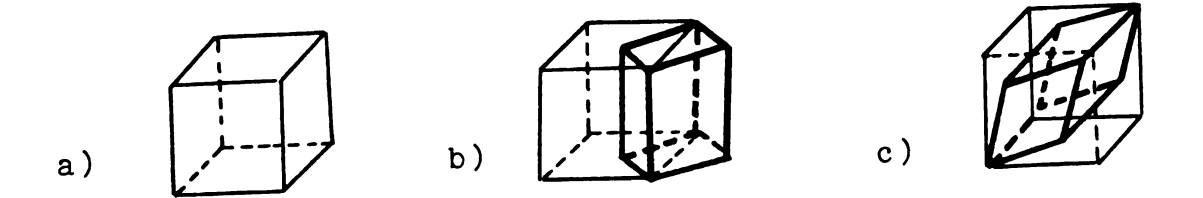
Vernier structures have now been identified for other elements. In the  ${}^{M}_{5}{}^{X}_{11}$  series we find  ${}^{H}_{0}{}^{C}_{11}$ ,  ${}^{53}$  Sm $_{5}{}^{B}_{11}$ ,  ${}^{54}$  Cf $_{4}$ GdCl $_{11}$  and Cf $_{4}$ GdBr $_{11}$ ,  ${}^{55}$  while the  ${}^{M}_{6}{}^{X}_{13}$  series is represented by Dy $_{6}{}^{C}_{13}$ ,  ${}^{52}$  Sm $_{6}{}^{B}_{13}$ ,  ${}^{54}$  and possibly Sm $_{5}{}^{Y}_{B}_{13}$ . In addition, the phase Sm $_{11}{}^{B}_{24}$  appears to be an intergrowth of the 5/11 and 6/13 phases. (See Figure 10.)

Greis and co-workers have employed a systematic indexing of superstructure lines of powder diffraction patterns to examine the crystal chemistry of yttrofluorite species in the systems  $\text{LnF}_2\text{-LnF}_3$  (Ln=Sm,Eu,Tm,Yb) and  $\text{MF}_2\text{-REF}_3$  (M=Ca,Sr,Ba; RE=Y,La,Sm,Eu,Tm,Yb).57-63 They have identified two different series of homologous compounds,  $\text{M}_m\text{F}_{2m+5}$  and  $\text{M}_m\text{F}_{2m+6}$ . For the composition region where m = 13, 14, 15 or 19, both tetragonal and rhombohedral structures were found (See Figure 11) and cationic ordering was present.

Anionic ordering is known to exist in the fluorine-rich rhombohedral phases which Greis designates as  $\beta$  and  $\gamma$ . In these species, anionic clustering occurs as a result of cation ordering. At intermediate fluorine concentrations, anion clusters appear to be built up from both interstitial and shifted fluorite-structure anions. At fluorine concentrations where cubic symmetry prevails the microdomains are too small to be revealed by X-ray diffraction, but Greis believes that partial ordering occurs.



The 5/11, 6/13 and 11/24 Vernier structures. Figure 10.



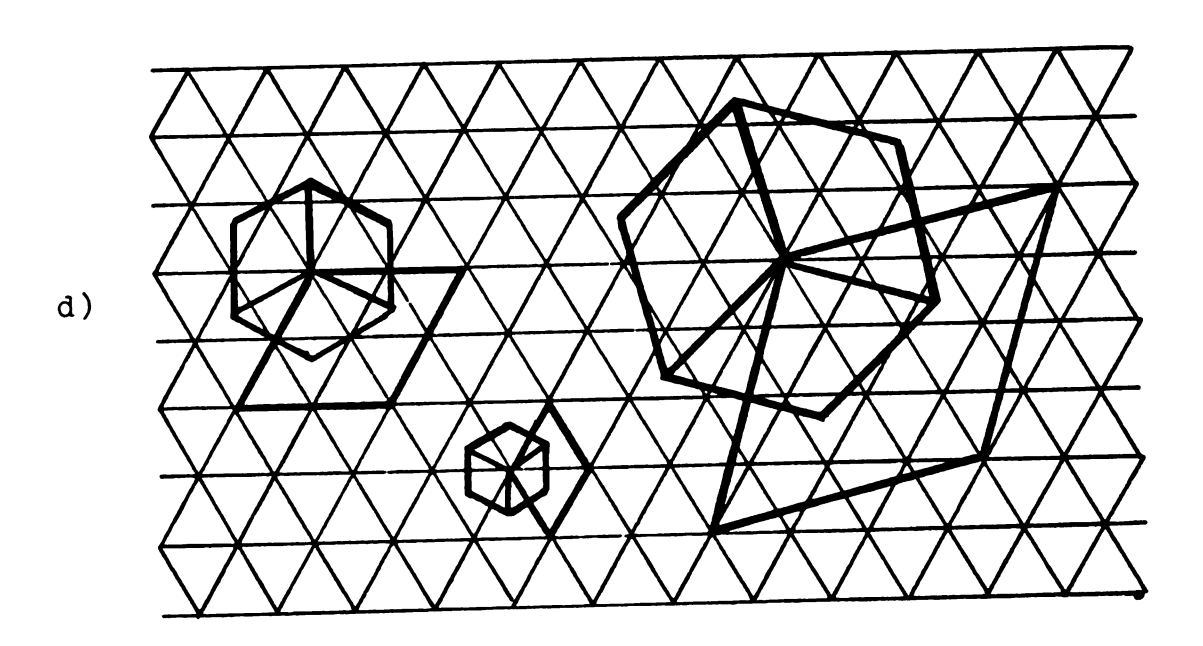


Figure 11. a) The cubic fluorite unit cell. b) Tetragonal basis cell derived from the fluorite cell. c)
Rhombohedral basis cell derived from fluorite unit cell. d) The rhombohedral basis cell and suggested superstructures. (Figure redrawn from Reference 57.)

The Russian literature reports europium  $^{64}$ ,  $^{65}$  and samarium  $^{66}$  chlorides as having the Vernier-type  $^{M}$ <sub>n</sub> $^{X}$ <sub>2n+1</sub> stoichiometry and also reports mixed metal species containing  $^{SrCl}$ <sub>2</sub> and  $^{BaCl}$ <sub>2</sub> with trivalent rare earth ions.  $^{66}$  Unfortunately, no structural details are available.

Fedorov and co-workers  $^{68}$  have identified fluoritederived structures in the  ${\rm CaF_2-LnF_3}$  systems for Ln=Y, Ho-Lu. These phases have an idealized composition  ${\rm Ca_8Ln_5F_{31}}$ , the same  ${\rm M_mF_{2m+5}}$  composition as that described by Greis, but have been indexed on the basis of pseudocubic unit cell parameters with each axis approximately 13 times that of  ${\rm CaF_2}$ . More recently, phase diagrams have been investigated for the systems  ${\rm SrF_2-LnF_3}$  for Ln=Y, La-Nd, Sm, Gd-Lu. The phases identified have had either fluorite, fluorite-derived, or tysonite (LaF3) structures.

To date, only Lüke and Bäringhausen have studied the rare earth Vernier phases through the analysis of single crystals: all structures except Yb5ErCl13 and Dy5Cl11 have been solved by refinement of powder diffraction data. Because of the similarity of electron density of Yb(II) and Er(III), not to mention the similarity of Dy(II) and Dy(III), the site symmetry of the +2 and +3 ions has never been specified crystallographically. In addition, no studies of either single crystal or powder diffraction data have indicated whether these structures are stable in the complete absence of f-block elements. It is also of

interest to investigate the limits of cell size: what are the limits of "n" in  $^{M}_{n}X_{2n+1}$  when the Vernier structure is maintained?

As initially planned, the objectives of this research were to grow single crystals of Vernier compounds and to solve their structures to determine:

- i) whether f-block metals are necessary to stabilize the Vernier structure;
- ii) what, if any, is the site symmetry of the metal coordination? What are the specific locations of the +2 and +3 ions?

Many combinations of divalent and trivalent ions were proposed on the basis of radius ratios in known Vernier structures. However, in view of the overwhelming difficulty in identifying crystallographically suitable crystals, investigation was eventually limited to combinations containing  $SrCl_2$ , a compound noted for its ability to accommodate high concentrations of chemical defects, and form high quality crystals even in the presence of heteroion dopants. Furthermore,  $Sr_4DyCl_{11}$  exists as a precedent for the incorporation of Sr(II) into the Vernier structure. The similarity of size of Y(III) to that of Dy(III) (at CN=VIII,  $R_{Y(III)}=1.019 \mbox{Å}$ ;  $R_{Dy}(III)=1.027 \mbox{Å} \mbox{\rotate}^{70}$  suggested YCl<sub>3</sub> as a component worth investigating. A mixture of  $SrCl_2$  and  $YCl_3$  would address the first objective. It would be reasonable to anticipate the formation of

 $\mathrm{Sr_{n-1}^{YCl}_{2n+1}}$ , analogous to  $\mathrm{Sr_{4}DyCl}_{11}$ . A mixture of  $\mathrm{SrCl}_{2}$  and  $\mathrm{YbCl}_{3}$  was chosen to elucidate the site symmetry and ordering of the cations. It was hoped that substitution of  $\mathrm{Sr}(\mathrm{II})$  for  $\mathrm{Yb}(\mathrm{II})$  would aid in the formation of a crystallographically suitable crystal in the same manner as the substitution of  $\mathrm{Er}(\mathrm{III})$  for  $\mathrm{Yb}(\mathrm{III})$ .

Although a high quality crystal of  $(Sr/Y)Cl_{2+x}$  was identified, it proved to have a different structure. The research project completed is not the project originally envisioned. The question of the necessity of f-block elements in the Vernier structures has not yet been addressed: absence of proof is not proof of absence.

The structure of  $(Sr/Y)Cl_{2.05}$  appears to be related to the cluster model of  $UO_{2.13}$  proposed by Willis. This is the first Willis-cluster chloride described.

#### EXPERIMENTAL

## Preparation of (Sr/Y)Cl<sub>2+x</sub> and (Sr/Yb)Cl<sub>2+x</sub>

The rare earth halides and, to a lesser extent,  $SrCl_2$  are hygroscopic. Heating the hydrated species leads to the formation of oxide halides rather than to simple dehydration. To avoid oxide halide formation, a modification of the method of Taylor and Carter, dehydration of hydrated chlorides in the presence of excess  $NH_4Cl$ , was used to prepare the starting materials.

 $Yb_2O_3$  and  $NH_4Cl$  were dissolved in 6  $\underline{N}$  hydrochloric acid. The resultant hydrated  $YbCl_3$  and coprecipitated  $NH_4Cl$  were placed in a glass bulb attached to a high vacuum line, and the water and  $NH_4Cl$  were eliminated by heating to about  $320^{\circ}C$  overnight under dynamic vacuum. After dehydration was complete, the glass bulb was cut free with a torch and opened only in an Argon atmosphere glove box.

Anhydrous  $SrCl_2$  was prepared similarly from  $Sr(OH)_2$ . The overall reactions are:

$$Yb_2O_3 + 6 NH_4C1 \xrightarrow{6N HC1} 2 YbCl_3 + 3 H_2O(g) + 6 NH_3(g)$$

$$Sr(OH)_2 + 2 NH_4C1 \xrightarrow{6N HC1} SrCl_2 + 2 H_2O(g) + 2 NH_3(g)$$

The YCl<sub>3</sub> was used as purchased from Research Inorganic Chemicals.

Since the major interfering impurities were expected to be hydrolysis products, X-ray powder diffraction was used to check for purity. Powder patterns include a characteristic grouping of additional lines when hydrolysis products are present even in low concentrations.

The mixed valent chlorides were prepared by high temperature reactions. Samples containing 5:1 molar ratios of SrCl<sub>2</sub> and YCl<sub>3</sub> or YbCl<sub>3</sub> were sealed in evacuated outgassed quartz ampoules which were placed in a tube furnace and heated to about 900°C for two hours to insure complete melting. Thereafter, crystals grew from the melt as the

temperature was automatically lowered at an average rate of 1.5° per hour. After the samples were annealed at 400°C for several hours or overnight, the furnace was shut off and allowed to cool to room temperature.

The ampoules were opened in the glove box. In all cases, the sample had formed a hard, compact mass which adhered to the glass. As great a portion of the contents as possible was chipped free and lightly ground in a mortar. The crushed material was transferred to a Schlenk tube fitted with an optical window and removed to the outside of the glove box where the sample was protected by flowing Argon and examined under a microscope. Individual crystals were selected and sealed into Lindemann capillaries. (See Figure 12.)

The selected crystals were subjected to microscopic examination under polarized light. Those which did not exhibit birefringence were examined by the precession method to determine the approximate cell parameters and the space group. Particular attention was directed to searching for weak reflections indicative of superstructure.

It was necessary to examine many crystals before one of suitable quality was identified. Eventually, a rather extensive collection of photographs of (Sr/Y)Cl<sub>2+x</sub> was acquired. The habit of these crystals was such that the preferred orientation in the capillary characteristically led to a zero-layer photograph showing an apparent six-fold

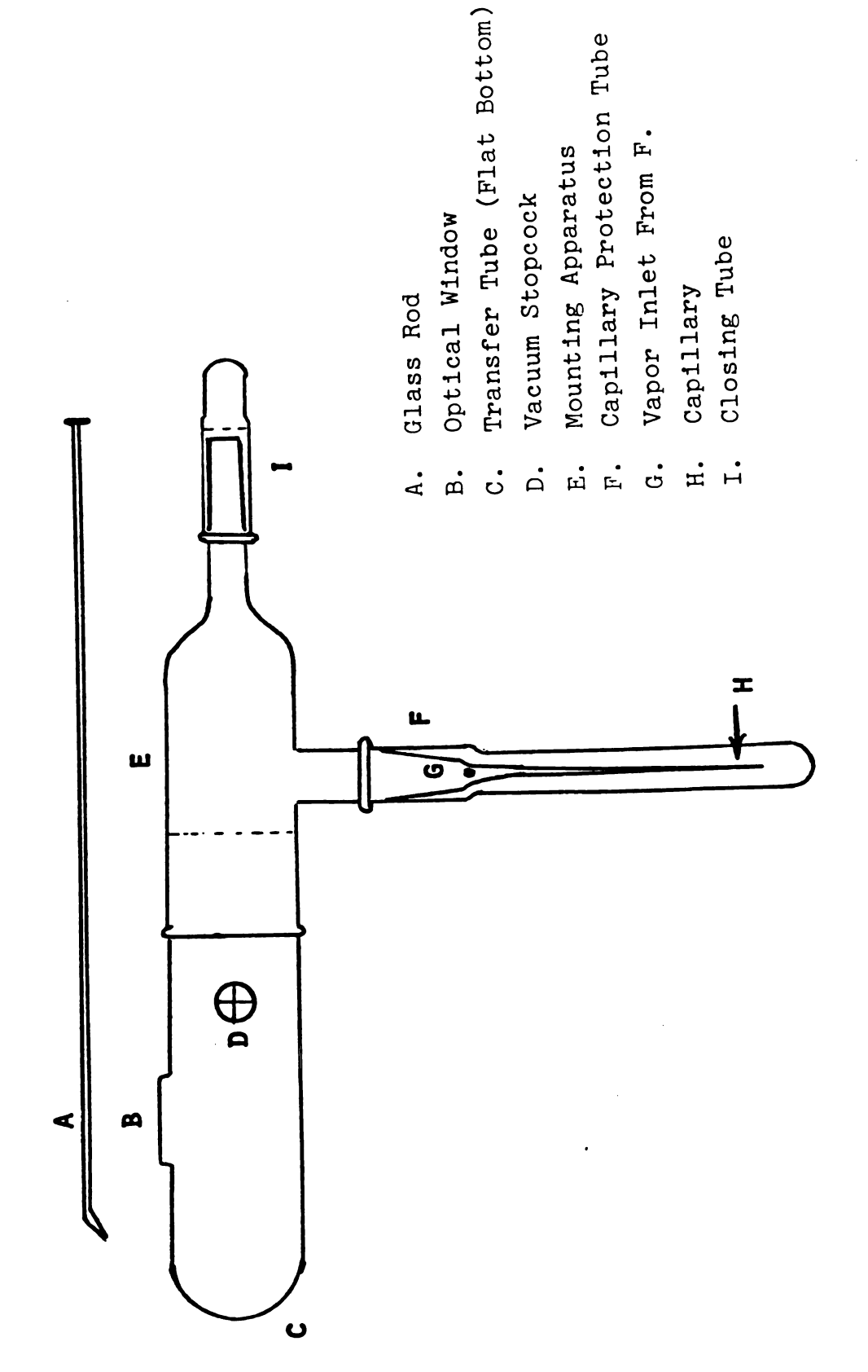


Figure 12. Crystal mounting apparatus.

axis, and a perpendicular zero-layer showing an unusual pattern of triplets separated by a row of reflections of greatly reduced intensity. (See Figure 13.) Camera geometry prevented me from obtaining a complete set of upper layer photographs.

After calculation of cell parameters the crystal was referred to Dr. Donald Ward for data collection.

### Data Collection and Refinement of (Sr/Y)Cl2+x

Crystal data are listed in Table 5.

Volume calculations based on  $SrCl_2$  and  $YCl_3$  indicate that the chloride anion when associated with cation occupies about 43 or 44 ų. The calculated cell volume of 252.8 ų should hold about 5.7 anions. Possible formulas would be  $SrYCl_5$ , or, if the cell were doubled,  $Sr_4YCl_{11}$ . Unfortunately, there was no basis for enlarging the unit cell: a search had been made along the 00ℓ and 0k0 axes for evidence of superstructure, but none was found.

The data were reduced and standard deviations were calculated as a function of counting statistics. 9 Refinement was attempted using the entire system of Zalkin's programs (MAGPIK, ABSOR, INCOR, ORDER2, FORDAP, LESQ, DISMAT, DISTAN) as modified for local use. 11 Eventually refinement was accomplished using ORFLS. 13

Work was begun using an unmerged data set because ORDER was not operational at the time. An analytic absorption

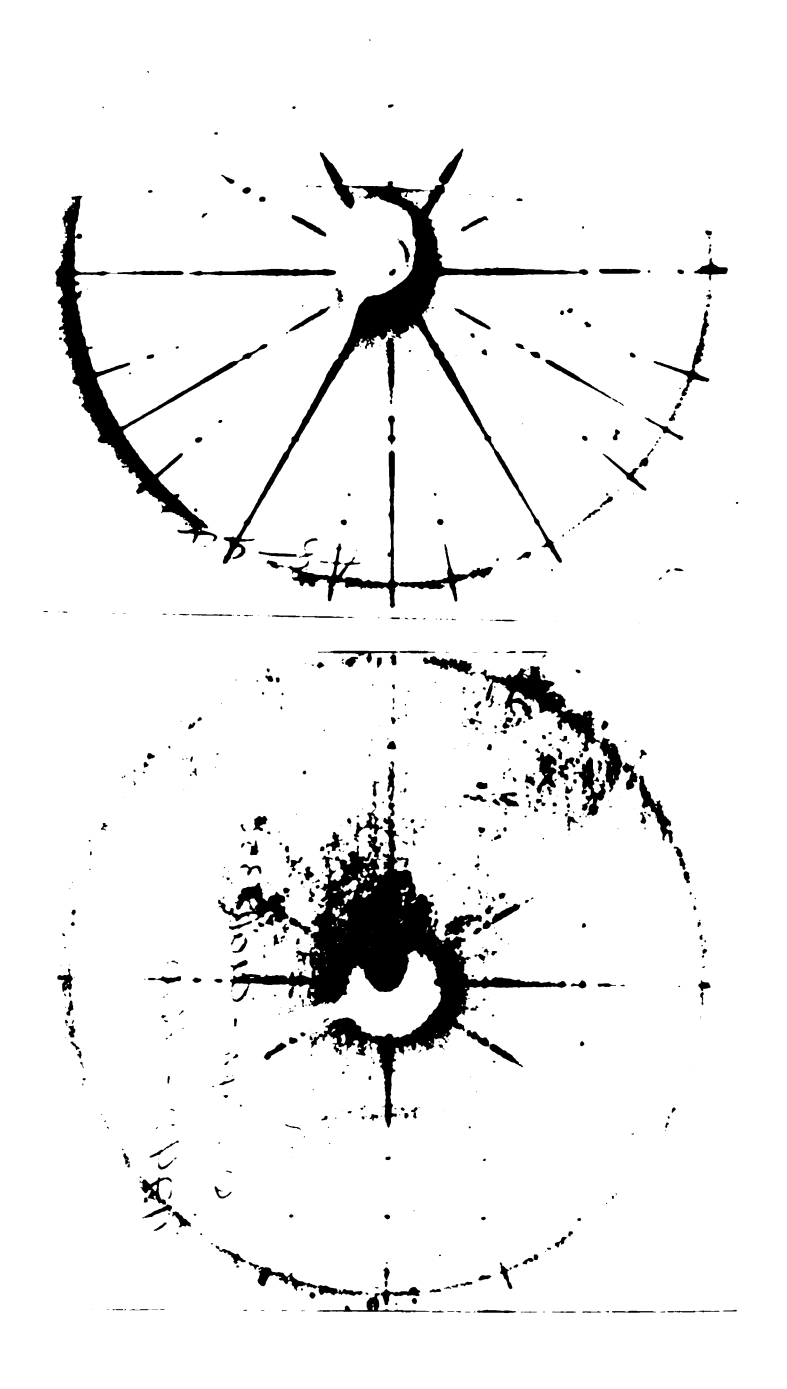


Figure 13. Zero layer precession photographs of (Sr/Y)-  $\text{Cl}_{2+x}$ . Above: an apparent six-fold axis. Below: a pattern of triplets.

Table 5. Crystal Data for (Sr/Y)Cl<sub>2.05</sub>, First Data Collection.

formula	(Sr/Y)Cl <sub>2+x</sub> , x unknown
space group	R3 or $R\overline{3}$
systematic absences	-h+k+l≠3n (hexagonal axes)
unit cell, hexagonal axes:	
a,b,Å	4.923(1)
c,Å	12.046(5)
γ,deg	120.0
Unit cell parameters were calcufit of 18 strong reflections in	
v, Å <sup>3</sup>	252.8
crystal description	colorless, approximately 0.5 x 0.77 x 0.84 mm
radiation	Mo $K_{\alpha}$ , graphite monochromatized
$\mu$ , cm <sup>-1</sup>	157
scan type	θ-2θ
limit Bragg angle, deg	0 <u>&lt;</u> 20 <u>&lt;</u> 60
background count time	20 sec.
scan speed, deg in $2\theta/\min$	2.0
unique data, no.	503
unique data with $F^2 > 2\sigma(F)$ , no.	477
P - See Reference 9	0.02
Q - see Reference 9	0
scan range	1.0° below $\alpha_1$ to 1.0°
	above $\alpha_2$

correction was applied to the raw data. The path length on which this correction was based was calculated from measurements of the crystal through the protective capillary.

Preliminary ion positions were determined from a Patterson synthesis and were reasonable in the context of the space group chosen. Refinement was begun with a succession of least squares calculations and difference maps. With a metal ion located at approximately 0 0 3/8 and a chloride at approximately 0 0 7/8, the structure refined quickly to R = 0.1716 and  $R_{w} = 0.1951$ . (See Table 6.) Unfortunately, attempts to add more anions to the structure resulted in higher residuals and unacceptable bond distances. Without additional anions, the cation: anion ratio was 1:1 with both species located in special positions of the type 00z. Placing a chloride ion in a general position, however, would result in a cation:anion ratio of 1:4. Stoichiometry could be satisfied by placing anions at selected special positions, but these were not consistent with either Patterson synthesis or bond length requirements.

This impasse suggested that either the wrong unit cell or the wrong space group had been chosen. Since ORDER was operational again, the data set was merged in rhombohedral symmetry. A comparison of supposedly equivalent reflections revealed that their intensities were drastically different. If the correct space group were chosen and if

Table 6. Results of Rhombohedral Refinement Positional and Thermal Parameters with Associated ESD's.

Atom	x	У	Z	В
Sr	.00	.00	.3729(2)	.91(7)
Cl	.00	.00	.830 (3)	10.1(7)

$$R_1 = (\Sigma |F_0 - F_c|)/\Sigma F_0) = .1716$$
 for 477 data with  $F^2$ 

$$2\sigma (F)^2$$

$$R_2 = \{ \Sigma(\text{wtg x } | F_0 x F_c |^2) / \Sigma \text{wtg x } F_0^2 \}^{1/2} = .1951.$$

Shift-to-error ratios: maximum .355

average .129

#### Final difference map:

max. positive density:  $(e^{X-3}) = 53.3$ 

max. negative density:  $(eA^{-3}) = -3.0$ 

the data had been adequately corrected for absorption, the intersities of these reflections should be similar. Because an analytic absorption correction had already been applied to the data, it appeared that the wrong unit cell and hence the wrong space group had been chosen.

Precession photographs of (Sr/Y)Cl<sub>2+x</sub> were reexamined for evidence of a different unit cell. Both orthorhombic and monoclinic cells were tentatively identified and the indices of the reflections were transformed by matrix multiplication. Neither transformation was pursued, since merger of the data set in neither of the new symmetry classes reduced the discrepancy index of ORDER significantly.

The failure of this value to respond to changes of space group suggested that the problem lay in the absorption correction and not in the symmetry. A stereogram confirmed that there were distinct areas where the reflections were either more or less intense than average. Corresponding discrepancies were noted in a series of four azimuthal scans, and remained unaffected when the physical description of the crystal was changed in the absorption correction program. Comparison of the intensities of the azimuthal scans before and after the analytic correction was applied showed that this method was ineffective in eliminating the absorption problem. The necessary data for an empirical correction could not be obtained because the crystal had deteriorated.

I had been unable to solve the structure of (Sr/Y)Cl<sub>2+x</sub> in the rhombohedral space group and had been unable to identify evidence of a more promising space group. Therefore, because of the strong precedent for the retention of the fluorite subcell in related anion-excess species, I set about to locate a cubic unit cell with edges of about 7Å. After finding this SrCl<sub>2</sub> subcell, I hoped to find additional reflections which would reveal the presence of superstructure.

A new crystal was selected and a new series of precession photographs was examined. Because of the orientation of the crystal in its protective capillary and the geometry of the goniometer head, it was not possible to obtain photographs showing a cubic unit cell. Examination of a scale model however revealed the relationship between the desired cubic cell and the rhombohedral cell. (See Figure 14.)

The second crystal was moved to the diffractometer.

Once the cubic cell had been identified all three axes

were scanned for superlattice reflections. No evidence of

superstructure was found.

Because of the difficulties encountered with the first crystal extraordinary efforts were directed towards anticipating additional complications with the second crystal. A triclinic data set was collected over the region h,  $\pm k$ ,  $\pm \ell$  with the 20 range extending to 65°. This crystal was found to have a primitive cubic cell, even though SrCl<sub>2</sub>

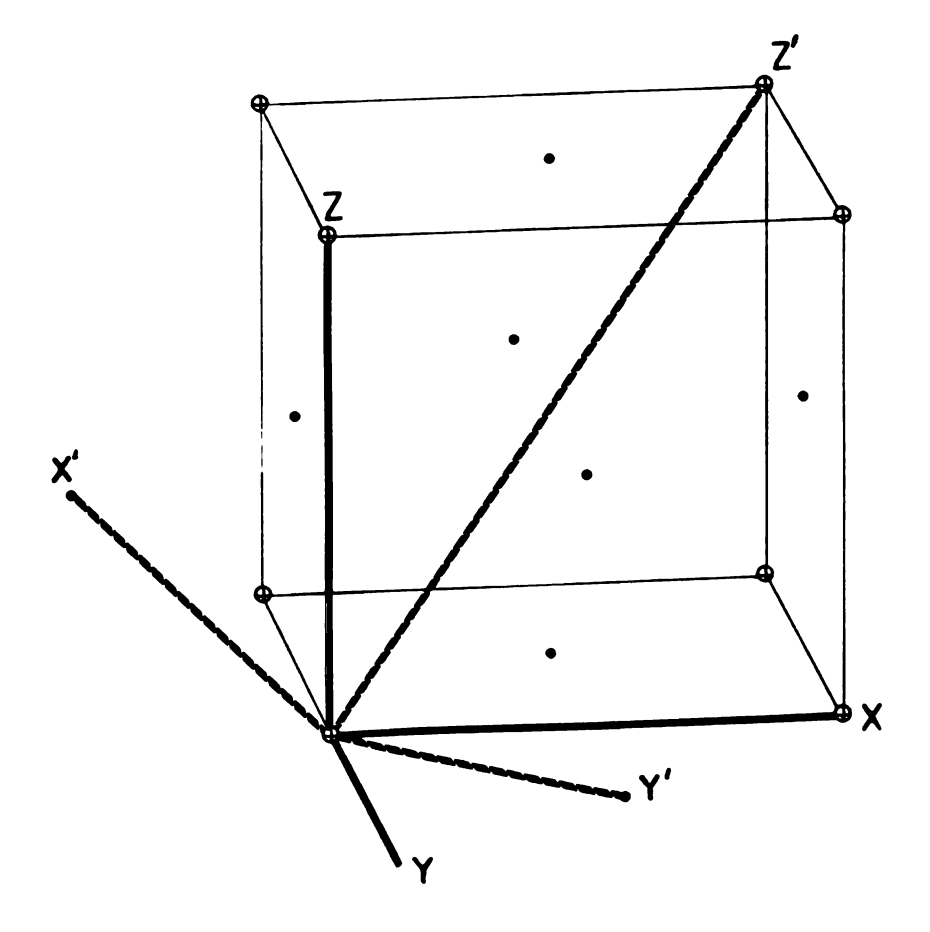


Figure 14. Relationship between the axes of the rhombo-hedral and cubic unit cells.

Table 7. Crystal Data - Second Data Collection.

formula	(Sr/Y)Cl <sub>2.05</sub>
space group	apparently cubic. A triclinc data set was collected. Solutions in space groups Pl, P23, P43m and Fm3m are proposed
a,b,c,A	6.967(1)
α,β,γ,deg	90.0
	re calculated from a least reflections in the range
crystal description	Colorless, broad, flat wedge with larger dimensions approximately 0.3-0.4 mm
radiation	Mo K, graphite monochromatized
μ, cm <sup>-1</sup>	157
scan type	θ-2θ
limit Bragg angle, deg.	θ < 2θ = 65
background count time, sec.	20
scan speed, deg in 20/min	2.0
unique data, no.	425
unique data with $F > \sigma(F)$	221 - primitive 114 - face centered
P - see Ref. 9.	0.02
Q - see Ref. 9	0
scan range	1.0° below $\alpha_1$ to 1.0° above $\alpha_2$

The second crystal was shaped like a broad, flat wedge and the intensity variations due to absorption were extreme. A series of azimuthal scans indicated that the intensity of a given reflection might vary by an order of magnitude as  $\phi$  varied over 180°. Seven azimuthal scans were collected at  $\chi$  = 90° and these were used to calculate an empirical absorption correction. Unfortunately, this correction was less effective as  $\chi$  deviated from 90° and variations as great as four-fold were noted for individual reflections in azimuthal scans collected at other values of  $\chi$ .

Because of the limited success of the absorption correction, first attempts at refinement were made using only a portion of the data -- i.e., that collected in the \$\phi\$ region where absorption effects were most consistent. It was necessary to strike a balance between obtaining the greatest number of data points and the smallest variations in intensity. (See Figure 15.) The best compromise was identified by comparing the residual values when the data in each slice were averaged in space group Pm3 (#200) by ORDER.

.1508 .1813 .3062

310 428 583

175-200 170-205 165-210

# Reflections

	300
	- 200 - degrees
	1000
9.00	1.0-1

No absorption corscans.  $I_{\text{max}}/I$  vs  $\phi$  for two representative azimuthal rection has been applied. Figure 15.

The data collected over the region 170°  $\leq \phi \leq$  205° seemed to offer the best balance between a reasonable number of data points and a low discrepancy index.

Preliminary atom positions were deduced from a Patterson map. Major peaks were found at (000), (½%0), (½%%) and lesser peaks at (½½%) and (0%0). All other peaks were insignificant. If one assumes that the origin is occupied by an ion, these Patterson peaks are consistent with the SrCl<sub>2</sub> structure.

In SrCl<sub>2</sub>, all atoms are located in special positions. Even when the symmetry is lowered from face-centered cubic to primitive cubic, the positions remain non-refinable. Furthermore, attempts to refine thermal parameters with all atoms in special positions resulted in massive, random fluctuations of the temperature factors and the scale factor. Invariably, LESQ failed unless only the scale factor was refined and it refined in one cycle. After that, no further change was noted.

The data from the first crystal were then transformed from rhombohedral to cubic coordinates. When atoms were placed at the same sites the residual was comparable to that of the second data collection. (See Table 8.)

Due to the symmetry chosen for data collection, many reflections were not counted during the first data collection. (See Chapter 1, section on Transformation of Unit Cells.) Since all reflections counted were compatible

Table 8. Comparison of Refinement in Space Group Pm3m Using Both Data Collections.

Atom	Х	Y	Z	В	Mult.	% Occupancy
Sr <sub>l</sub>	0	0	0	. 7	.0208	100
Sr <sub>2</sub>	0	.50	•50	• 7	.0625	100
Cl	.25	.25	.25	1.0	.1667	100

For the first data collection, transformed to cubic indices:

$$R_1 = (\Sigma | F_0 - F_c | / \Sigma F_0) = .1832$$
 for 186 data with  $|F|^2$  greater than  $2\sigma(F^2)$ 

$$R_2 = \{\Sigma \text{ wtg } x \mid F_0 x F_c \mid^2 \}/\Sigma \text{wtg } x F_0^2 \}^{1/2} = .2499$$

For the second data collection:

$$R_1 = (\Sigma | F_o - F_c | / \Sigma F_o) = .2374$$
 for 97 data with  $|F|^2$  greater than  $2\sigma(F^2)$ 

$$R_2 = \{\Sigma \text{ wtg } x \mid F_0 x F_c \mid^2 \}/\Sigma \text{ wtg. } x F_0^2 \}^{1/2} = .2666.$$

with face-centered symmetry, this may have biased the data in favor of the fluorite structure. The lower residual noted for the first data collection is perhaps due to the selective nature of the collection.

An attempt to use MULTAN<sup>10</sup> to extract additional information from the second data set was not successful. Because the reflections which violated the face-centered extinction conditions were relatively weak, assignment of phase relationships was difficult. Information obtained from MULTAN either reiterated that obtained from the Patterson synthesis or was of questionable validity.

The cubic space group may place restrictions on refinement. As noted, an impasse was reached when all atoms were located in unrefinable special positions. Furthermore, the true symmetry of the unit cell is almost certainly not cubic: if the position of the trivalent heteroion is not random, this in itself would destroy the cubic symmetry.

Because there was no evidence to suggest that the unit axes had been chosen incorrectly, the same lattice was considered in terms of other, less restrictive space groups. Data were merged using ORDER, and the discrepancy index of ORDER was assumed to be a reliable criterion of the correctness of the space group chosen. This strongly suggested that the true symmetry was triclinic, space group Pl, however, since very few values were averaged in Pl, the low discrepancy index may reflect only the small number of

equivalent positions.

Subsequently, least squares fits were carried out with the entire data set merged according to Pl symmetry. Atomic positions were specified individually. It was hoped that this approach would (1) avoid biasing the data in favor of any particular structure and (2) eventually allow positional refinement.

With all positional and thermal parameters fixed, the residual, R, was found to be 0.2028 for 665 data of intensity greater than 2 $\sigma$  and R $_{\rm W}$  was found to be 0.2774. A difference map revealed that all major remaining peaks were satellites of the atoms already positioned. Fixing the scale factor and positions while the thermal parameters were refined was not successful: all temperature factors became negative. The same sequence was tried with ORFLS with similarly discouraging results.

It appeared that the high symmetry of the cell was limiting the efficiency of the programs. When the cubic unit cell was used, I was unable to refine either positional or thermal parameters with LESQ, even when the system was described as triclinic. The discrepancy index values of ORDER had already suggested that describing the cubic cell in terms of lower symmetry would have little effect on the goodness of fit. For this reason, I attempted to lower the symmetry by actually changing the unit cell to tetragonal symmetry, using the relationships:

$$a_{tet} = a_{cu} + b_{cu}$$
  $a_{tet} = 2a_{cu} + 2b_{cu}$ 

$$b_{tet} = -a_{cu} + b_{cu} \quad \text{and} \quad b_{tet} = -2a_{cu} + 2b_{cu}$$

$$c_{tet} = c_{cu}$$
  $c_{tet} = c_{cu}$ 

The first is a face-diagonal of the cubic cell, while the second, supported by measurements of the precession films, equates  $b_{ au e t}$  and  $c_{ au e t}$  to twice the face diagonal of the cubic cell.

Attempts to average the transformed data with ORDER resulted in residual discrepancy indices so large that it was obvious that the matrix multiplication cell transform was not operating correctly. The approach was abandoned.

Until this time, two assumptions underlay all attempts at refinement:

- (1) that the residual discrepancy index of ORDER was a reliable guide to the true symmetry of the unit cell; and
- (2) that the additional positive charge of the trivalent heteroion would be balanced by interstitial
  anions.

Although the first assumption was reasonable in view of the quantified data collected by the diffractometer, the qualitative information from the precession films clearly indicated a high degree of symmetry. This information

casts doubt on the first assumption, as the continuing failure to identify a different sized unit cell that would refine casts doubt on the second assumption.

The SrCl<sub>2</sub> lattice is too closely packed to accommodate interstitial anions without displacing the parent structure anions. One would then expect to find reduced anion site occupancy and residual peaks in the difference synthesis at the locations of the interstitials. The difference synthesis had not revealed any obvious interstitial sites.

Assumption (1) could be tested by merging the data in the lowest cubic symmetry and examining the results of further refinement. If Assumption (2) were to be discarded, another means of maintaining charge balance had to be postulated. This could be achieved by the deletion of ions: perhaps by the removal of three Sr<sup>2+</sup> ions for every two Y<sup>3+</sup> ions incorporated (a net loss of one cation) or by paired Schottky defects, with two Sr<sup>2+</sup> ions and a Cl<sup>-</sup> ion removed for every Y<sup>3+</sup> ion included (net loss of one cation and one anion). Since there are twice as many anion sites as cation sites, if the second mechanism were in operation, a 2x% reduction in cation occupancy would accompany an x% reduction in anion occupancy.

The entire set of reflection data was averaged in cubic symmetry, space group P23. Atomic positions were input according to the equivalent positions of space group Pm3m. Thermal parameters, positions, and 100% occupancy were all

fixed and the scale factor was refined. Then the scale factor was fixed and occupancy was refined.

A sudden, dramatic decrease in the weighted residual was noted, and after two cycles of refinement, the occupancies were:

Atom	Occupancy Found	Normalized Values
cı-	149%	100%
Sr <sup>2+</sup> (000)	102%	68%
Sr <sup>2+</sup> (0½)	112%	75%

Clearly, these values indicated a differential in occupancy and suggested that partial occupancy of sites was a good model for the structure.

To obtain a better value for the ratio of cation:anion occupancy, I selected several reasonable values and refined the scale factor for one cycle. Atoms were input in space group Pm3m. A minimum value of the residual was noted at 80% Sr:90% Cl and these values were chosen as a first approximation of the relative occupancies. (See Table 9.) Atomic positions were assigned and refined individually. Cycles of refinement alternated between the occupancy, while the thermal parameters and scale factor were fixed, and the thermal parameters and scale factor, while the occupancy was fixed.

Variations in occupancy and thermal parameters appeared

Table 9. Discrepancy Indices for Refinements with Different Cation: Anion Occupancy Ratios.

INPUT P	OSITIONS	Space Gr	oup Pm3m	
	<u> </u>	Y	Z	Biso
Srl	0	0	0	1.5
Sr2	0	•5	•5	1.5
Cl	.25	.25	.25	3.0

	R(F)		
Occupancy	All Data	l Sigma Data	
100%	.3447	.3027	
<b>Sr</b> =90/C1=95	. 3444	.3024	
Sr=80/C1=90	•3437	.3016	
Sr=70/C1=85	. 3465	.3046	

among the twelve positions. It was clear that they were not equivalent. The results of refining the positions individually suggested that the anions were divided into two sets of different occupancy forming interpenetrating tetrahedra.

Two refinements were begun at this point: one in space group Pl and one in space group P23.

Refinement of positional parameters in space group Pl resulted in only insignificant shifts, and no further attempt was made to refine these values. The final difference map on the Pl refinement did not indicate the absence or gross mispositioning of any atoms, although the lowest valley of -5.7 eÅ-3 in the difference map of the P23 refinement was suspect. Occupancy values gave a composition of MCl<sub>2.17</sub>, close to the expected stoichiometry.

Only after this structure analysis had been completed did it become possible to analyze the crystal chemically. Quantitative metal determination had not been done earlier because of the small amount of compound available. The ampoule contents were frequently inhomogeneous and the sample for analysis had to be selected crystal by crystal using a microscope joined to a glove bag.

About 30 crystals which were visually similar to the  $(Sr/Y)Cl_{2+x}$  data crystal were submitted to Dr. W. E. Braselton for analysis by induction coupled plasma spectrometry. The results of this investigation proved that phase

separation had occurred, for the Sr:Y ratio of the sample was 18:1, corresponding to a formula of  $MCl_{2.05}$  rather than the expected 5:1 ratio and  $MCl_{2.17}$  stoichiometry.

Subsequently, the  $(Sr/Y)Cl_{2+x}$  data crystal and several visually dissimilar crystals of  $(Sr/Yb)Cl_{2+x}$  were analyzed. The results are listed in Table 10. The  $(Sr/Y)Cl_{2+x}$  crystal on which data were collected was similar in composition to the bulk sample analyzed previously. The cation ratio of the strontium-ytterbium mixtures was highly variable and visual appearance proved to be a poor indication of composition.

Hamilton's test $^{74}$  provided no evidence that either solution was the more probable. To insure conformity with the analytic results, the P23 structure was constrained to the composition  $MCl_{2.05}$ .

The final results of the Pl refinement and the constrained P23 refinement are summarized in Table 11.

The vacancy model solution of (Sr/Y)Cl<sub>2.05</sub> had been obtained empirically. Every attempt had been made to avoid biasing the refinement in favor of a predetermined solution. However, an unprejudiced opinion is not necessarily true. The data were now approached in terms of the Willis cluster model. He are now approached in terms of the Willis cluster model was specifically developed for fluorite solutions in this composition range, the investigation was undertaken even though the model required that certain constraints be placed on

Table 10. Results of Chemical Analysis by Induction Coupled Plasma Spectrometry.

		ppb		
Sample	Yb	Y	Sr	Ratio
Sr/Yb-white	119.7(2.4)		1657.0(33.1)	27.
Sr/Yb-clear 2 crystals	94.2(1.9)		827.6(16.6)	17.
Sr/Yb-clear l crystal	35.9(7)		85.1(1.7)	4.7
Sr/Y-clear data crystal		831.2(16.6)	15756(315)	19.
Sr/Y-clear oulk sample		210(4)	3750(80)	18.1
ICP opera	ating condit	ions:		
-	C	Comp - Jarrel	1-Ash	

forward power (kw)
flame height, mm 1.1 16. nebulizer pressure, 14 argon coolant flow, 18 lpm auxiliary flow, 0.5 0.4 lpm sample flow, lpm

Table 11. The Vacancy Model Results of Refinement.

Space Group Pl
Positional and thermal parameters with associated esd's.

Atom	Х	Y	Z	В	Mult.	% Occupancy
Cll	•75	.25	.25	2.8(2)	.95(3)	95.2
C12	.75	.75	.75	1.3(2)	.87(2)	87.4
C13	.25	.75	.25	2.0(2)	.89(3)	89.1
C14	.25	.25	.75	1.8(2)	.87(3)	87.4
C15	•75	.25	.75	2.5(3)	.72(3)	72.2
C16	•75	.75	.25	2.8(3)	.74(3)	74.1
C17	.25	.75	.75	.2(1)	.73(2)	73.6
C18	.25	.25	.25	.8(2)	.72(2)	72.4
Srl	.00	.00	.00	1.04(6)	.759(7)	75.9
Sr2	.00	.50	.50	1.02(6)	.750(8)	75.0
Sr3	.50	.00	.50	.57(4)	.767(7)	76.7
Sr4	.50	.50	.00	1.62(7)	.753(8)	75.3

Final Cycle Refinement Indicators

 $R_1 = (\Sigma | F_0 - F_c |)/\Sigma F_0) = .0873$  for 117 data with  $|F|^2$  greater than 2 $\sigma$  ( $F^2$ )

 $R_2 = \{ \Sigma (\text{wtg x } |F_0 - F_c|^2) / \Sigma \text{wtg x } F_0^2 \}^{1/2} = .0839.$ 

Shift-to-error ratios: maximum .2836 average .08815

Final difference map maximum positive density  $(e^{\lambda^{-3}}) = .802$  maximum negative density  $(e^{\lambda^{-3}}) = -1.476$ 

Table 11. Continued.

Space Group P23

Positional and Thermal parameters with associated esd's

Atom	х	Y	Z	В	Mult.	% Occupancy
ClA	.25	. 25	.25	.80(6)	.209(8)	62.8
ClB	.75	.75	.75	1.95(7)	.310	93.0
Srl	.00	.00	.00	.24(3)	.0642(4)	77.0
Sr2	.00	.50	.50	1.31(2)	.1892(9)	75.7

Cl set A includes positions .25 .25 .25, .25 .75 .75,

.75 .25 .75, .75 .75 .25.

Cl set B includes positions .75 .75 .75, .75 .25 .25,

.25 .75 .25, .25 .25 .75.

Final Cycle Refinement Indicators

 $R_1 = (\Sigma | F_o - F_c |)/\Sigma F_o) = .1013$  for 218 data with  $|F|^2$  greater than  $\sigma$   $(F)^2$ 

$$R_2 = \{ \Sigma (\text{wtg x } |F_0 - F_c|^2) / \Sigma \text{wtg x } F_0^2 \}^{1/2} = .0849.$$

Shift-to-error ratios: maximum .3578

average .0597

Final difference map

maximum positive density  $(e^{-3}) = 1.458$ maximum negative density  $(e^{-3}) = -4.869$  the data.

All reflections inconsistent with face centering were deleted from the data set because both  $\rm UO_{2.13}$  and  $\rm (Ca/Y)-F_{2.10}$  had been solved in Fm3m symmetry. As indicated previously, none of the primitive reflections deleted was very intense, and refinement of the face-centered data would provide a good indication of the validity of the model.

To begin evaluation of the Willis cluster model for  $(Sr/Y)Cl_{2.05}$ , coordinates and occupancy values were input exactly as given for  $(Ca/Y)F_{2.10}$ . (See Table 12.) Positional, thermal and occupancy factors were fixed while the scale factor was refined. Then thermal parameters, anion multiplicity, the scale factor and the positional parameters of the displaced anions were refined separately with ORFLS in alternating cycles. Separate refinements were necessary because of the high correlation of many of the variables.

Although fewer parameters were varied in this refinement than in that of the triclinic vacancy model, the residual of the Willis cluster model quickly fell below that obtained with the vacancy model. The total anion occupancy was constrained to equal 8.20 (4 x 2.05) for the entire unit cell. After refinement of the site occupancies with ORFLS had stabilized, refinement was continued with LESQ for evaluation of an empirically determined

Table 12. Structural Parameters of Average Cells. 48\*

(Ca/Y)F <sub>2.10</sub>								
	х	Y	Z	Contribution to 2+x in (Ca/Y)F <sub>2+x</sub>				
Lattice F	0.25	0.25	0.25	1.88(.04)				
Interstitial F'	•50	v	v	.14(.03)				
Interstitial F"	W	W	W	.08(.03)				
v = 0.36(.0)	L) v	v = 0.42	2(.01)					
<sup>UO</sup> 2.12				Contribution to 2+x in UO 2+x				
Lattice 0	0.25	0.25	0.25	1.87(.03)				
Interstitial 0'	.50	v	v	.08(.04)				
Interstitial 0"	W	W	W	.16(.06)				
v = 0.38(.0)	.)	w =	0.41(.0	01)				

<sup>\*</sup>Data from Reference 48.

extinction factor. A final difference map did not indicate either the absence or gross mispositioing of any atom.

Final cycle refinement indicators and the final values of all parameters are presented in Table 13.

Refinement of the entire primitive data set was attempted in space group  $P^{\overline{4}}3m$ , the symmetry of the composite  $U_4O_9$  cell described by Willis: <sup>45</sup> Refinement of thermal parameters was not possible: they fluctuated without restraint until the program failed. The result of the incomplete refinement is also summarized in Table 13.

Direct, quantitative comparison by Hamilton's method  $^{74}$  of the two refinements is not possible unless both are based on the same number of data. Since the P $\overline{4}$ 3m refinement was incomplete, the vacancy model was refined in space group F23, with final discrepancy indices of  $R_1$  = .0914 and  $R_2$  = .0711 for 114 data with F greater than  $\sigma(F)$ . These values were compared to those for the Fm3m refinement of the Willis cluster model.

## Preliminary Investigation of (Sr/Yb)Cl<sub>2+x</sub>

The bulk sample of  $(Sr/Yb)Cl_{2+x}$  was visibly less uniform than that of  $(Sr/Y)Cl_{2+x}$ . At least three types of ytterbium-substituted species were seen: water clear crystals, white crystals which seemed to be of marginal quality, and a white powder. The clear crystals were chosen for X-ray investigation and precession photographs

The Willis Cluster Model Results of Refinement. 13. Table

Space Posit:	Space Group Fm3m Positional and t	n hermal par	Fm3m and thermal parameters with	associated	esd's	
Atom	X	Y	2	В	Mult.	Contribution to (2.05) in (Sr/Y)Cl <sub>2.05</sub>
C11	.25	.25	.25	.91(3)	.0362	1.74
C12	.50	.402(2)	.402(2)	6.9(2.5)	(9)6700.	.24
C13	.341(5)	.341(5)	.341(5)	2.9(5.1)	(919100.	.08
Sr	00.	00.	00.	.96(2)	.0208	!
Ext:	Extinction factor = 5.25	tor = $5.25$	x 10-8			
	$R_1 = (\Sigma   F)$	$R_1 = (\Sigma   F_o - F_c   / \Sigma F_o)$	= .0633 for	= .0633 for 114 data with $ F ^2$	th  F  <sup>2</sup> greater	ter than $\sigma$ (F <sup>2</sup> )
	$R_2 = \{\Sigma(w)\}$	rex FoxF	$R_2 = \{\Sigma(\text{wtg x }   F_o x F_c  ^2) / \Sigma \text{wtg x } F_o^2\}^{1/2}$	$F_0^{2}$ 1/2 = .0696	969	
Shi	Shift to error ratios:	ratios:	maximum . 494	η <b>.</b>		
Final	al difference map:		average .197 maximum positive density $(eA^{-3})$ maximum negative density $(eA^{-3})$	.197 positive density $(e^{-3})$ negative density $(e^{-3})$	11 11	1.068 718

Table 13. Continued.

Space Group Positional	Ω	. P43m and thermal param	meters			
	- 1	- 1				
Atom	×	Ы	2	Д	Mult	Contribution to 2.05 in $(Sr/Y)Cl_{2.05}$
CIAI	.25	.25	.25	(9)02.	.1291	.7746
CIA2	.75	.75	.75	.87(5)	.144(5)	.864
ClBl	.50	.597(2)	.597(2)	10.8	.006(2)	.036
C1B2	.50	.402(2)	.402(2)	η.	.006(2)	.036
C1B3	.50	.902(2)	.902(2)	7.6	.005(3)	.030
C1B4	.50	.098(2)	.098(2)	10.8	.005(3)	.030
C1B5	00.	.902(2)	.402(2)	7.6	.015(4)	060.
C1B6	00.	.098(2)	.597(2)	7.6	.015(4)	060.
CICI	.341(5)	.341(5)	.341(5)	9.4	.0006(30)	.003
C1C2	.659(5)	.659(5)	(2)659.	4.6	.004(3)	,024
C1C3	.841(5)	.841(5)	.841(5)	2.7	.004(3)	.024
C1C4	.159(5)	.159(5)	.159(5)	2.7	.007(3)	.042
SrA	00.	00.	00.	2.12(5)	9140.	
SrB	00.	.50	.50	.68(1)	.1250	

Thermal parameters for the interstitial anions do not converge.

Table 13. Continued.

(F).
ø
than
greater
ഥ
with
reflections with
221
$\mathbf{for}$
.1125
H
ORFI,S
R(F)
ĸ

 $WR(YO)_{ORFLS} = .0878.$ 

R(F) and WR(YO) in ORFLS correspond to  $\rm R_1$  and  $\rm R_2$  in LESQ but WR(YO) is based on  $|\rm F|$  rather than  $|\rm F|^2$ .

suggested that they were isostructural with the clear crystals of  $(Sr/Y)Cl_{2+x}$ . In fact, the best photograph showing the cubic unit cell was a zero-layer picture of a crystal of  $(Sr/Yb)Cl_{2+x}$ . (See Figure 16.).

A good quality crystal was transferred to the diffractometer and data collection was begun. Cell parameters were analogous to those of the yttrium-substituted species, however, the non-face-centered reflections were absent. These extra reflections were critical since they indicate that the crystal is not pure SrCl<sub>2</sub>. The ICP analysis requires destruction of the crystal and there was no other means of confirming that Yb(III) had been incorporated into the lattice. Data collection was terminated. A second clear crystal was examined and rejected for the same reason. Two white crystals were rejected because of poor quality.

ICP analysis later confirmed that the metals ratio of the clear crystals of  $(Sr/Yb)Cl_{2+x}$  is the same as that of  $(Sr/Y)Cl_{2.05}$ , while the composition of the white crystals is different. It is also interesting to note that two white crystals analyzed together had a Sr:Yb ratio of 27:1 while a third white crystal, originally intended to be analyzed with the others, had a Sr:Yb ratio of 4.7:1. This third crystal is close to the composition of the reaction mixture.

X-ray powder diffraction patterns of the white and clear portions of  $(Sr/Yb)Cl_{2+x}$  exhibit subtle but undeniable

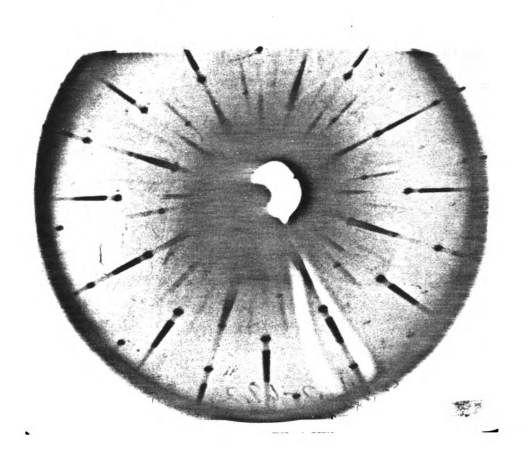


Figure 16. A zero layer precession photograph showing two of the cubic axes.

differences. Unfortunately, the significance of these differences is obscure, since at least the clear crystals include more than one phase.

#### RESULTS AND DISCUSSION

When only the face centered data are considered, Hamilton's test<sup>74</sup> substantiates the intuitive conclusion that the Willis cluster model is more accurate than the vacancy model in describing the structure of  $(Sr/Y)Cl_{2.05}$ . The discrepancy index of even the incomplete  $P\overline{4}3m$  refinement with the primitive data is also much lower than that of the complete P23 refinement. However, in the  $P\overline{4}3m$  case, thermal parameter refinement does not yield convergence. This failure to converge indicates that although the Willis cluster is an excellent approximation of the true structure, the model should not be viewed as the definitive solution.

The Willis cluster represents a disordered model. The individual crystals of  ${\rm UO}_{2.13}$  and  $({\rm Ca/Y}){\rm F}_{2.10}$  investigated respectively by Willis 44,45 and Cheetham, et al.,46 produced only reflections consistent with face centering, and no evidence of ordering was found. Clustering was deduced primarily from the physical requirements of atomic sizes. The phase  ${\rm U_4O_9}$ , however, did exhibit weak, mixed index superstructure reflections. Belbeoch and coworkers 75 had determined that its unit cell was four times as large in each dimension as that of  ${\rm UO_2}$  and that it belonged to

space group 143d. Willis ascribed these reflections to ordering of the interstitial oxygen atoms, but chose to ignore their influence. He describes  $U_4O_9$  in terms of a disordered model with symmetry  $P\overline{4}3m$ , noting that the majority of the reflections are ascribable to face centered symmetry. The size of the cell Willis selected is essentially equal to that of  $UO_2$ .

Cheetham 46 extended Willis' model and postulated specific groupings of defects, designated clusters, which would be consistent with stoichiometric and diffraction data. (See Figure 17.) It is possible that these clusters are themselves ordered over a measurable domain. In fact, Greis claims to have found some evidence of precisely this type of ordering in the cubic phases of  $(M/RE)F_{2+x}$  57-63 (M=Ca, Sr, Ba; RE=Y, La, Sm, Eu, Tm, Yb). Since the rhombohedral phases arise as superstructures of  $CaF_2$ , the rhombohedral cells may describe the ordering of Willis-type clusters.

The crystal of (Sr/Y)Cl<sub>2.05</sub> chosen for study unambiguously produced reflections which were inconsistent with face centered symmetry. In addition, when refinement was freed from the constraints of high symmetry, the atomic positions were seen to be inequivalent. Both of these observations substantiate the assertion that symmetry cannot be as high as Fm3m and may be much lower. The evidence suggests an as yet unidentified superstructure, where the symmetry of the atoms in the substructure unit is different

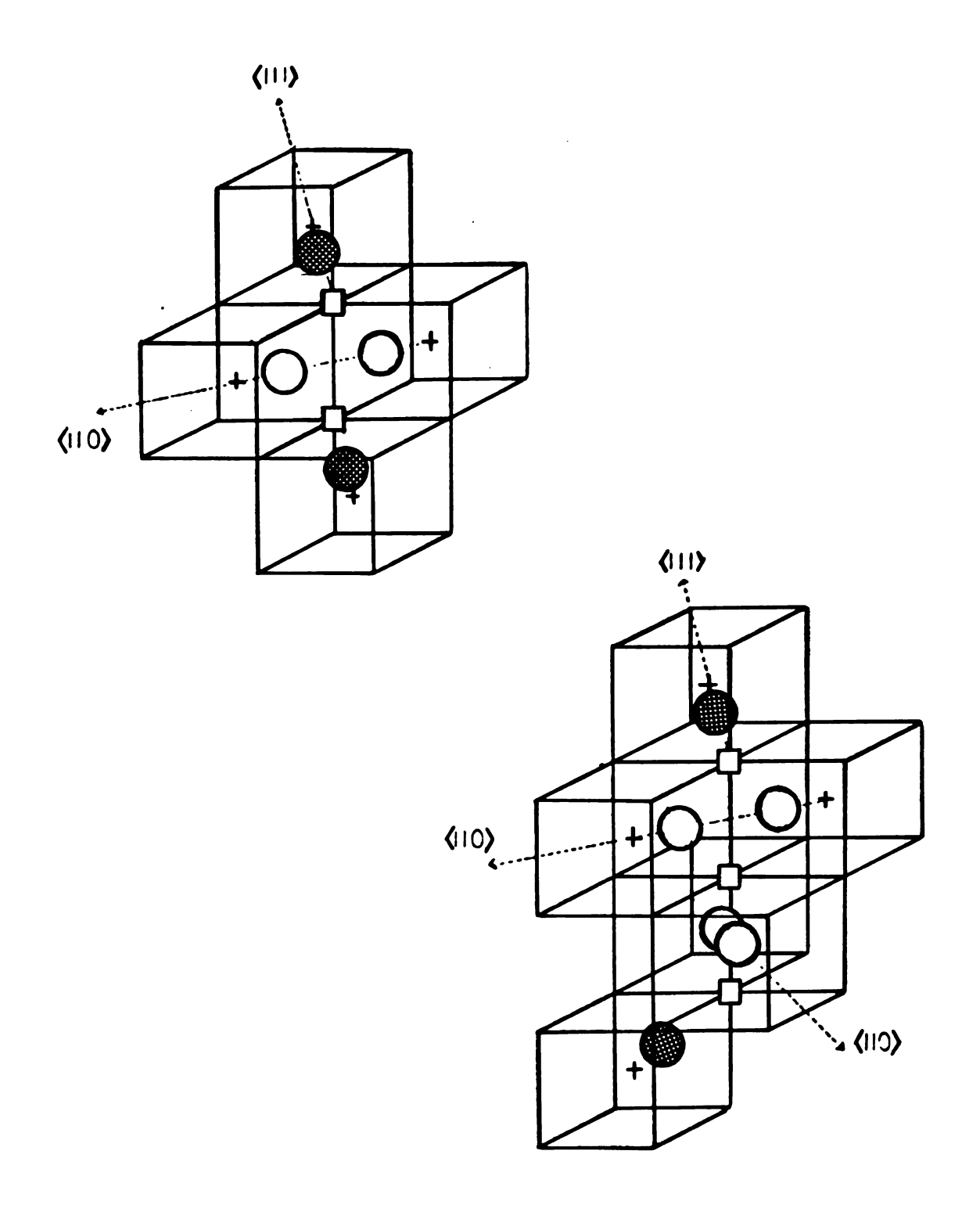


Figure 17. Above: 2:2:2 Willis cluster containing two normal anion vacancies ( ) two X' interstitials ( ), two X" interstitials ( ), and cubic (½,½,½) sites (+). Below: A 3:4:2 Willis cluster. Figure redrawn from Reference 47.

from that of the atoms in the composite structure with partial occupancy of one or more sites. In this case, the symmetries of the substructure and the composite structure are very similar because the majority of the sites occupied in the composite are identical to those of the fluorite subcell. This fact makes identification of the true cell extremely difficult.

Because the vacancy model is also closely related to the fluorite cell it should not be rejected out of hand, even though the Willis cluster model appears preferable.

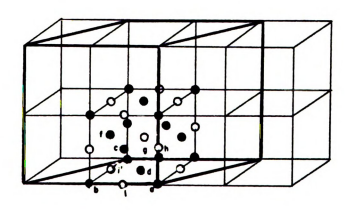
The discrepancy index of the vacancy model is reasonable. Furthermore, it is possible to refine the entire data set, not merely the face centered portion, in terms of this model, and the difference map reveals no great peaks.

Precedent exists for this type of structure. Other vacancy structures are well documented. ZrS is a nonstoichiometric compound with a range of homogeneity extending from  ${\rm Zr_{0.67}S}$  to  ${\rm ZrS_{1.2}}$ . The ideal 1:1 compound has the NaCl-type structure, but X-ray examination of a single crystal of  ${\rm Zr_{0.77}S}$  revealed a superstructure of the NaCl cell with partial occupancy of certain sites, as summarized in Table 14 and Figure 18. The pattern of vacancies becomes apparent if  ${\rm Zr_{0.77}S}$  is described as a monoclinic superstructure of NaCl.

Titanium monoxide is another grossly nonstoichiometric species, with a composition range extending from  ${
m TiO}_{0.9}$ 

Table 14. Percent Occupancy of Zr Sites in Zr<sub>0.77</sub>S.

Zr Site (Wycoff Notation)	Position in Fm3m	% Occupancy	Error
a	(000)	107	±8
b	(555)	27	±8 ±8 ±8
С	(3/4 3/4 3/4)	27 63	±8
c d	(0½½0, (½0½), (½½0) (0½3/4) (3/4 0 1/4)		
	((1/4 3/4/0)	79 69	±8 ±7
e	$(\underline{x}00)$ , $(0x0)$ , $(00x)$		
	$(\bar{x}00)$ , $(0-x0)$ , $(00-x)$	69	±7
f	(xxx), (x-x-x), (-xx-x), (-xx-x), (-x-xx), (-x-x-x), (-xx-x), (-		
	((x-xx),(xx-x)	85	±7



- Zr positions a,b,c,d,f labels correspond to table
- O S positions.

Figure 18. Illustration of the atomic positions in the monoclinic superstructure, space group C2/m. The monoclinic unit cell is shown by the heavy lines. The NaCl-type ZrS cells are shown as thin-lined cubes. Redrawn from Reference 57.

to TiO<sub>1.25</sub> at temperatures below 990°C. Depending on composition, either the cation or anion lattice can be nearly perfect, with vacancies in the counterion lattice. Even in the 1:1 compound, TiO, about 15% of both cation and anion sites are vacant. The observed electron microscope data can be explained if half the titanium and half the oxygen atoms are alternately missing in every third (110) plane of the original cubic cell.

The high percentage of vacancies in these species can be supported only by long range ordering. The equilibrium concentration of defects in a solid can be approximated, but this value is characteristically on the order of 10<sup>-7</sup> even at 400°C. This calculation is based on short range electrostatic forces operating within an essentially unchanged lattice. Structural modulation arises from the interaction of long range forces, such as stress and strain, with the short range forces. The ordering of defects to produce a new structure permits an overall lowering of internal energy through a balancing of long and short range forces.

In the vacancy model of  $(Sr/Y)Cl_{2.05}$ , occupancy values for both anions and cations appear to be less than 100%. Balance of charge appears to be achieved not by incorporation of interstitial ions, but by the removal of ions. Anion occupancy as well as cation occupancy is reduced, and suggests that for each metal site occupied by  $Y^{3+}$ ,

another metal site and a chloride site are vacated. The alternative scheme of removing three  $\mathrm{Sr}^{2+}$  ions whenever two  $\mathrm{Y}^{3+}$  ions are incorporated, seems less likely, as it cannot explain the partial occupancy of the anion sites.

If the absences occurred on a purely random basis, all sites would be equivalent. If the procedure used in the data handling had any effect at all, it would tend to obscure this inequivalence rather than enhance it. Averaging the data to alleviate the absorption discrepancies would tend to make the sites more equivalent rather than less equivalent, and the persistence of the inequivalencies argues for their significance. The obvious inequivalence of both the cation and anion sites, especially in the Pl refinement, strongly suggests an ordered structure. As in the cases of ZrS and TiO, the high percentage of vacancies also supports the hypothesis of long range ordering: such a high concentration of disordered defects would be thermodynamically impossible. While the level of confidence is greater for the Willis cluster model than for the vacancy model, both hypotheses are consistent with a structure based on a fluorite-like subcell. There is reason to believe that long range ordering of these subcells exists, but unfortunately the refinements of these data do not reveal the extended period of the crystal.

It is highly possible that superstructure reflections which would define a larger unit cell are present but are

too weak for easy detection. Other hypotheses can be advanced to explain why the exact modulation of the structure cannot be specified at this time:

- (1) Crystal imperfections, either specific to the crystal chosen for data collection, or characteristic of the bulk sample. A longer period of annealing would minimize crystal imperfections unless the composition of the crystal is at a boundary region between two phases of different structure. If the crystal represents such a metastable state, longer annealing will lead to continued separation of the phases.
- (2) Absorption problems obscuring the ordering.

  More powerful absorption correction techniques and
  grinding the crystal to a spheroidal shape before data
  collection would minimize this problem.

Density measurements would unambiguously determine whether a vacancy model was reasonable for this structure. The calculated density of the vacancy structure is about 2.3 g cm<sup>-3</sup>, while the calculated density of a structure with interstitial ions is about 3.1 g cm<sup>-3</sup>, slightly greater than that of SrCl<sub>2</sub>. Unfortunately, these measurements could not be performed because of the difficulty of obtaining a sufficiently large, unhydrated sample of homogeneous compound. Each crystal should be selected individually and even in a glove bag the material is attacked by

atmospheric moisture. The experience of selecting crystals for ICP analysis indicated that 50 mg. of visually similar crystals would be a relatively large sample. On such small amounts of compound, inherent weighing errors and weight changes due to hydrolysis could easily exceed the difference in weight calculated for the two models.

The samples analyzed typically contained a much smaller percentage of trivalent ion than expected. Walker's work with  $\mathrm{SrCl_2}^{78}$  suggests a solubility limit of 5-6% RECl\_3 in  $\mathrm{SrCl_2}$ , and it appears that a separation of phases has occurred. Since analysis of visually dissimilar portions of the bulk sample did not identify a fraction rich in trivalent ion, I conclude that the MCl\_3 component combined with the reaction container either physically or chemically and was discarded with the used ampoules.

If precipitated YbCl<sub>3</sub> were in contact with the glass, side reactions must be considered. Ayasse<sup>79</sup> has characterized the compound Yb<sub>3</sub>(SiO<sub>4</sub>)<sub>2</sub>Cl, formed by a side reaction when YbOCl is heated under a chlorine atmosphere in a quartz container. He also noted, but did not characterize, another phase of "thin white sheets and slivers found adjacent to and on the tube wall". This description is consistent with the etching of the ampoule walls which occurred during the reaction of SrCl<sub>2</sub> and YbCl<sub>3</sub> or YCl<sub>3</sub>. Yttrium species analogous to the ytterbium products would not be unexpected. Chlorosilicate formation with SrCl<sub>2</sub> would not be anticipated.

 $(Sr/Y)Cl_{2.05}$  is the first chloride formally described in terms of the Willis cluster and the first Willis cluster compound in its composition region to exhibit superstructure reflections. The significance of the primitive reflections must be emphasized. They appear to arise from the anion superlattice, and study of these reflections may be the key to understanding long range ordering in fluorite related phases of the composition  $MX_{2+x}$  for  $0 \le x \le 0.2$ . Neither the Vernier structures nor the ordered superstructures discussed by Greis has been found in this composition region. It should be noted that the cubic fluoride phases may exhibit similar superstructures, but the chloride systems are more likely to yield to X-ray investigation than the fluorides because of the greater electron density of the chloride ion.

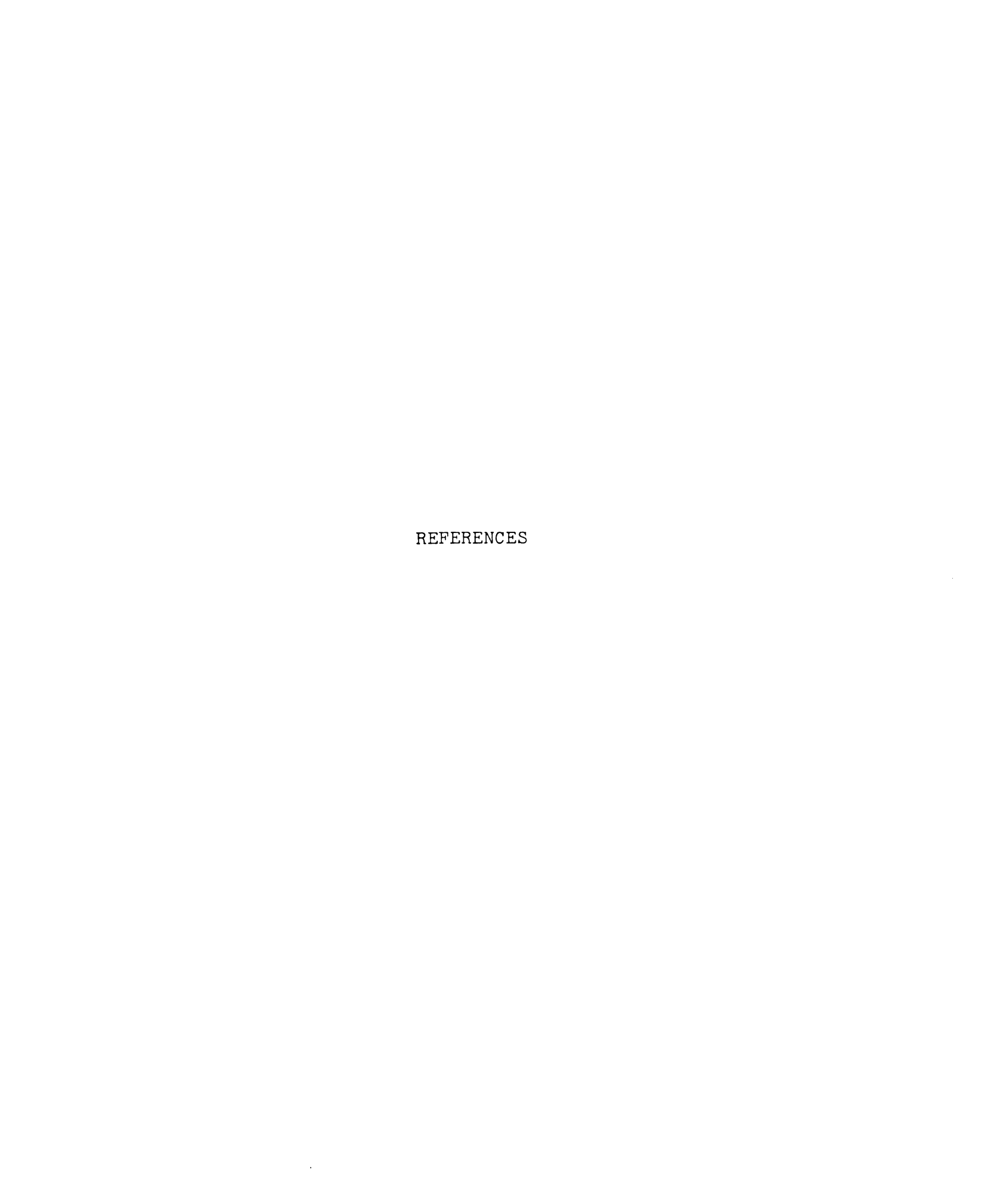
The major significance of this work lies in the scope of the future work it suggests: namely, an investigation of the phase diagrams for systems of the type  $SrCl_2-MCl_3$  with emphasis on the identification of ordered phases in the composition region of 0 to 25 mole percent  $MCl_3$ .

A number of phase diagrams  $^{67,80}$  have specified a phase  $^{M_3M'Cl_9}$  where M=Sr or Ba, and M'=Ce,Nd,Pr,Sm or Pu. The identification of a Willis cluster structure for  $(Sr/Y)Cl_{2.05}$  now suggests that these  $^{M_3M'Cl_9}$  phases may be analogous to the known structure of  $U_4O_9$ .

It would also be interesting to look for a structural

basis for the eutectic found in these systems at about 40 mole percent  $\mathrm{M'Cl}_3$ .

The evidence of an ordered structure for  $(Sr/Y)Cl_{2.05}$  suggests that the crystal chemistry of fluorite derivatives is even more complex than it has seemed.



### REFERENCES

- 1. Hughes, B. B., Haltiwanger, R. C., Pierpont, C. G., Hampton, M., and Blackmer, G. L. <u>Inorg. Chem.</u>, 1980, 19, 1801.
- Popov, A. I., and Lehn, J.-M., "Physicochemical Studies of Crown and Cryptate Complexes" in Chemistry of Macrocyclic Compounds, G. A. Melson, Ed., Plenum, N.Y., 1979.
- Cahen, Y. M., Handy, P. R., Roach, E. T., and Popov,
   A. I., J. Phys. Chem., 1975, 79, 80.
- 4. Cahen, Y. M., Dye, J. L., and Popov, A. I., <u>J. Phys.</u> Chem., 1975, 79, 1289.
- 5. Cahen, Y. M., Dye, J. L., and Popov, A. I., <u>J. Phys. Chem.</u>, 1275, <u>79</u>, 1292.
- 6. Smetana, A. J., and Popov, A. I., <u>J. Solution Chem.</u>, 1980, <u>9</u>, 183.
- 7. van Remoortere, F. P., and Boer, F. P., Inorg. Chem., 1974, 9, 2071.
- 8. Boer, F. P., Neuman, M. A., van Remoortere, F. P., and Steiner, E. C., <u>Inorg. Chem.</u>, 1974, <u>13</u>, 2826.
- 9. Wei, K.-T., and Ward, D. L., <u>Acta Cryst. Sec. B</u>, 1976, <u>32</u>, 2768.

RAWI = COUNT - [TIME x (1/2)(B1 + B2)/CT]

 $SIGI = (COUNT + SIGBKG^2)1/2$ 

 $SIGBKG = SIGB12 \times (1/2)(TIME/CT)$ 

SIGB12 is the greater of (B1 + B2) $^{1/2}$  and  $\sqrt{2}$  (|B1 - B2|)

RAWI = raw intensity SIGI = standard deviation of RAWI

Bl and B2 = background counts measured at the ends of a scan of CT seconds duration.

COUNT = counts recorded while scanning for TIME seconds.

After applying factors to RAWI to correct for Lorentz polarization, decay, and absorption (where necessary) the square of the structure factor (FSQ) and its standard deviation are obtained.

Equivalent and duplicate data are combined to give averaged values for FSQ and SIGFSQ for unique reflections:

$$FSQ_{av} = (\sum_{i=1}^{N} FSQ_{i})/N$$

$$SIGFSQ_{av} = \left[\sum_{i=1}^{N} (SIGFSQ)_{i}^{2}\right]^{2}/N$$

When the scatter of data from the averaged value exceeded SIGFSQ $_{av}$  by a factor of four or more, SCATTER was used in place of SIGFSQ $_{av}$  for this reflection.

SCATTER = 
$$\{(\sum_{i=1}^{N} FSQ_i - FSQ_{av}|^2)/[(N-1)N]\}^{1/2}$$

The factors P and Q can also be used in the full-matrix least squares calculation to modify SIGFSQ:

$$SIGFSQ_{mod} = [SIGFSQ^2 + (P \times FSQ)^2 + Q^2]^{1/2}$$

The structure factor, FOBS =  $(FSQ)^{1/2}$ , can be corrected by using an extinction factor, EF:

$$FOBS_{cor} = (1 + EF \times RAWI) \times FOBS$$

The standard deviation of the structure factor (SIGMA) is given by the equations:

$$SIGMA = SIGFSQ^{1/2}$$
 when RAWI < SIGI

and,

SIGMA = FOBS - 
$$(FSQ - SIGFSQ)^{1/2}$$
 for  $FSQ \ge SIGFSQ$ .

In the least squares refinement, structure factors are weighted by  $1/(SIGMA)^2$ .

- 10. Main, P., Hull, S. E., Lessinger, L., Germain, G., De Clerca, J. P., Woolfson, M. M. Multan 78, "A System of Computer Programmes for the Automatic Solution of Crystal Structures from X-ray Diffraction Data", 1978, Univ. of York, England.
- 11. These programs were acquired from Dr. Allan Zalkin by Dr. Donald Ward and modified for use on the MSU CDC 6500 and Cyber 750.
- 12. Johnson, C. K., ORTEP, Report ORNL-3794, Oak Ridge National Laboratory, Oak Ridge, TN, 1965.
- 13. Busing, W. R., Martin, K. O., and Lerry, H. A., ORFLS4 based on ORFLS, Oak Ridge National Laboratory, Oak Ridge, TN, June 1978.
- 14. "International Tables for X-Ray Crystallography", Kynoch Press: Birmingham, England, 1974, Vol. IV, pp. 72 ff.
- 15. <u>Ibid</u>, p. 149.
- 16. Shannon, R. D., Acta Cryst. Sec. A., 1976, 32, 751.
- 17. Bush, M. A., and Truter, Mary R., J. Chem. Soc., Perkin, 1272, 341.
- 18. Dobler, M., Dunitz, J. D., and Seiler, P., <u>Acta Cryst</u>. <u>Sec. B</u>, 1974, <u>30</u>, 2741.
- 19. Raston, C. L., White, A. H., and Wilks, A. C., <u>Aust</u>. <u>J. Chem.</u>, 1978, <u>31</u>, 415.
- 20. Griggs, C., Hasan, M., Henrick, K., F., Matthews, R. W., and Tasker, P. A., <u>Inorganica Chimica Acta</u>, 1977, 25, 129.
- 21. Fair, C. K., and Schlemper, E. O., Acta Cryst. Sec. B,  $\frac{1978}{2000}$ ,  $\frac{34}{436}$ .
- 22. Maluszynzka, H., and Okaya, Y., <u>Acta Cryst., Sec. B</u>, 1977, 33, 3049.
- 23. Enders, H., Keller, H. J., Martin, R., and Traeger, U., <a href="Acta Cryst.">Acta Cryst.</a>, <a href="Sec. B">Sec. B</a>, <a href="1980">1980</a>, <a href="36">36</a>, <a href="35">35</a>.
- 24. Drew, M. G. B., and Hollis, S., <u>Acta Cryst.</u>, <u>Sec. B</u>, 1980, <u>36</u>, 2629.
- 25. West, D. X., Pavhovic, S. F., Brown, J. N., Acta Cryst., Sec. B, 1980, 36, 143.

- 26. Vance, T. B., Jr., and Holt, E. M., <u>Acta Cryst.</u>, <u>Sec.</u> B, 1980, 36, 1950.
- 27. Vance, T. B., Jr., Holt, E. M., and Holt, S. L., Acta Cryst., Sec. B, 1980, 36, 153.
- 28. Mellors, G. W. and Sanderoff, S., J. Phys. Chem., 1959, 63, 110.
- 29. Keneshea, F. J., Jr. and Cubicciotti, David, <u>J. Chem.</u> Engr. Data, 1961, 6, 507.
- 30. Druding, Leonard F, Corbett, John D., and Ramsey, Bob N., Inorg. Chem. 1963, 2, 869.
- 31. Mee, Jack E. and Corbett, John D., Inorg. Chem., 1965,  $\underline{4}$ , 88.
- 32. Corbett, John D., Pollard, David L. and Mee, Jack E., Inorg. Chem., 1966, 5, 761.
- 33. Corbett, John D. and McCollom, Bill C., <u>Inorg. Chem.</u>, 1266, <u>10</u>, 938.
- 34. Caro, P. E. and Corbett, John D., <u>J. Less Common Met.</u>, 1969, <u>18</u>, 1.
- 35. Löckner, Ulrick and Corbett, John D., <u>Inorg. Chem.</u>, 1975, <u>14</u>, 426.
- 36. Druding, Leonard F. and Corbett, John D., <u>J. Am. Chem.</u> <u>Soc.</u>, 1961, <u>83</u>, 2462.
- 37. Simon, Arndt, Mattausch, Hansjürgen, and Holzer, Norbert, Angew Chem., 1978, 88, 685.
- 38. Adolphson, Douglas G. and Corbett, John D., Inorg. Chem., 1976, 15, 1820.
- 39. Daake, Richard L. and Corbett, John D., <u>Inorg. Chem.</u>, 1977, <u>16</u>, 2029.
- 40. Poeppelmeier, Kenneth R. and Corbett, John D., <u>Inorg.</u> Chem., 1977, 16, 1107.
- 41. Poeppelmeier, Kenneth R., Corbett, John D., McMullen, Tom P., Torgeson, David R. and Barnes, Richard G., Inorg. Chem., 1980, 19, 129.
- 42. Bevan, D. J. M., "Non-Stoichiometric Compounds. An Introductory Essay", in <u>Comprehensive Inorganic Chemistry</u>, Vol. IV ed, (Oxford: Pergammon Press, 1973) 453, ff.

- 43. Brauer, G., and Müller, O., Z. Anorg. Allg. Chem., 1958, 295, 218.
- 44. Willis, B. T. M., <u>Nature</u>, 1963, 197, 755.
- 45. Willis, B. T. M., <u>Journal de Physique</u>, 1964, 25, 431.
- 46. Cheetham, A. K., Fender, B. E. F, and Steele, D. and Taylor, R. F. and Willis, B. T. M., Solid State Commun., 1970, 8, 171
- 47. Cheetham, A. K. Fender, B. E. F., and Cooper, M. J., J. Phys. C., 1971, 4, 3107.
- 48. Fender, B. E. F., "Theories of Non-Stoichiometry" in Solid State Chemistry, MTP International Review of Science, Inorganic Chemistry, Series 1, vol. 10, 1972, 243.
- 49. Fishel, Norman A., Ph.D. Thesis, Michigan State University, East Lansing, MI, 1970.
- 50. Fishel, Norman A. and Eick, Harry A., <u>J. Inorg. Nucl.</u>
  Chem., 1971, 33, 1198.
- 51. Lüke, H. and Eick, Harry A., <u>Proc. Rare Earth Res.</u> Conf. 12th, 1976, <u>1</u>, 424.
- 52. Bärnighausen, H., Proc. Rare Earth Res. Conf., 12th., 1276, 1, 404.
- 53. Löckner, U., Bärnighausen, H., and Corbett, John D., Inorg. Chem., 1977, 16, 2134.
- 54. Bärnighausen, M. and Haschke, John M., <u>Inorg. Chem.</u>, 1978, <u>17</u>, 18.
- 55. Haire, R. G., Young, J. P., Peterson, J. R., Fellows, R. L., Proc. Rare Earth Res. Conf., 13th, 1977.
- 56. Pezzoli, Paul A., M. S. Thesis, Michigan State University, East Lansing, MI 1977.
- 57. Greis, O. Z. Anorg. Allg. Chem., 1977, 430, 175.
- 58. Greis, O. and Petzel, T., Z. Anorg. Allg. Chem.,  $\frac{1977}{434}$ , 89.
- 59. Greis, O., <u>J. Solid State Chem.</u>, 1978, 24, 227.
- 60. Greis, O., Z. Anorg. Allg. Chem., 441, 39.

- 61. Gettman, W. and Greis, O., <u>J. Solid State Chem.</u>, 1978, <u>26</u>, 255.
- 62. Greis, O., <u>Proc. Rare Earth Res. Conf., 14th</u>, 1979, 2, 167.
- 63. Kieser, M. and Greis, O., Z. Anorg. Allg. Chem., 1980, 469, 164.
- 64. Astakhova, S. S., Laptev, D. M., Kulagin, N. M., Zh. Neorg. Khim., 1977, 22, 1702.
- 65. Astakhova, S. S., Laptev, D. M., Kulagen, N. M., Zh. Neorg. Khim., 1977, 22, 2003.
- 66. Polyachenok, O. G., and Morozov, G. S., Russ. J. Inorg. Chem., 1963, 8, 1478.
- 67. T'en, Fam Ngok and Morozov, J. S., Russ. J. Inorg. Chem., 1971, 16, 1215.
- 68, Fedorov, P. P., Izotova, O. E., Alexandrov, V. B., and Sobolev, B. P., J. Solid State Chem., 1974, 9, 368.
- 69. Sobolev, B. P. Seranian, K. B., Garashina, L. S. and Federov, P. P., J. Solid State Chem., 1979, 28, 51.
- 70. Shannon, R. D., <u>Acta. Cryst., Sect. A.</u>, 1976, <u>32A</u>, 751.
- 71. Wendlandt, Wesley W., J. Inorg. Nucl. Chem., 1957, 5, 118.
- 72. Wendlandt, Wesley, J. Inorg. Nucl. Chem., 1959, 9, 136.
- 73. Taylor, M. P. and Carter, C. P., <u>J. Inorg. Nucl. Chem.</u>, 1962, <u>24</u>, 38.
- 74. Hamilton, Walter C., Acta Cryst., 1965, 18, 502.
- 75. Belbeoch, B., Piekarski, C. and Perio, P., <u>Acta Cryst.</u>, 1961, 14, 837.
- 76. Conrad, B. R. and Franzen, B. F., "The Crystal Structure of ZrS and Zr<sub>0.17</sub>S" in <u>The Chemistry of Extended</u> Defects in Non-Stoichiometric Solids, ed Eyring, LeRoy and O'Keeffe, Michael (Amsterdam: North-Holland Publishing, 1970), 207.

- 77. Watanabe, D. and Terasaki, O., "Electronmicroscopic Study on the Structure of Low Temperature Modification of Titanium Monoxide Phase", <u>Ibid</u>, 238.
- 78. Walker, P. J., <u>J. Crystal Growth</u>, 1978, <u>44</u>, 187.
- 79. Ayasse, Conrad, and Eick, Harry A., Inorg. Chem., 1973, 12, 1140.
- 80. Leary, T. A., and Johnson, K. W. R., <u>J. Metals</u>, 1961, <u>13</u>, 670.

### AN ANNOTATED BIBLIOGRAPHY OF CRYSTALLOGRAPHY

This bibliography is intended as an introductory guide to some of the crystallography books which are readily available at Michigan State University. It is not intended to be comprehensive: many other volumes may be equally useful or perhaps of even greater value.

The reader is encouraged to examine the longer bibliographies included in most of these works.

Ahmed, F. R., with Hall, S. R. and Huber, C. P., <u>Crystal-lographic Computing</u>, Copenhagen: Munksgaard, 1969.

These articles were presented at an International summer school and hence address specific computing problems, detailed and specific discussion of computing methods used in crystallography.

Ahmed, F. R., ed., <u>Crystallographic</u> <u>Computing Techniques</u>, Copenhagen: Munksgaard, 1976.

Highly technical and mathematical discussions of current computing practice. Articles written by the authors of the programs. Best detailed discussion of MULTAN, but the utility of the material is limited by its difficulty.

Arndt, U. W. and Willis, B. T. M., <u>Single Crystal Dif-</u> fractometry. Cambridge: Cambridge University Press, 1966.

Unintelligible due to the obscurity of excessive detail. Avoid it.

Buerger, Martin J., <u>Crystal Structure Analysis</u>. New York: John Wiley and Sons, Inc., 1960.

Fundamental crystallography written clearly and in detail. Contains both theoretical and "nuts and bolts" discussions.

. The Precession Method in X-Ray Crystal-lography. New York: John Wiley and Sons, Inc., 1964.

Everything you always wanted to know about the precession method but didn't have time to ask. Written by the man who invented it. The definitive discussion.

<u>Crystal Structure</u> Investigation. New York: John Wiley and Sons, Inc., 1959.

Verbose. May tell you more than you really want to know. Excellent discussion of Patterson functions.

Glusker, Jenny Pickworth and Trueblood, Kenneth N., Crystal Structure Analysis: a Primer. New York: Oxford University Press, 1972.

Do not confuse simplicity with triviality. This is an excellent introductory and reference text. Good index, glossary and bibliography.

"International Tables for X-Ray Crystallography". vol I-IV. Birmingham, England: Kynoch Press.

Useful discussions of theory and methods as well as invaluable tabulated data. Index is at the end of Volume IV. Use it: it may save you hours of hunting for the original articles.

Ladd, M. F. C. and Palmer, R. A., <u>Structure Determination</u> by X-Ray <u>Crystallography</u>. New York: Plenum Press, 1979.

Similar to Stout and Jensen (below) but more up to date. Includes examples.

Main, Peter, Hull, Se. E., Lessinger, L., Germain, G., DeClercq, J. P., Woolfson, M. M., <u>MULTAN78</u>: "A System of Computer Programmes for the Automatic Solution of Crystal Structures from X-Ray Diffraction Data". University of York, England, 1978.

The manual maintained by Dr. Ward is well documented and includes specific references to the original publications. Understanding of the program is enhanced by reading the manual.

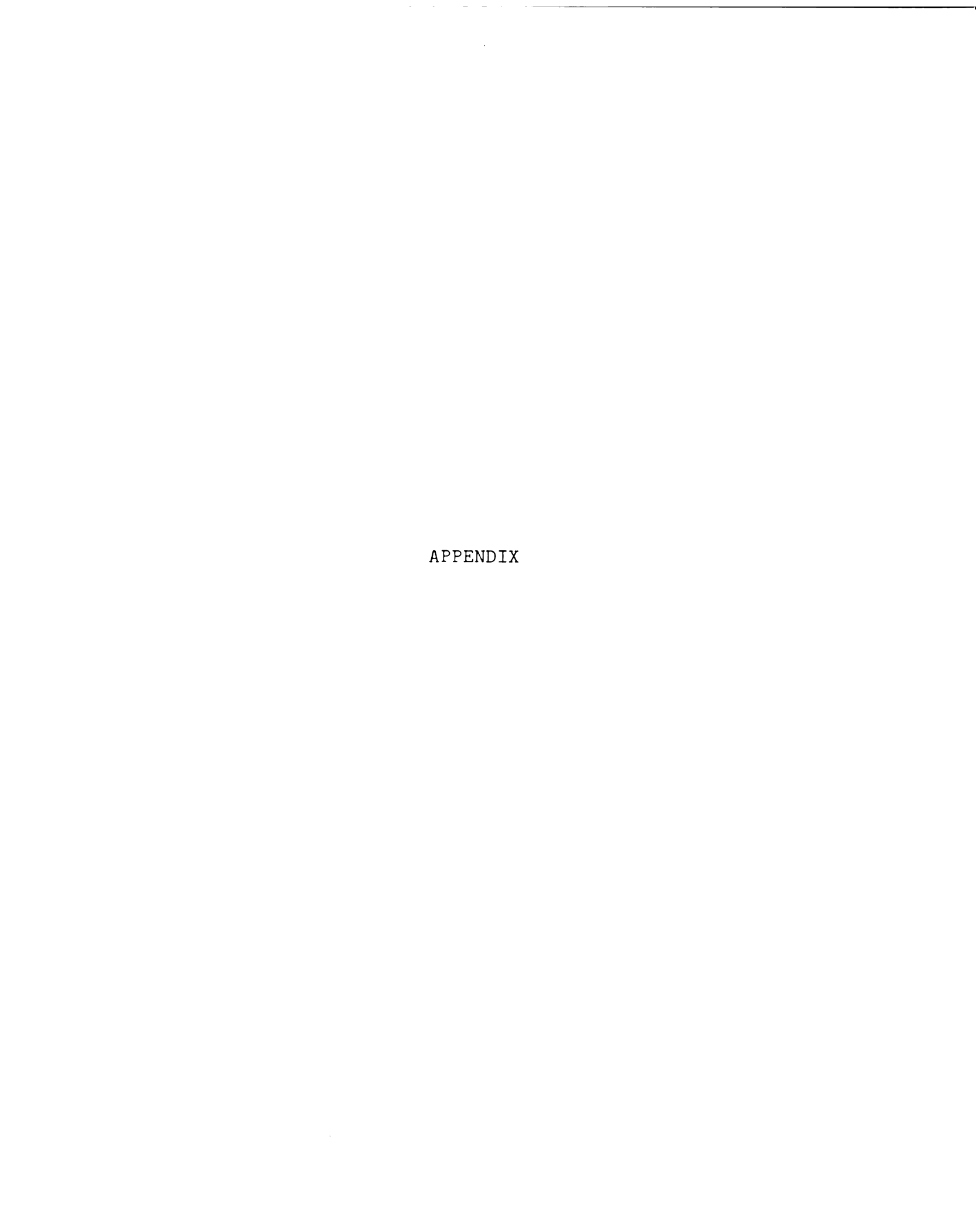
Rollett, J. S., ed., <u>Computing Methods in Crystallography</u>. Oxford: Pergamon Press, 1965.

Based on a lecture series in crystallography. Covers algebra, statistics, phase determination and programming.

The last section is out of date, but the rest is valuable and not overly obscure. Illuminating illustrations.

Stout, George H. and Jensen, Lyle, R., X-Ray Structure Determination. New York: Macmillan Co., 1968.

Crystallographic theory as well as "how to" sections. Readable and well illustrated.



DASCRUED STRUCTURE FACTORS FOR #15-12-CROWN-4 (CONTINUED) PAGE ? PE BCHL 04416 | March | Marc | Martin | M 

CSSERVED STRUCTURE FACTORS, STANDARD DEVIATIONS, AND DIFFERENCES (X 1.0) FOR (SR/Y)CL2.05, VACANCY MODEL F(0,0,0) = 224

FOB AND FCA ARE THE OBSERVED AND CALCULATED STRUCTURE FACTORS.

SG = ESTIMATED STANDARD DEVIATION OF FOB. DEL = /FOB/ - /FCA/.

\* INDICATES ZERO WEIGHTED DATA.

H FOB SG DEL K.L= 0. 0 3 1 2 -1\*  $K_{\bullet}L = 3_{\bullet} - 2$ 5 1 2 -1\* K.L= 4. 2 4 2 2 -1\* K,L= 3, -1 4 3 1 1 K.L= 3. -3 3 63 1 5 0 1 0+ K.L= 5 4 1. 3 K.L= 1. -1 5 53 4 1 K,L= 4. 3 1 62 3 -33 K.L= 3. -2 K.L= 1. 4 5 1 0 K.L= 1. 0 3 2 1 K.L= 3. 5 2 3 -1\* 0 0 K.L= 4, 4 1 0 K.L= 3. -1 4 3 1 1 K.L= 2. -4 5 3 3 -1\* K,L= 1, 1 3 66 6 0 K.L= 3. 1 5 3 3 0 K.L= 5. -5 4 2 3 -1+ 1 52 25 -47 K.L= 2. -3 5 34 K.L= 3. 0 3 1 K.L= 0. n 3 2 1 0 K.L= . 3. 2 5 3 0 K.L= 5. -4 1 4 3 2 K,L= 3, K.L= 2 18 3 7 K.L= 3. 1 0 2, -2 5 2 4 -2+ 3 61 7 -6 1 K.L= 0. 5 3 2 K.L= 3 0 5, -3 4 3 1 2 1 0 0 K.L= 3. 2 0 K.L= 2. -1 5 41 3 2 K.L= 1. -1 3 2 2 K.L= 4. -4 0 \* 5 3 1 0 K.L= 5. -2 K.L= 3. 3 4 88 5 12 K.L= 2. 0 2 1 1 0 \* 5 2 3 -2\* K.L= 1. 0 3 56 11 -2 K.L= 4. -3 5 1 2 -1\* K.L= 5. -1 2 3 -1\* K,L= 4, -2 1 1 0 \* K.L= 0. 0 K.L= 2, 1 5 44 3 2 1 K.L= 1, 4 98 13 -26 5 2 2 -1\* K,L= 5• 0 4 20 2 6 2 1 1 0 + K.L= K.L= 0. 1 5 3 2, 2 3 -1 K.L= 2. -2 4 2 1 0 K.L= 4. -1 5 2 3 -1\* K.L= 5. 1 5 42 4 -1 2 27 1 11 K.L= 0. 2 2 3 -1+ K.L= 2. 3 K.L= 2. -1 4 20 1 K.L= 4. 0 5 3 1 ٠ 0 K.L= 5. 2 2 1 1 1 0 4 2 0 0 \* K.L= 0, 3 4 87 6 -7 4 5 2 3 -1\* K.L= 2. K.L= 2 -1\* K<sub>0</sub>L= 4<sub>0</sub> 1 4 2 3 -1 4 5 2 3 -1+ K.L= 5. 3 K.L= 1. -3 2 100 8 -53 -1+ K.L= 3, -4 5 42 2 3 4 2 2 -1\* K.L= 4. 2 K.L= 2. 1 5 3 3 -1\* K.L= 5. 4 K.L= 1. -2 4 19 2 2 1 2 0 \* K.L= 3. -3 5 4 5 0 + K.L= 2. 2 K.L= 4. 3 • 2 2 -1\* 5 46 0 K.L= 5. 5 4 2 22 8 K.L= 1. -1 4 2 3 -1\* 6 K.L= 3. -2 5 33 1 n 4. K.L= 0. 0 3 1 1 K.L= 4 5 2 3 -1\* K,L= 0. 0 3 1 1 -1\* K.L= 1. 0 4 82 9 6 K.L= 3, -1 6 19 2 5 K.L= 0. 1 K.L= 4 1 2 -1+ 5 55 4 0 • 0 3 K.L= 0. 1 1 2 -1\* K.L= 1. 1 5 2 2 -1\* K.L= 3. 0 6 2 3 -1\* K.L= 0. 2 2 1 K.L= 0. 1 5 1 2 -2\* 0 K.L= 0. 2 3 1 1 0 + 5 1 2 -1\* K.L= 1. 2 K.L= 3, 1 6 83 5 -1 4 2 2 -1\* K.L= 1. -2 K.L= 0. 2 5 51 K.L= 0. 6 0 - 3 3 0 \* K.L= 1, 3 1 1 5 2 2 -1+ K.L= 3. 2 6 3 2 0 K.L= 4 2 K.L= 1. -1 2 0 \* 0. 3 5 2 2 -1+ K,L= 0. 4 3 70 7 -9 K.L= 2. -3 5 3 2 K+L= 3+ 3 0 6 13 0 1 K.L= 1. 0 4 2 2 -1+ K.L= 0. 4 5 46 3 -1 K.L= 0. 5 3 1 1 0 + K.L= 2, -2 5 1 3 -2\* K.L= 3, 4 6 3 3 -1\* K.L= 1, 1 4 98 9 -9 K.L= 1. -4 5 4 2 1 K.L= 1. -5 5 3 3 K•L= 1• 3 67 7 -9 K.L= 2. -1 5 0 \* K.L= 4, -4 0 \* 6 3 4 K.L= 1. 2 4 2 0 + 1, -3 5 2 4 -2+ K.L= 1, -4 K.L= 55 5 2. 0 2 -1\* 5 O 2 K.L= 4. -3 6 3 3 -1\* K.L= 2, -2 4 19 2 2 K.L= 1. -2 5 4 2 0 K.L= 1. -3 1 2 -1\* K.L= 2. 1 2 2 -1\* K.L= 4. -2 6 2 3 -1\* K.L= 2. -1 4 2 1 0 K,L= 1, -1 5 4 1 1 K.L= 1. -2 5 58 6 3 0 2 1 K.L= 2. 2 K.L= 6 3 2 1 4. -1 0 K.L= 1. K.L= 2. 0 4 95 10 -12 0 5 3 4 0 + K.L= 1. -1 2. 3 2 1 0 \* K • L = 5 2 -1+ K.L= 0 6 4 1 1 K.L= 2. 1 4 2 3 -1\* K.L= 1. 1 K.L= 1. 5 2 2 -1\* 0 5 57 5 -2 K.L= 3. -3 1 6 1 2 -2\* 3 0 2 -2\* K.L= 4. K.L= 2. 2 K.L= 1. 2 5 3 4 K.L= 1. 1

# STRUCTURE FACTORS CONTINUED FOR (SR/Y)CL2.05. VACANCY MODEL

PAGE 2

H FOB SG DEL	H FOR SG DEL	H FOS SG DEL	H FOB SG DEL	H FOB SG DEL
6 3 3 -1+	K.L= 43	6 11 1 1	K.L= 22	7 3 4 0+
K,L= 1, 2	5 <b>4</b> 4 0 <b>*</b>	K.L= 6. 3	7 3 4 0+	K.L= 4. 1
6 3 3 0*	K.L= 42	6 3 4 -1*	K.L= 21	7 4 2 0
K.L= 1. 3	6 69 4 0		7 5 2 2	· · · · · · · · · · · · · · · · · · ·
6 3 2 0	K.L= 41	6 53 1 4	K.L= 2. 0	7 5 2 1
K,L= 1, 4	6 4 4 0+	K.L= 6. 5	7 5 2 1	K.L= 4. 3
6 3 2 0	K•L= 4• D	6 5 5 1*	K•L= 2• 1	7 3 5 -1*
K.L= 1. 5	6 13 0 0	K.L= 6. 6	7 4 2 0	K,L= 4, 4
6 5 2 1	K.L= 4. 1	6 13 2 4	K.L= 2. 2	7 4 5 0*
K.L= 25	6 3 4 -1*	K.L= 0. 0	7 4 3 0	K.L= 4. 5
6 2 4 -2*	K.L= 4. 2	7 2 3 -1*	K.L= 2. 3	7 7 2 3
K.L= 24	6 67 6 -3	K.L= 0. 1	7 3 4 -1+	
	K.L= 4. 3		K.L= 2. 4	7 5 6 1+
K.L= 23	6 4 4 0*	K.L= 0. 2	7 5 2 1	K.L= 56
6 3 3 -1*	K.L= 4. 4	7 4 1 1	K.L= 2. 5	7 5 6 1*
K.L= 22	6 13 1 2	K.L= 0. 3	7 2 4 -2*	K.L= 55
6 15 2 1	K.L= 4. 5	7 3 2 0	K.L= 2. 6	7 26 1 0
K.L= 21	6 4 5 0+	K.L= 0. 4	7 5 4 1	K.L= 54
6 3 3 0*	K.L= 55	7 3 3 -1	K.L= 36	7 5 6 1*
K.L= 2. 0	6 7 1 3	K.L= 0. 5	7 5 2 1	K.L= 53
6 74 7 -10	K.L= 54	7 3 4 -1*	K.L= 35	7 30 2 -1
	6 3 4 -1*	K.L= 0. 6	7 30 2 -1	K.L= 52
6 3 2 0	K.L= 53	7 3 4 -1+	K.L= 34	7 6 1 2
K.L= 2. 2	6 4 4 0*	K.L= 16	7 5 2 1	K.L= 51
6 15 0 1	K.L= 52	7 4 5 0+	K.L= 33	7 34 3 1
K.L= 2. 3	6 4 4 0	K.L= 15	7 38 3 2	K.L= 5. 0
6 2 3 -2*	K.L= 51	7 35 3 2	K.L= 32	7 1 3 -3*
K.L= 2. 4	6 4 4 0+	K.L= 14	7 4 2 0	K.L= 5. 1
6 69 4 -1	K.L= 5. 0	7 3 4 -1+	K.L= 31	7 32 3 -1
K.L= 2. 5	6 4 3 0	K.L= 1, -3	7 39 3 0	
6 4 2 0	K.L= 5. 1			
			K.L= 3, 0	7 3 4 -1*
K,L= 3, -5	6 4 2 0	K.L= 12	7 3 3 -1*	K.L= 5. 3
6 3 4 -1+	K.L= 5, 2	7 4 2 0	K.L= 3. 1	7 32 1 1
K.L= 34	6 4 3 0	K.L= 11	7 38 4 -1	K.L= 5. 4
6 3 2 0	K•L= 5• 3	7 41 3 -2	K•L= 3• 2	7 1 5 -3+
K,L= 3, -3	6 5 2 1	K.L= 1. 0	7 3 4 -1*	K.L= 5, 5
6 4 2 0	K.L= 5. 4	7 2 3 -1+	K.L= 3, 3	7 30 1 3
K.L= 32	6 4 5 0+	K.L= 1. 1	7 38 2 2	K.L= 5. 6
6 1 4 -3+	K.L= 5. 5	7 40 3 -3	K.L= 3. 4	7 4 5 0+
K,L= 3, -1	6 5 6 1*	K.L= 1, 2	7 3 4 -1*	K.L= 65
6 1 3 -2*	K.L= 66	7 3 3 -1+	K.L= 3. 5	7 5 5 0*
K.L= 3. 0	6 8 6 -1	K.L= 1, 3	7 31 1 1	K.L= 64
6 2 2 -2*	K.L= 65	7 39 3 -1	K.L= 3. 6	7 4 5 0*
$K_{\bullet}L=3_{\bullet}$ 1	6 3 5 -1*	K <sub>9</sub> L= 1 <sub>9</sub> 4	7 0 5 -4*	K <sub>1</sub> L= 6, -3
6 2 4 -2*	K.L= 64	7 3 4 0+	K.L= 46	7 5 5 0 *
K•L= 3• 2	6 49 3 0	K.L= 1. 5	7 6 3 2	K.L= 62
6 2 3 -1*	K,L= 6, -3	7 34 2 1	K.L= 45	7 2 4 -2*
K.L= 3. 3	6 4 5 0*	K.L= 1. 6	7 3 4 -1+	K.L= 61
6 3 3 -1*	K.L= 62	7 5 2 1	K.L= 44	7 5 2 1
K.L= 3. 4	6 12 1 1	K.L= 26	7 3 5 -1*	K.L= 6. 0
6 3 4 0*	K.L= 61	7 5 5 1+	K.L= 43	7 4 4 0*
•	6 3 4 -1*	K.L= 25	7 5 2 1	K.L= 6. 1
6 4 4 0+	K.L= 6. 0	7 3 4 -1+	K+L= 4+ -2	7 5 6 1*
K.L= 45	6 60 4 2	K.L= 2, -4	7 5 3 1	K,L= 6, 2
6 2 4 -2*	K•L= 6• 1	7 3 4 -1*	K.L= 41	7 6 2 2
K.L= 4, -4	6 5 3 1	K.L= 23	7 2 4 -2*	K.L= 6. 3
6 13 1 2	K.L= 6, 2	7 3 3 -1+	K.L= 4. 0	7 6 3 2
<b>-</b>	,			

# STRUCTURE FACTORS CONTINUED FOR (SR/Y)CL2.05, VACANCY MODEL

· ·

PAGE 3

H FJB SG D		SG DEL		SG DEL	H FOB			SG DEL
K.L= 6.	4 8 2	5 -3*	K,L=	43	9 4	5 0+	K,L=	3. 0
	-3+ K.L=	2• -6	8 2	4 -2*	K.L=	0 • 4	9 4	<b>4</b> 0
K.L= 6.	5 8 42	3 0	K.L=	42	9 5	3 1	K,L=	3. 1
7 7 3	2 K.L=	2, -5	8 10	1 0	K.L=	0. 5	9 26	2 -2
	-3 8 5	4 1	K.L=	41	9 4	5 0+	K+L=	3. 2
7 25 1	1 K.L=	2, -4	8 3	4 -1+	K,L=	15	9 3	5 -1+
	-2 8 10	2 0	K.L=	4. 0	9 24	1 -1	K.L=	3. 3
7 4 5	0+ K.L=	2• -3	8 49	3 -5	K.L=	14	9 24	1 -2
	<b>-1</b> 8 3	4 -1+	K.L=	4, 1	9 5	3 1	K+L=	3, 4
7 26 1	0 K.L=	2• -2	8 5	5 1*	K.L=	1, -3	9 2	5 -2*
K.L= 7.	0 8 57	4 -1	K.L=	4, 2	9 27	2 -1	K,L=	4, -3
	-1* K.L=	2, -1	8 11	1 1	K.L=	12	9 5	5 0÷
K.L= 7.	1 9 5	2 1	K.L=	4. 3	9 5	3 0	K,L=	4, -2
7 24 1	-2 K.L=	2.0	8 3	5 -1+	K.L=	11	9 5	5 1*
K.L= 7.	2 8 11	1 0	K,L=	4. 4	9 29	2 -2	K.L=	41
7 7 2	2 K.L=	2. 1	8 46	2 1	K.L=	1, 0	9 5	3 1
K.L= 7.	3 8 4	4 0+	K,L=	4. 5	9 3	4 -1+	K,L=	<b>4.</b> 0
7 27 1	2 K.L=	2, 2	8 4	7 0+	K.L=	1. 1	9 4	5 0 <b>*</b>
K•L= 0•	0 8 56	4 -3	K.L=	5, -4	9 29	1 -2	K.L=	4, 1
8 64 4	0 K.L=	2. 3	8 2	6 -2*	K.L=	1. 2	9 4	5 0 <b>*</b>
K.L= 0.	1 8 3	4 -1+	K.L=	5 <b>, -</b> 3	9 3	4 -1*	K.L=	4. 2
8 4 3	0 K.L=	2, 4	8 4	6 0*	K.L=	1. 3	96	3 2
K.L= 0.	289	1 -1	K.L=	52	9 27	1 -2	K.L=	4. 3
8 11 1	0 K.L=	2, 5	8 4	3 0	K.L=	1, 4	9 3	5 -1*
K.L= 0.	3 8 5	4 1	K.L=	5• <b>-</b> 1	9 3	5 -1*	K.L=	5• <b>-</b> 2
8 3 4	0* K.L=	2. 6	8 6	3 2	K.L=	1. 5	9 4	7 -1*
K.L= 0.	4 8 42	1 1	K.L=	5• O	9 23	1 -1	K.L=	5, -1
8 53 3	-1 K.L=	36	8 5	5 1*	K.L=	2• <b>-</b> 5	9 23	1 -2
K•L= 0•	5 8 6	5 2	K.L=	5. 1	9 4	5 -1+	K.L=	5 <b>•</b> 0
8 5 3	1 K.L=	3• <b>-</b> 5	8 5	5 0+	K.L=	2, -4	9 4	4 0+
K•L= 0•	6 8 5	4 1	K.L=	5, 2	9 4	6 0+	K,L=	5, 1
8 11 1	2 K.L=	3, -4	8 5	5 1*	K.L=	23	9 22	1 -2
K.L= 1.	<b>-6</b> 8 5	2 1	K.L=	5, 3	9 3	6 -1*	K.L=	<b>5</b>
8 3 5	-1* K.L=	3• <b>-</b> 3	8 4	5 -1*	K.L=	22	9 4	5 -1+
K•L= 1•	-5 8 4	4 0 •	K.L=	5• 4	9 6	3 2	K.L=	0 • 0
8 3 4	-1 * K.L=	3• <b>-</b> 2	8 5	7 0*	K.L=	2, -1	10 7	2 -2
K.L= 1.	-4 8 4	4 0 +	K.L=	6, -3	9 4	4 0+	K.L=	0, 1
8 3 4	-1* K.L=	3• <b>-</b> 1	8 4	5 0*	K.L=	2. 0	10 4	5 0+
K.L= 1.	-3 8 4	2 0+	K.L=	62	9 6	2 1	K.L=	0, 2
8 3 5	-1 * K.L=	<b>3</b> • 0	8 41	3 -1	K,L=	2. 1	10 41	1 -1
K.L= 1.	<b>-2</b> 8 5	2 1	K.L=	61	9 4	5 0*	K.L=	0, 3
8 4 3	1 K.L=	3, 1	8 7	2 3	K.L=	2, 2	10 6	3 2
K.L= 1.	-1 8 1	5 <b>-3</b> +	K.L=	6• O	9 2	4 -2*	K.L=	13
8 3 4	-1* K.L=	3, 2	8 8	1 -1	K.L=	2. 3	10 7	3 2
K.L= 1.	0 8 1	4 -3*	K.L=	6 1	9 4	6 0+	K,L=	12
	-1+ K.L=	3, 3	8 5	3 1	K.L=	2, 4	10 5	6 1*
K.L= 1.	1 8 5	4 1	K.L=	6 2	9 6	3 1	K.L=	11
8 4 2	1 K.L=	3, 4	8 42	2 0	K.L=	2. 5	10 5	3 1
K.L= 1.	2 8 4	5 O*	K.L=	6, 3	9 5	4 1	K.L=	1. 0
8 3 4	-1+ K+L=	3• ⋅5	8 3	5 -1*	K.L=	3, -4	10 2	5 -2*
K.L= 1.	3 8 3	5 -2*	K.L=	0 • 0	9 5	6 1*	K.L=	1. 1
8 4 3	0 K.L=	3	9 2	4 -2*	K,L=	3, -3	10 6	2 2*
K.L= 1.	4 8 7	2 3	K.L=	0. 1	9 24	1 -2	K,L=	1. 2
8 2 4	-2* K.L=	45	9 5	2 1	K.L=	3, -2	10 7	3 3
K.L= 1.	5 8 4	5 0+	K.L=	0 • 2	9 5	5 1+	K,L=	1, 3
8 4 5	0* K.L=	4, -4	9 4	5 -1*	K.L=	3, -1	10 3	6 -2*
K.L= 1.	6 8 43	3 -2	K.L=	0. 3	9 26		K.L=	
			-				-	-

OBSERVED STRUCTURE FACTORS. STANDARD DEVIATIONS. AND DIFFERENCES (x23.7) FOR (SF/Y)CL2.LE WILLIS CLUSTER F(0.0.0) = 1742

FOB AND FCA ARE THE SESERVED AND CALCULATED STRUCTURE FACTORS.

SG = ESTIMATED STANDARD DEVIATION OF FOB. DEL = /FOB/ - /FCA/.

\* INDICATES ZERO WEIGHTED DATA.

```
L FOB SG DEL
               L FOR SG DEL
                              L FOL SO DEL
  H.K= 1. 1
              -2 117 12
                                 86
                                    4 -2
-1 569 29-119
               0 615 57 -27
                              2 45: 35 -14
1 454219-234
                              4 72 11 -1
               2 115 3
                         -2
 H.K= 2, C
               4 566 34
                         21
                              £ 338 5
                                        -4
 0 144 25 -42
                H+K= 6+ 4
                               H+K= 8+ 4
 H.K= 2. 2
                          9
              -4 190 6
                             -4 344 26 -24
-2 216 12 32
              -2 568 37
                         22
                                 79 B
                                        5
                              390 27 -38
0 987 78-151
               0 130
                      3
                         -1
2 178 62 -5
                                    7 12
               2 547 49
                              3 85
                          2
                             4 368 16
 H.K= 3. 1
               4 105
                     € 10
                                        C
-1 610 63
          5
                H•K= 6•
                              H.K= 8. 6
                         6
1 584 62 -20
              -6 63 45
                          3
                             -2 328 22 -14
              -4 304 26
                              ° 62 11
 H•K= 3. 3
                         -2
                                        Ω
-3 526 9 63
              -2 94
                     5
                         .15
                              2 336 18
                                       -6
-1 552 48
               0 488 29
          39
                         22
                               H.K=
                                    9. 1
                             -5 191 5
1 514 60
          1
               2 89 6
                         10
                                         n
 3 458 93 -5
               4 423 5
                         27
                             -3 219 15 -11
 H.K= 4. C
               6 9 16 39
                             -J 230 12 -10
 904124
          - 4
                H.K= 7.
                         1
                             1 228 11 -13
2 160 11 -4
              -5 275 21 14
                              3 212
                                       -9
                                    4
  H,K= 4, 2
              -3 318 28
                          7
                                     6 -9
                              F 183
-2 872 79 75
                               H • K =
              -1 326 26
                         - ç
                                     9, 3
               1 319 23 -16
                             -3 193 5 -16
0 149 13 -15
2 840 89 44
               3 307 20
                        - 3
                             -1 209 14 -12
 H.K= 4. 4
               5 268 14
                          7
                             1 210 17 -11
-4 742 45 148
               H+K= 7.
                         - 3
                             3 189 5 -19
-2 158 12
              -5 23E 17
          27
                         -3
                               H.K=
                                     9. 5
0 744 51
          31
              -3 300 27
                         21
                             -1 182
                                     5 -9
                              1 176 5 -16
2 152 13
          21
              -1 313 26
                         2
4 690 75
                               H.K= 19. 0
          96
               1 305 28
                         -5
 H.K= 5.
          1
               3 299 19
                         20
                              9 54 18 -8
-3 445 37
                             2 323 5 -20
          34
               5 246 5
                          5
-1 478 50
          19
                H.K= 7.
                          5
                               H.K= 10. 2
1 468 41
           9
              -5 208
                      4
                            -2 55 22 -3
                              2 314 5 -29
3 428 36
              -3 239 15
          16
                         -2
 H.K= 5.
              -1 268 20
                             2 70 13 11
          - 3
                          7
-3 372 32
           7
               1 256 23
                         -5
-1 450 33
                          G
          38
               3 250
                      5
1 417 47
           5
               5 235
                         30
                      6
3 369 27
           5
                H.K=
                      7,
                          7
 H.K= 5.
           5
              -3 200
                      5
                          R
-5 268 21 10
              -1 209
                      5
                          4
-3 330 23
          24
               1 191
                      6 -14
-1 356 27
         19
               3 211
1 337 28
          - 1
                H.K= 8.
                          7
3 337 16
          31
               0 517 34
                         14
5 261
           3
                 89
       6
                          Ċ
 H.K= 6.
               4 425 25
           n
0 152 16
               6 87 10
          15
                         24
2 703 42
                      8.
          62
                H.K=
                         2
      3
4 106
           5
              -6 334 23
                         -8
 H.K= 6. 2
              -4 80 12
                         6
-4 563 42 18
              -2 460 36
```